AD-A067 280 SRI INTERNATIONAL MENLO PARK CA F/G 20/14
EMP SIMULATOR - SITE INTERACTION.(U)
MAR 78 A L WHITSON, W E SCHARFMAN DNA001-76-C-0026
UNCLASSIFIED DNA-4553F NL

1 OF 2
AD
A067 280

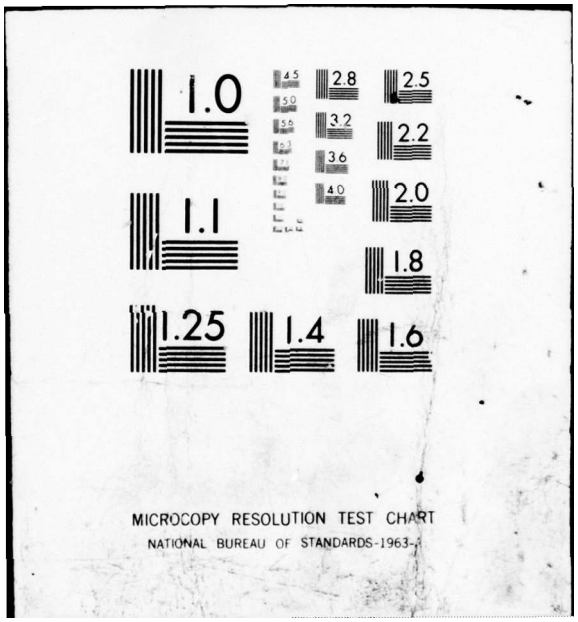
1.0
1.1
1.25
1.4
1.6
1.8
2.0
2.2
2.5
2.8
3.2
3.6
4.0
4.5
5.0
5.6
6.3
MICROCOPY RESOLUTION TEST CHART
NATIONAL BUREAU OF STANDARDS-1963-A

(12) LEVEL III

DNA 4553F

EMP SIMULATOR–SITE INTERACTION

SRI International
333 Ravenswood Avenue
Menlo Park, California 94025

March 1978

Final Report for Period 1 March 1976–31 October 1976

CONTRACT No. DNA 001-76-C-0226

APPROVED FOR PUBLIC RELEASE;
DISTRIBUTION UNLIMITED.

THIS WORK SPONSORED BY THE DEFENSE NUCLEAR AGENCY
UNDER RDT&E RMSS CODE B323076464 R99QAXEB08866 H2590D.

Prepared for
Director
DEFENSE NUCLEAR AGENCY
Washington, D. C. 20305

Destroy this report when it is no longer needed. Do not return to sender.

PLEASE NOTIFY THE DEFENSE NUCLEAR AGENCY, ATTN: TISI, WASHINGTON, D.C. 20305, IF YOUR ADDRESS IS INCORRECT, IF YOU WISH TO BE DELETED FROM THE DISTRIBUTION LIST, OR IF THE ADDRESSEE IS NO LONGER EMPLOYED BY YOUR ORGANIZATION.

UNCLASSIFIED

SECURITY CLASSIFICATION OF THIS PAGE *(When Data Entered)*

REPORT DOCUMENTATION PAGE		READ INSTRUCTIONS BEFORE COMPLETING FORM
1. REPORT NUMBER DNA 4553F	2. GOVT ACCESSION NO.	3. RECIPIENT'S CATALOG NUMBER
4. TITLE *(and Subtitle)* EMP SIMULATOR—SITE INTERACTION		5. TYPE OF REPORT & PERIOD COVERED Final Report for Period 1 Mar 76—31 Oct 76
		6. PERFORMING ORG. REPORT NUMBER SRI Project 4988
7. AUTHOR*(s)* A. L. Whitson W. E. Scharfman		8. CONTRACT OR GRANT NUMBER*(s)* DNA 001-76-C-0226
9. PERFORMING ORGANIZATION NAME AND ADDRESS SRI International 333 Ravenswood Avenue Menlo Park, California 94025		10. PROGRAM ELEMENT, PROJECT, TASK AREA & WORK UNIT NUMBERS NWED Subtask R99QAXEB088-66
11. CONTROLLING OFFICE NAME AND ADDRESS Director Defense Nuclear Agency Washington, D.C. 20305		12. REPORT DATE March 1978 13. NUMBER OF PAGES 110
14. MONITORING AGENCY NAME & ADDRESS*(if different from Controlling Office)*		15. SECURITY CLASS *(of this report)* UNCLASSIFIED 15a. DECLASSIFICATION/DOWNGRADING SCHEDULE

16. DISTRIBUTION STATEMENT *(of this Report)*

Approved for public release; distribution unlimited.

627094

17. DISTRIBUTION STATEMENT *(of the abstract entered in Block 20, if different from Report)*

18. SUPPLEMENTARY NOTES

This work sponsored by the Defense Nuclear Agency under RDT&E RMSS Code B323076464 R99QAXEB08866 H2590D.

19. KEY WORDS *(Continue on reverse side if necessary and identify by block number)*

EMP Simulator
HEMPS
TEMPS Interation
Site Interation
Simulator Utilization

20. ABSTRACT *(Continue on reverse side if necessary and identify by block number)*

EMP simulators interact with test objects and subsequently do not provide a test excitation environment that equals that of the threat EMP. This study compares the excitation from a horizontal simulator (TEMPS) to that from a horizontal EMP (HEMP). This comparison is made on a geometric scale model of an idealized communications facility.

TEMPS is shown to be able to excite the facility and its external penetrations at threat-like levels, but cannot duplicate threat excitations. By

(over)

DD FORM 1 JAN 73 1473 EDITION OF 1 NOV 65 IS OBSOLETE

UNCLASSIFIED

SECURITY CLASSIFICATION OF THIS PAGE *(When Data Entered)*

20. ABSTRACT (Continued)

analyzing a site for its critical penetration-to-critical-circuit coupling paths, often a TEMPS position can be found that will excite the site to threat-like levels.

SUMMARY

Large, full-scale simulators are often used in testing the survivability of weapon systems against nuclear electromagnetic pulse (EMP) effects. However, the test environment provided by a simulator does not always duplicate the EMP threat environment. To develop quantitative information that can assist in the evaluation of the degree to which EMP simulators can be useful, SRI compared the excitation from the Defense Nuclear Agency (DNA) Transportable EMP Simulator (TEMPS) on a ground-based facility with that provided by a high-altitude nuclear explosion.

Ideally, an EMP simulator should duplicate the response caused by the threat EMP at all critical circuits. However, no simulator actually does this. For a large ground-based facility with many conducting facility penetrations, EMP excitation can be provided by duplicating the facility threat excitation and the interference excitations on each facility penetration.

This study used geometric scale modeling to compare a high-altitude EMP (modeled as a horizontal dipole) with TEMPS as excitation sources on an idealized ground facility. The facility was modeled as a large metal building with aboveground and buried wire penetrations and with a radio tower penetration.

The currents flowing on wires due to excitation by a horizontal electromagnetic pulse (HEMP) and a TEMPS simulator are compared in time and frequency. Scale modeling techniques are used for the measurements on aboveground and buried wires. In general, the results show that the spectral content of the two excitation methods are within a few decibels of each other when the simulator does not cross over the wire. For aboveground wires straddled by the simulator, much larger differences are observed.

For aboveground penetrations, TEMPS can duplicate or exceed HEMP excitation. For buried wires, it may be necessary to position TEMPS over the wire to achieve HEMP excitation levels.

TEMPS is shown to be a threat-relatable test simulator if it is positioned to excite the critical penetrations of the facility. Test positions can be found to duplicate the EMP threat at any critical circuit by identifying the penetration-to-critical circuit coupling paths. This critical path can be determined by analysis, on-site testing, or scale modeling.

CONTENTS

ILLUSTRATIONS

TABLES

1. INTRODUCTION

In testing the EMP hardness of a system using an EMP simulator, there are invariably differences between the threat field produced by an actual nuclear burst and the fields produced by a simulator. These differences may stem from a number of possibly important factors such as:

- Polarization
- Angle of incidence
- Non-plane-wave field components
- Waveform (or spectral content).

Furtermore, when the test object is large, as most systems are, the simulated fields interact with the test object in a nonthreat way by:

- Multiple scattering between the test object and the simulator
- Differential time of excitation across the test object
- Nonuniform or partial illumination.

The interaction between large test objects and simulators will cause excitation currents on external surfaces and conducting penetrations that must be related to the excitations from the HEMP threat to assess the hardness of the test object. More important, the simulator excitation of critical equipment items inside the test object must be relatable to threat. For an EMP simulator test to be useful, an assessment must be made of the errors introduced by differences between simulation and the threat field.

For simple structures such as cylinders and spheres, it would be a formidable task to compute the actual fields produced by the simulator, rather than the zeroth-order approximation to these fields, and then to compute the coupling to the structure. For example, in the simplest of simulators, the parallel plate line, the fields are

not simply those computed assuming a simple propagating TEM mode.[1]* When the structure height becomes larger than the wavelength, field nonuniformities appear both in space and in frequency. Computing these effects in structures that are many wavelengths long is beyond the capabilities of the largest computers.

EMP field simulators use either a radiating structure or antenna to create a propagating wave or a bounded-wave structure such as a transmission line to create a confined uniform field.[2] Hybrids that do both are often used in hardness testing. Table 1 lists some of the EMP simulators available in the United States,[3] many of which are permanent facilities. The TEFS, RES, TORUS, and TEMPS I are examples of simulators that can be transported to facilities for tests.

Some data already exist for the interaction of test objects with EMP simulator fields. Appendix A is a summary of three scale-modeling studies that addressed field linearity and planarity requirements.[4,5,6] Scale-model studies have also been used to determine test object interaction as a function of simulator position.[6,7,8] Comparisons between scale model and full-scale tests have been made.[9,10,11] Comparisons between HEMP excitation and simulator excitation of test objects have been made but not with sufficient detail to identify simulator-test object interactions.

The work described in this report was based on test measurements using electromagnetic scale-modeling techniques[3] to determine simulator-test object interactions necessary to define the usefulness of simulators in HEMP assessment programs for large systems. Horizontally polarized simulators, exemplified by the TEMPS, were studied, and the coupled currents produced by the simulator were compared to a HEMP incident field. The HEMP was approximated by a long dipole antenna far from the test site center.

---

*References are listed at the end of the report.

Table 1

REPRESENTATIVE EMP SIMULATORS

Simulator \ Parameter	Basic Pulser Voltage	Field Polarization	Peak Field Strength	Rise Time 10% to 90%	Fixed or Transportable	Sponsoring Agency	CW Capability
Bounded Arrays							
ALECS	2.2 MV	V	100 kV/m	6-8 ns	F	AFWL	Yes
ARES	3.7 MV	V	92.5 kV/m	8 ns	F	DNA	Yes
TRESTLE	H: 16 MV V: 4 MV	H or V	H: 100 kV/m V: 50 kV/m	20 ns	F	AFWL	Yes
TEPS	100 kV	H or V	65 kV/m	15-20 ns	T	HDL	Yes
HEMPS	100 kV	V	80 kV/m	10 ns	F	SAFCA	No
Vertically Polarized Radiators							
VPD	1.8 MV	V	6 kV/m at 80 m	5 ns	F	AFWL	No
DRI	1.4 MV	V	500 kV/m at 1 m	1 ns	F	DRI	No
LASL	240 kV	V	160 V/m at 1 km	1 ns	F	LASL	No
EMPRESS	2.5 MV	V	24 kV/m at 50 m	8-13 ns	F	NOL	No
Horizontally Polarized Radiators, or Hybrids							
LASL	120 kV	H	72 V/m at 1 km	1 ns	F	LASL	No
HPD	5 m or 1.8 MV	H	25 kV/m	4 ns	F	AFWL	No
Suspended RES	1.8 MV	H	7 kV/m at 54 m	5 ns	F	AFWL	No
TORUS	2.5 MV	H and V	50 kV/m	10 ns	T	SAMSO	No
EMPRESS	2.5 MV	H	11 kV/m at 50 m	4 ns	F	NOL	No
TEMPS I	4.1 MV	H	52 kV/m at 50 m	8 ns	T	DNA	No
TEMPS II	4.1 MV	H	52 kV/m at 50 m	8 ns	F	HDL	No
Martin Marietta longwire	250 kV	H	1100 V/m	5-20 ns (variable)	F	Martin Marietta	No
Sandia longwire	30 kV	H	400 V/m	9 ns	F	Sandia	No
RES	1.8 MV	H or V	900 V/m at 500 m	4-6 ns	T	AFWL	No

Source: Reference 3

The pulse excitation was based on the HEMP threat field. A pulser with capacitance designed to produce the proper decay time was applied to the simulator terminals to produce fields with the threat decay time.

In this study, the currents that are coupled into facilities on external conductors (such as power lines, communication cables, water pipes, and antenna tower waveguides) were measured on an idealized test model. Both above- and below-ground conductors were modeled.

2. MODELS OF HEMP, TEMPS, AND TEST FACILITY

The models used to represent the HEMP and TEMPS signals were all 1/50th scale. An overall view of the model test facility is illustrated in Figure 1.

2.1 MODELING RANGE

All of the electromagnetic field measurements were made on the SRI modeling range, which consists of a 12 x 25-m area covered by an air-supported 0.5-mm Mylar building. The soil within this area was treated with sodium chloride (salt) to a depth of 1 m to raise the soil conductivity to approximately 0.5 s/m* (0.01 s/m full scale). The moisture content was maintained at a level that kept the conductivity constant to within about 30% of its nominal value (Appendix B).

Conductivity is measured at an audio frequency by two techniques. In one, a sample of soil is removed from the ground and placed in the test facility in a parallel plate geometry that measures the resistance of a known length of soil. In the other, which is used for day-to-day monitoring of conductivity, probes are inserted into the ground and the actual resistance is measured. Both techniques give substantially the same result.

The technique for measuring fields and coupled currents is described in Appendix C, along with a description of the sensors and their calibration method. Briefly, the measurements used a mercury read switch with an appropriate capacitor to shape the pulse excitation connected to either the HEMP dipole or the TEMPS. Current was measured by a current transformer surrounding the wire. This signal was sent via a coaxial cable

---

*s/m (siemens/meter) = mho/meter.

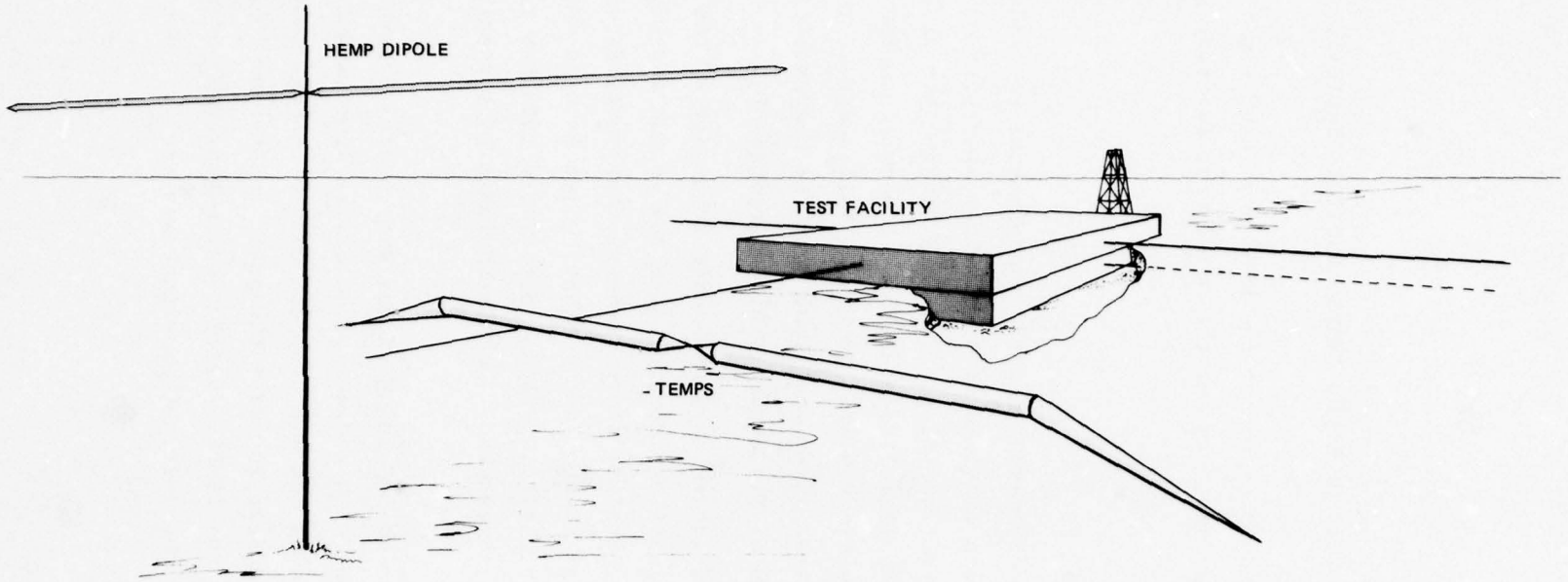

FIGURE 1 MODEL TEST FACILITY

to a sampling scope and an XY recorder, and these traces were digitized for spectral analysis.

Penetration on current was measured as the short-circuit wire current at the model building.

2.2 HEMP MODEL

The HEMP fields were produced by driving a dipole antenna with an overall length of 22 m, a sharp rise-time, and an exponentially decaying pulse (Figure 2). The dipole was fed through a broadband balun. The first 5.25 m of each half of the dipole was made of 2.5-cm diameter aluminum tubing. The feed points were tapered from a sharp point up to 2.5 cm in diameter over a length of 7.5 cm. Beyond the 5.25-m point, 5.75 m of 10-gauge wire was connected to reduce the discontinuity that would have resulted from leaving the dipole open-circuited at this point. This procedure reduced the discontinuity but did not eliminate it.

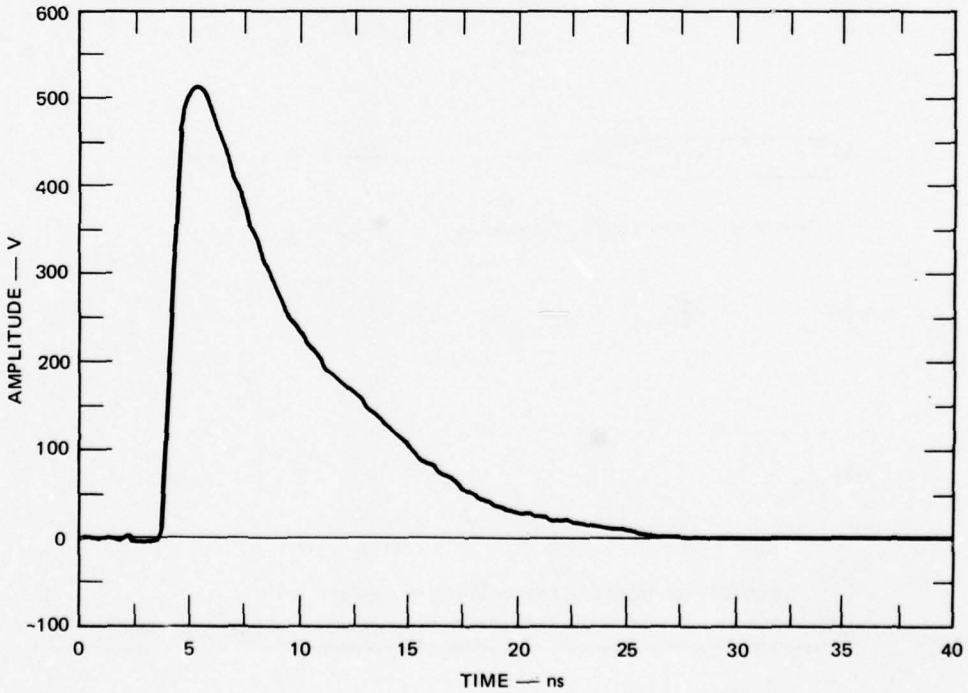

FIGURE 2 EXCITATION SOURCE WAVEFORM

The dipole antenna was mounted at a horizontal range of 7.5 m from the center of the test range. The dipole height was 2.4 m, giving an elevation angle of 21°. A top view of the dipole and its relation to the center of the test range is shown in Figure 3.

Of course, at no practical range scale could a perfect representation of a HEMP be achieved. However, at 7.5 m (corresponding to a full-scale range of 375 m), the linearity and planarity distortion caused by finite range effects are negligible (Appendix A), and they are so much

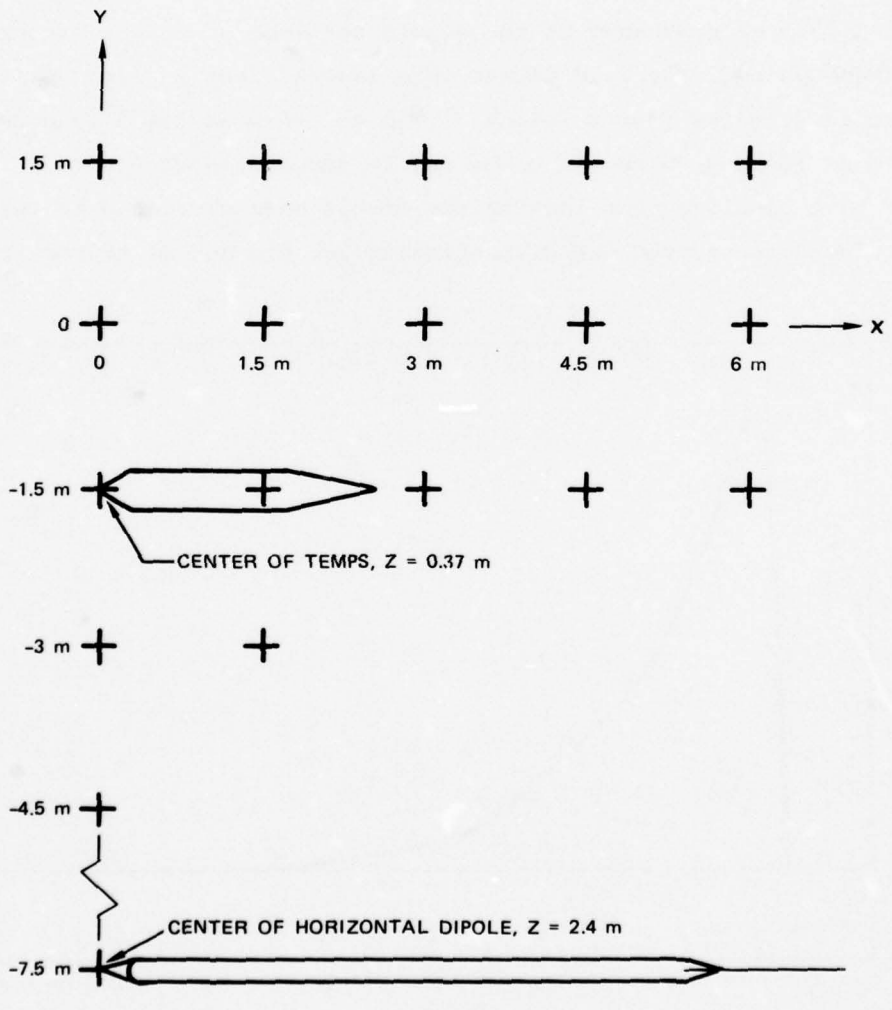

FIGURE 3 MODEL RANGE FIELD-MAPPING LOCATIONS

smaller than they are for the TEMPS location (Figure 2) that differences in coupled penetration currents can be attributed to differences in the TEMPS excitation from a HEMP excitation.

The fields produced by the HEMP model were mapped on the coordinates shown in Figure 3. For horizontal polarization, the Y-component of magnetic field is proportional to the incident horizontal electric field for this elevation angle.[12]

The Y-component of the magnetic field produced at a horizontal range of 7.5 m from the HEMP (dipole) is shown in Figure 4 at five values of X, where X is the horizontal distance measured from an axis drawn from the dipole feed-point perpendicular to the dipole axis. It can be seen from Figure 4 that the fields produced on the ground closely resemble an actual HEMP waveform. The results of the field mapping presented in Figure 4 show that at transverse distances up to 6 m (300-m full scale), the waveform is reasonably like a HEMP. The field strength decreases gradually, and the value at X = 6 m is about 65% of the value at X = 0.

2.3 TEMPS MODEL

A 1/50th scale model of the TEMPS was constructed of aluminum tubing. The many wires that form the TEMPS were replaced by solid conductors, but this had only a small effect on the impedance and field strength.[13] The TEMPS model was fed from a broadband balun with the waveform shown in Figure 2. The Y-component of the magnetic field produced by the TEMPS at the position shown in Figure 3 is shown in the lower half of Figure 4. The waveforms are consistent with full-scale mapping data.[14] The bump in field (X = 0) at about 10 ns is characteristic of the field produced by the current that flows down the terminating cones and is present in the full-scale TEMPS. As can be seen in Figure 4, the field at greater than X = 1.5 m is no longer a typical HEMP waveshape since, for TEMPS, a HEMP threat environment only exists within the bicone angle (±57°).

It should be mentioned that in addition to the field components shown in Figure 4 and the corresponding electric fields, TEMPS also produces a strong vertical electrical field at positions off the Y axis.

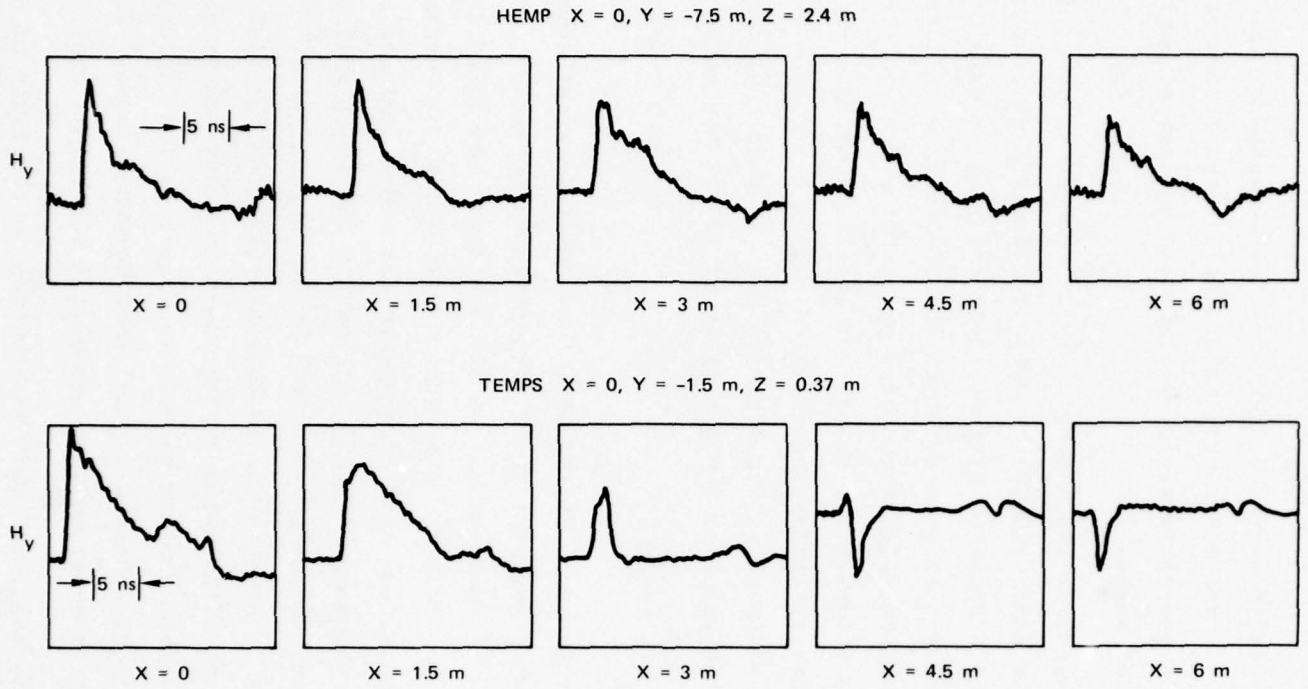

FIGURE 4 FIELD-MAPPING WAVEFORMS ALONG Y = 0

Also, TEMPS was sometimes located at X = 0, Y = -0.6 m and at X = 0.43 m, Y = -0.43 m with *TEMPS* at 45°.

2.4 TEST FACILITY

The modeled test facility and external penetrations are shown in Figure 5. The building was modeled as a solid shield 60 x 90 x 23-cm (30-x-45-x-11.5-m full scale). The brass model was buried 10 cm and was in direct contact with the model range soil (5-m full scale). The modeled penetrations were No. 16 wire soldered to the center of the model faces for above-ground penetrations and to the bottom center of the model for buried penetrations. Penetrations were labeled RIGHT, FAR, LEFT, and NEAR (Figure 5).

The test model shown in Figure 5 was located on the model test range with the RIGHT facility penetration junction at X = 0, Y = 0 (Figure 3). Measurements were made for single penetrations and for multiple penetrations, above and below ground, and for a mixture of above and below ground.

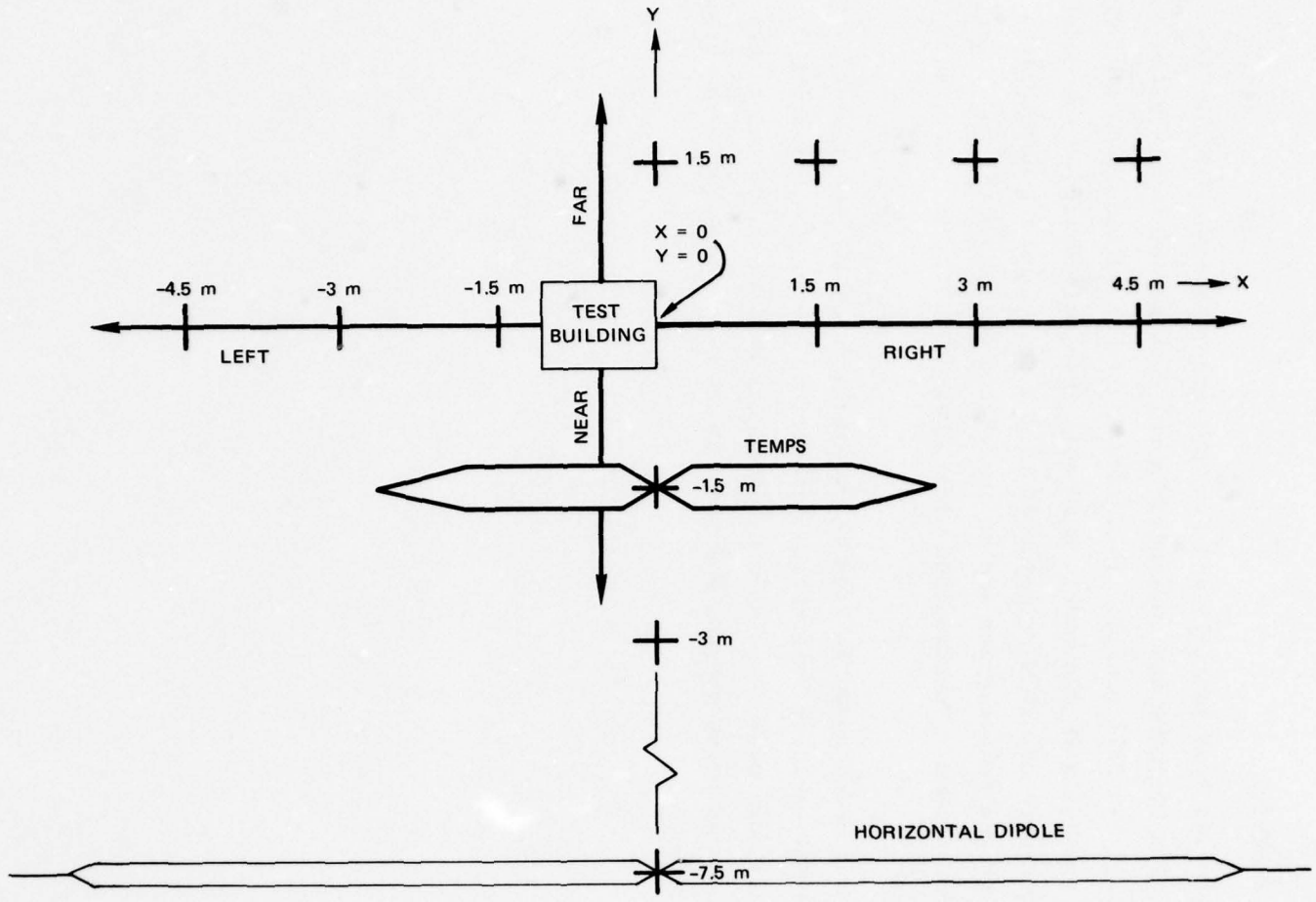

FIGURE 5 MODELED TEST FACILITY

3. MODEL DATA

Measurements were made of the short-circuit current for penetration wires, both above and below ground, for large buildings. The interaction of penetrations for a number of geometries was also determined. For each geometry, the structure was excited with the HEMP at a ground range 7.5 m from the center of the site and at an elevation angle of 21°. In addition, the TEMPS model was used to excite the same structure. Measurements were made with TEMPS 1.5 and 0.6 m from the center of the site, and with the TEMPS axis parallel to the HEMP dipole axis. The TEMPS was moved 0.6 m from the center of the site and rotated for a number of measurements. The latter orientations are typical of the use of TEMPS when it is used to achieve threat-level fields at the center of a site.

The data for the modeled HEMP excitation (dipole at 7.5 m) are, by definition, the expected penetration current waveform. The data for TEMPS excitations were, therefore, compared to the HEMP excitation. The data were taken in a time-domain so that when the waveforms of the coupled currents from the two excitations were similar, a comparison of peak field and decay time provided a fair characterization of the difference between a HEMP and a TEMPS excitation. In other cases, the waveforms were quite dissimilar. In these cases, the Fourier-transformed signals were compared in the frequency domain (always labeled as full-scale frequency).

3.1 ABOVEGROUND PENETRATIONS

3.1.1 Data

For the aboveground penetrations, a 7.5-m No. 20 wire 7.5 cm (3.75-m full scale) above ground was the RIGHT penetration. The FAR penetration was a 30-cm (15-m full scale) high-wire tower 7.5 cm (3.75-m full scale) from the building. A single waveguide, modeled as a No. 12

wire, was attached to the tower top and building. The tower legs were grounded with wire ground rods 10 cm in length and 0.38 cm in diameter.

The LEFT aboveground penetration was a No. 20 wire, 3 m in length, and 7.5 cm (3.75-m full scale) above ground. The NEAR penetration was identical to the LEFT penetration, and extended under TEMPS.

Figure 6 shows the short-circuit current* (solid line) measured on the RIGHT aboveground penetration, which was parallel to the HEMP dipole axis. For the first 23 ns (scale-model time), the measured waveform is similar to the driving waveforms shown in Figure 4, except for the

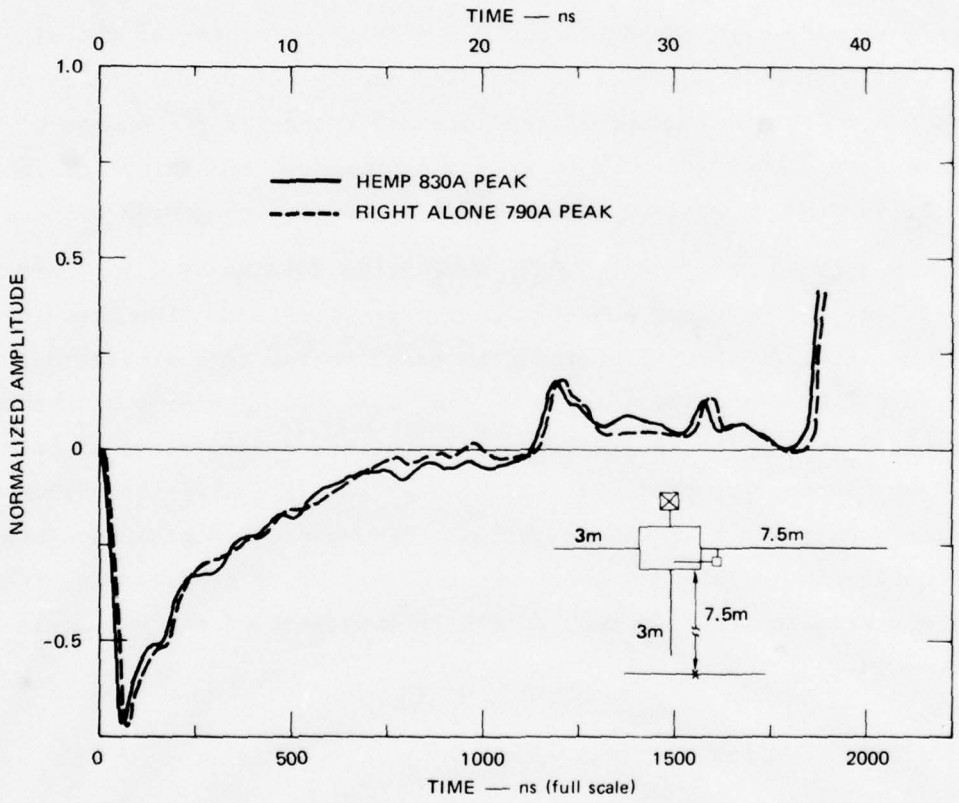

FIGURE 6 HEMP EXCITATION FOR A RIGHT ABOVEGROUND WIRE

*Current waveforms are normalized to 50,000 V/m for HEMP and for TEMPS at 50-m (1-m scale model) full scale. The waveform short-circuit magnitude is given for the first peak in amperes (full scale).

generally constant level of the data for times between 15 and 23 ns. The large discontinuity at 37 ns was caused by the open-circuit on the 7.5-m wire. Thus, the easily usable portion of this waveform was the first 37 ns. Using the entire waveform produces some frequency distortion. Figure 6 also shows the RIGHT aboveground penetration current waveform (dashed line) with the other three aboveground penetrations removed. The similarity between the two waveforms can be clearly seen.

The upper half of Figure 7 shows the RIGHT aboveground penetration waveform when excited by the TEMPS at a range of 1.5 m and the HEMP waveform from Figure 6. The gross waveform is similar to the HEMP excitation--a sharp rise and a slow decay--but it is clearly different in detail. The early time peak level for these waveforms is similar (within 20%). The transforms of the TEMPS and HEMP spectra are compared in the lower half of Figure 7.* A comparison of the spectra in Figure 7 shows some distinct differences between 1- and 10-MHz full scale in addition to the two-to-one excitation level of TEMPS and HEMP.

Figures 8 and 9 show the effects of bringing TEMPS into a range of 0.6 m (30-m full scale). Figure 8 shows the RIGHT aboveground wire current waveform and spectra for TEMPS at 0.6 m parallel to the wire. Figure 9 shows the same data for TEMPS at 0.6 m at 45°. The current waveform in Figure 8 is similar to the waveform for HEMP excitation--sharp rise and slow decay--except for the waveform crossover at 16 ns and the late time overshoot.

Sometimes the TEMPS is located as shown in Figure 9, when the primary concern is achieving threat-level excitation. The time-domain waveform for the angled TEMPS location is changed at its leading edge and in its relatively rapid decay and crossover at 7 ns, compared with the waveforms produced by a TEMPS parallel to the RIGHT aboveground

---

*Spectra are normalized to 50,000-V/m full scale at X = 0, Y = 0. Spectra are presented adjusted to the same full-scale value, which is listed for each spectrum.

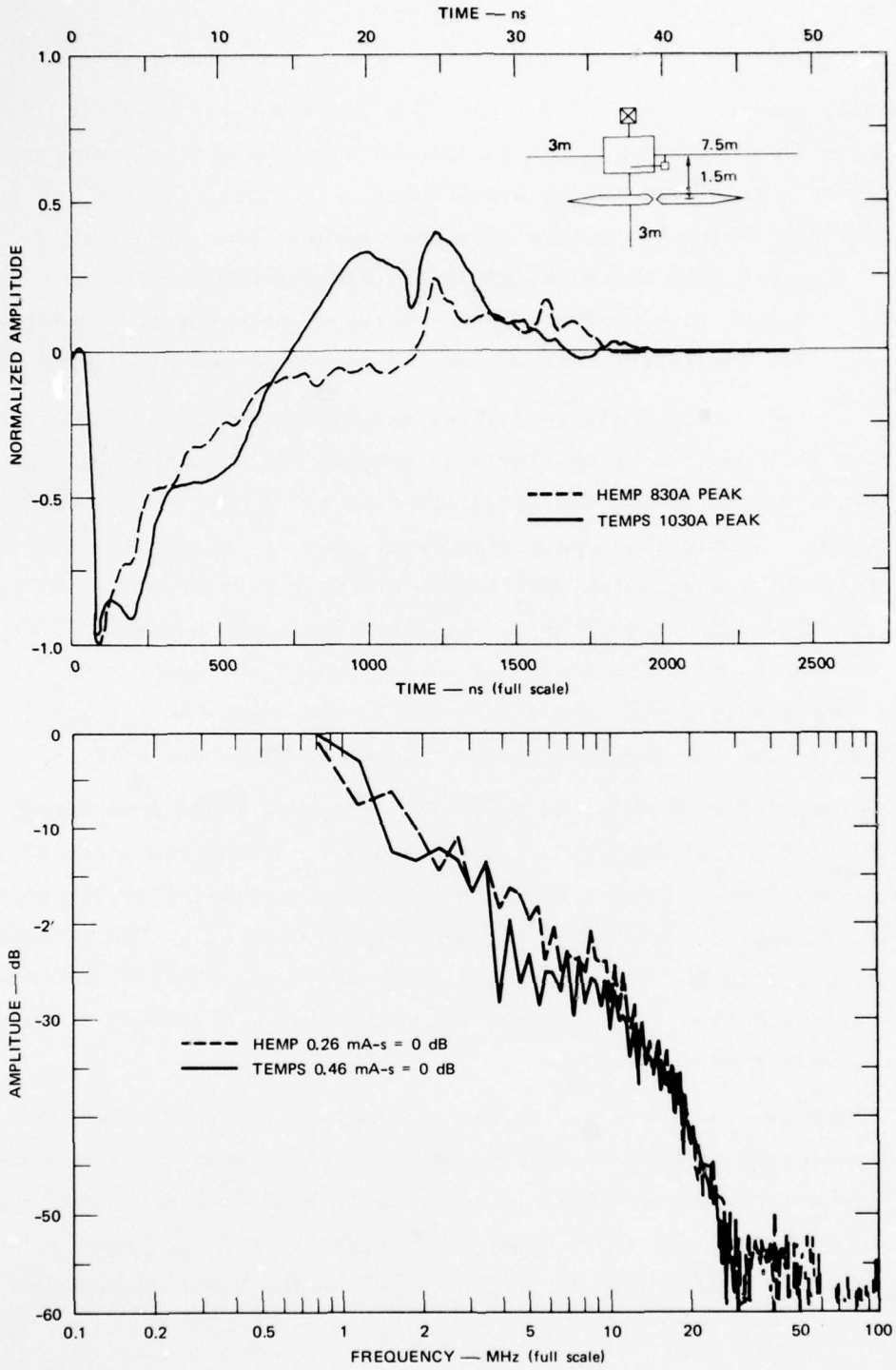

FIGURE 7 TEMPS AT 1.5 m (75-m full scale) AND HEMP EXCITATIONS ON THE RIGHT ABOVEGROUND WIRE

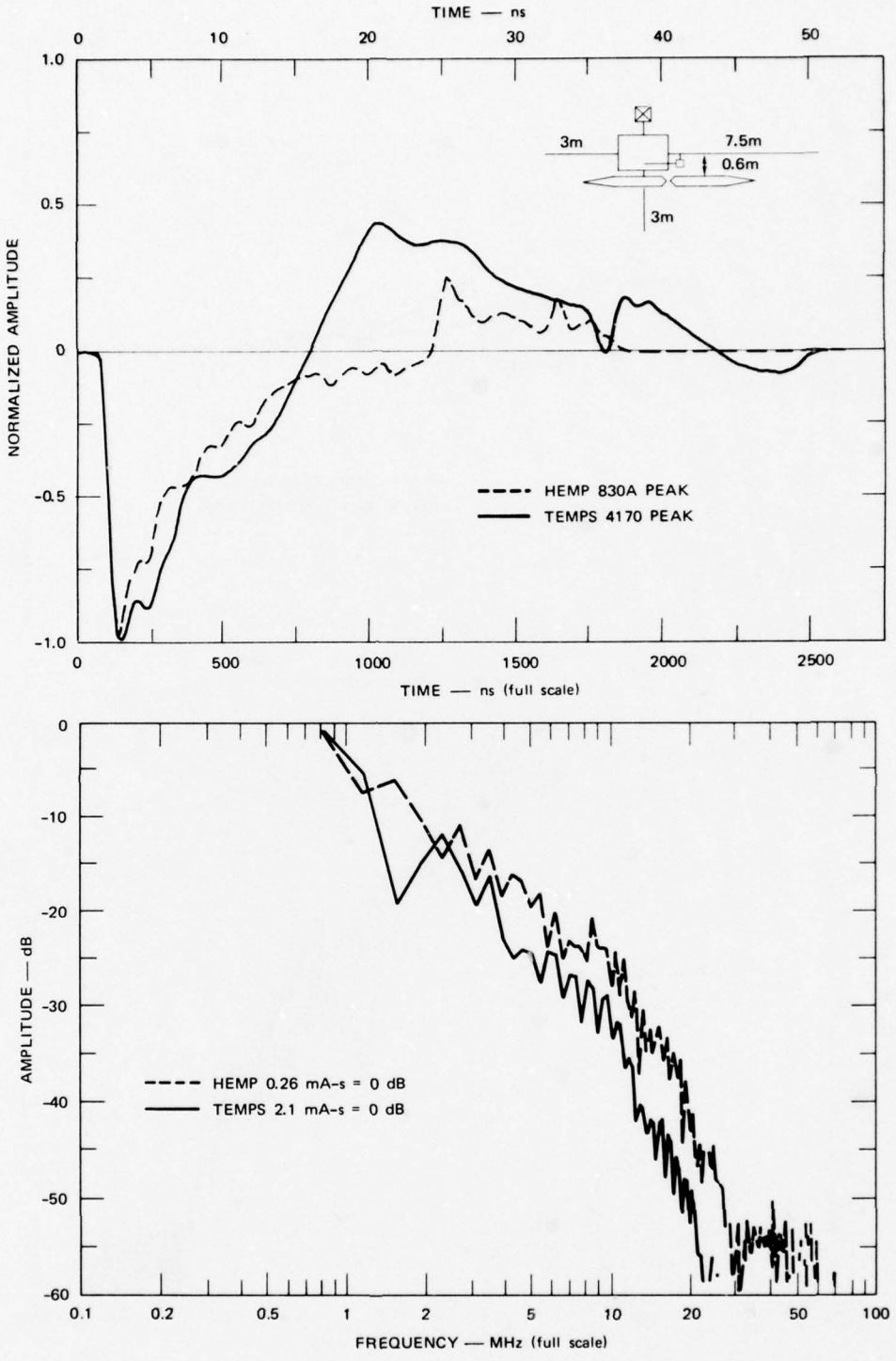

FIGURE 8 TEMPS AT 0.6 m (30-m full scale) AND HEMP EXCITATIONS ON THE RIGHT ABOVEGROUND WIRE

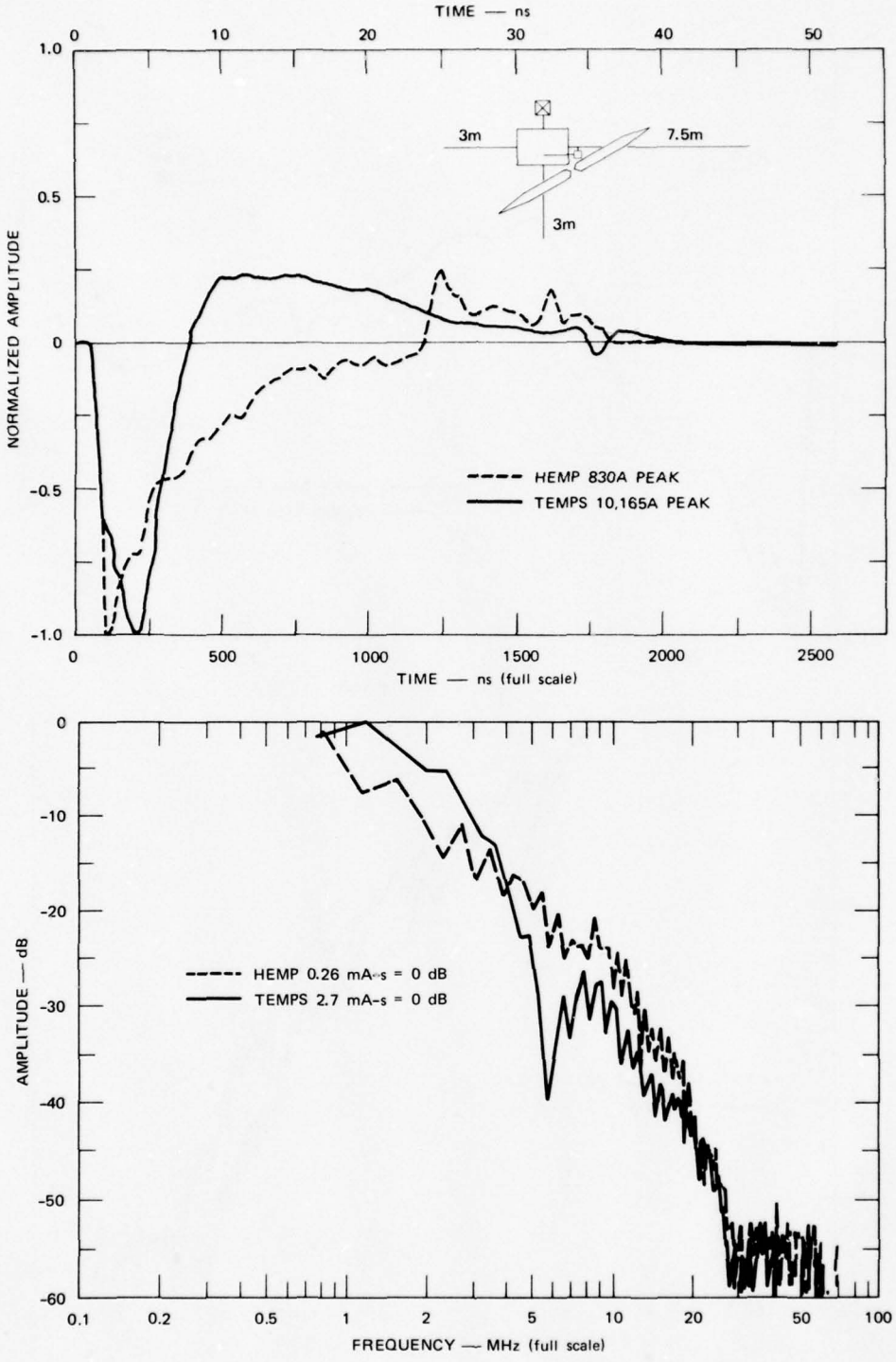

FIGURE 9 TEMPS AT 0.6 m (30-m full scale) AT 45° AND HEMP EXCITATIONS ON THE RIGHT ABOVEGROUND WIRE

wire (Figures 7 and 8). The resultant peak current has been increased by a factor of about 2.5.

The spectrum shape for TEMPS at 0.6 m and parallel to the RIGHT wire (Figure 8) is within ±4 dB of the HEMP excitation. The TEMPS excitation below 3 or 4 MHz is about an order of magnitude (18 dB) greater than HEMP and is at least 10 dB greater at all higher frequencies.

The spectrum shape for angled TEMPS (Figure 9) is greater than HEMP for frequencies below 4 MHz, and smaller than HEMP for frequencies between 4 and 20 MHz. Again, the TEMPS excitation is 15 dB greater than HEMP from 4 to 20 MHz, and at least 20 dB greater at all other frequencies.

The current waveform for HEMP excitation of a 3-m LEFT aboveground wire is shown in Figure 10 (solid line). The large reversal of current at about 12 ns after the peak current, and again at 33 ns, is caused by current excited on the wire, which hits the open circuit at the end and arrives at the current sensor after traveling the length of the wire. Until current reversal, the waveform for the LEFT aboveground wire is nearly identical to the RIGHT aboveground wire (Figure 6). This demonstrates what was predicted theoretically--that the early time peak depends only upon the wire configuration as a function of the dimensions of the order of the wire height. The wire length affects the late-time response.

The current waveform for the LEFT wire alone (other three penetrations removed) is shown (dashed line) in Figure 10.* The other penetrations have little effect, as was observed for the RIGHT wire (Figure 6).

---

*The LEFT wire alone shown in Figure 10 is from an early measurement on a slightly different sized building and wire, as is evident from the reflection at 11 ns.

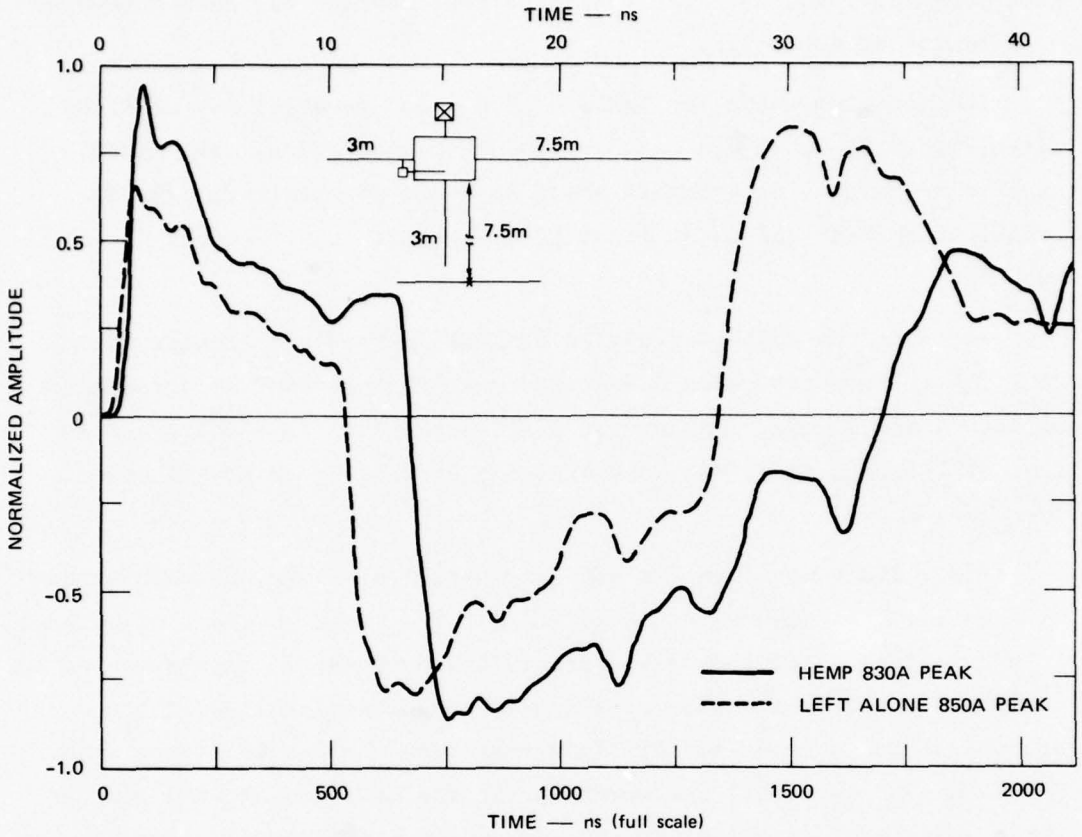

FIGURE 10 HEMP EXCITATIONS ON THE LEFT ABOVEGROUND WIRE

The current waveform for a 3-m long LEFT wire excited by TEMPS 1.5 m from the site is shown (solid line) in Figure 11. The waveform shows a sharp reversal about 17 ns after the initial peak time. This is again caused by the open circuit at the end of the LEFT wire. The time at which the reversal occurs has increased compared with the HEMP (dashed line, Figure 11) because of the differential propagation time from the TEMPS feedpoint to the current-sensor and to the end of the line.

The early time peak for TEMPS is about 3 dB less than the HEMP excitation. This peak is also 4 dB less than the peak from the RIGHT aboveground wire for HEMP (Figure 6). This small initial peak was probably caused by the building partially blocking the excitation of

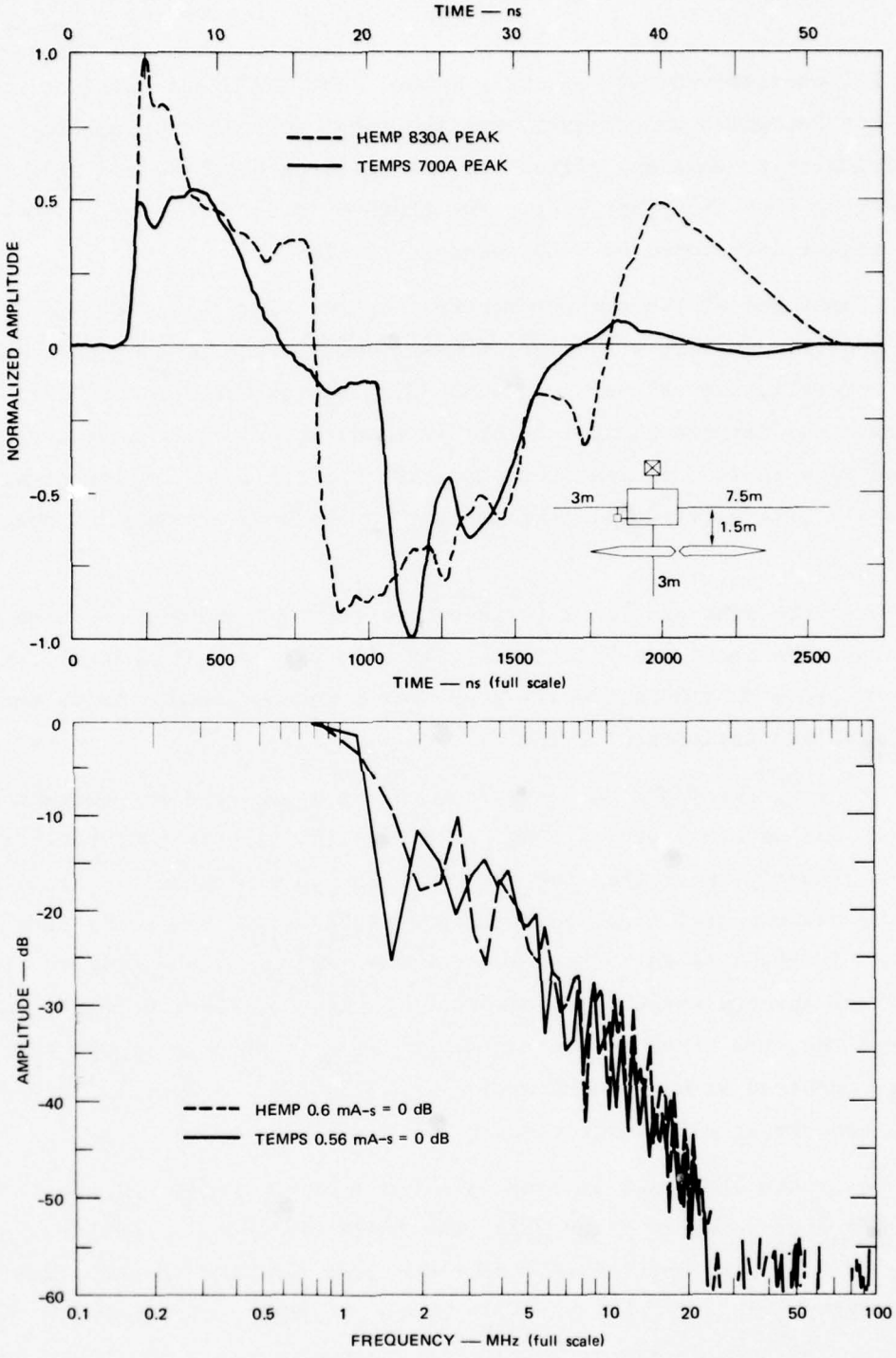

FIGURE 11 TEMPS AT 1.5 m (75-m full scale) AND HEMP EXCITATIONS ON THE LEFT ABOVEGROUND WIRE

the LEFT aboveground wire at early times. The TEMPS was centered so that its feedpoint was aligned with the right edge of the building specifically to show any effects of the building blocking one side in comparison with the other side. For TEMPS at 1.5 m, the early time-peak signal is reduced by 6 dB compared to HEMP.

Comparison of the current spectra for the TEMPS excitation of the LEFT aboveground wire with RIGHT aboveground wire current spectra shows that, overall, they compare within 5 dB. The spectra for the RIGHT aboveground wire are about 5 dB higher than those for the LEFT aboveground wire at frequencies over about 10 MHz. This is consistent with the early time building-blockage effect on the LEFT aboveground penetration.

When the HEMP and TEMPS currents for the LEFT aboveground wire are compared, the spectra substantially agree in the mean (Figure 11), with only minor ±5 dB fluctuations, except for a hole of about -15 dB for the TEMPS excitation at 1.5 MHz.

Bringing the TEMPS to 0.6 m from the site produced the current spectra and waveform (solid line) of Figure 12. The current reversal occurs slightly later than for the TEMPS at 1.5 m because of the slightly greater differential time, as explained previously. The early time-peak current is about 14 dB higher than for the TEMPS at 1.5 m (Figure 11). The TEMPS spectra shape is comparable with that of HEMP; however, below about 3 MHz, the TEMPS at 0.6 m produces about 5 dB more signal than HEMP. Compared with the HEMP excitation, the TEMPS spectrum is about 12 dB greater at all frequencies.

Next, the TEMPS was located at 0.6 m from the center of the site, but angled as shown in Figure 13. The TEMPS time-domain waveform (solid line) at 0.6 m was considerably narrower than the HEMP (dashed line); the TEMPS peak current was slightly below the HEMP peak current. These effects are shown in Figure 13, in the frequency domain in which the frequencies above 20 MHz are greater than the HEMP values.

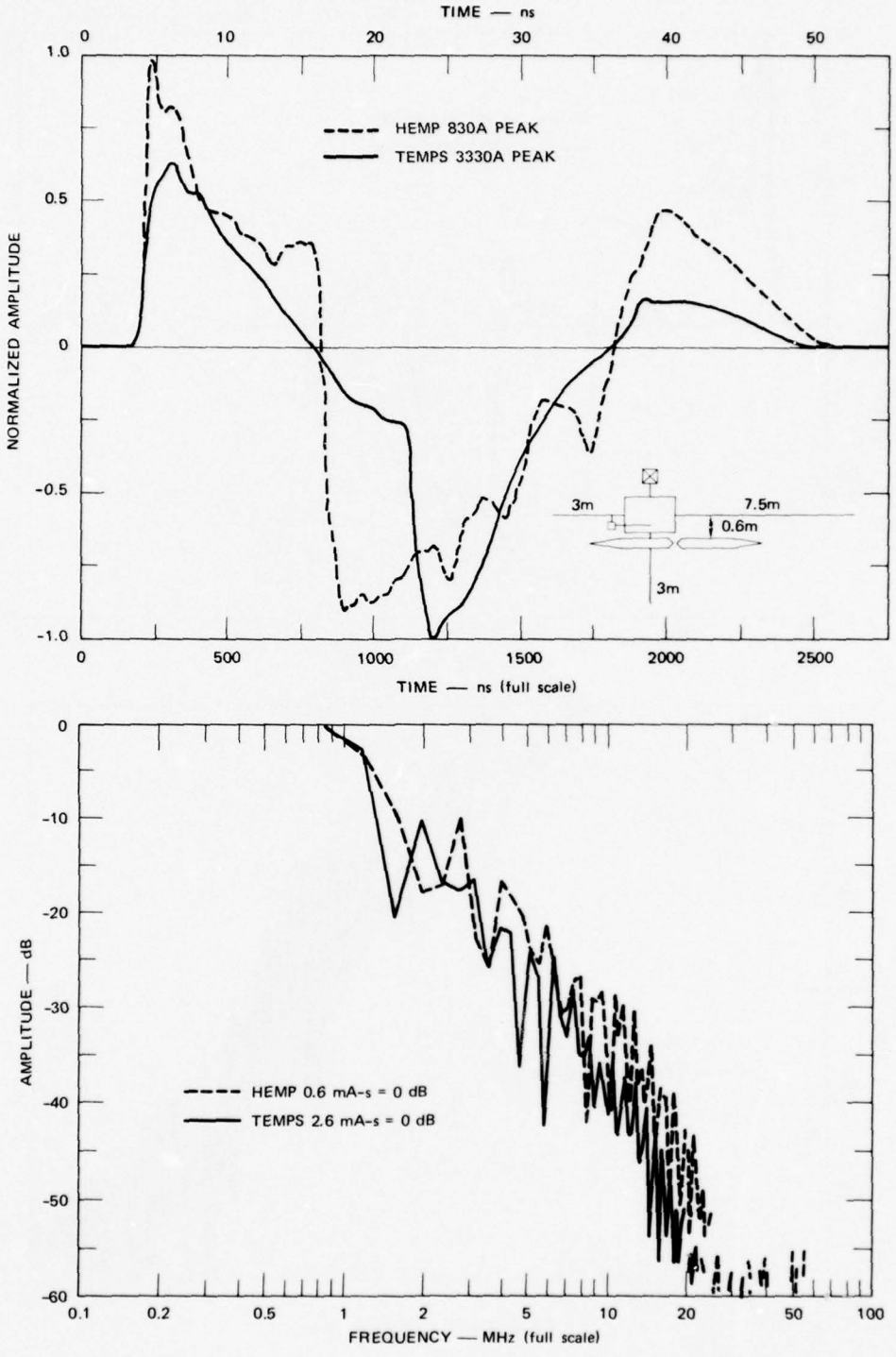

FIGURE 12 TEMPS AT 0.6 m (30-m full scale) AND HEMP EXCITATIONS ON THE LEFT ABOVEGROUND WIRE

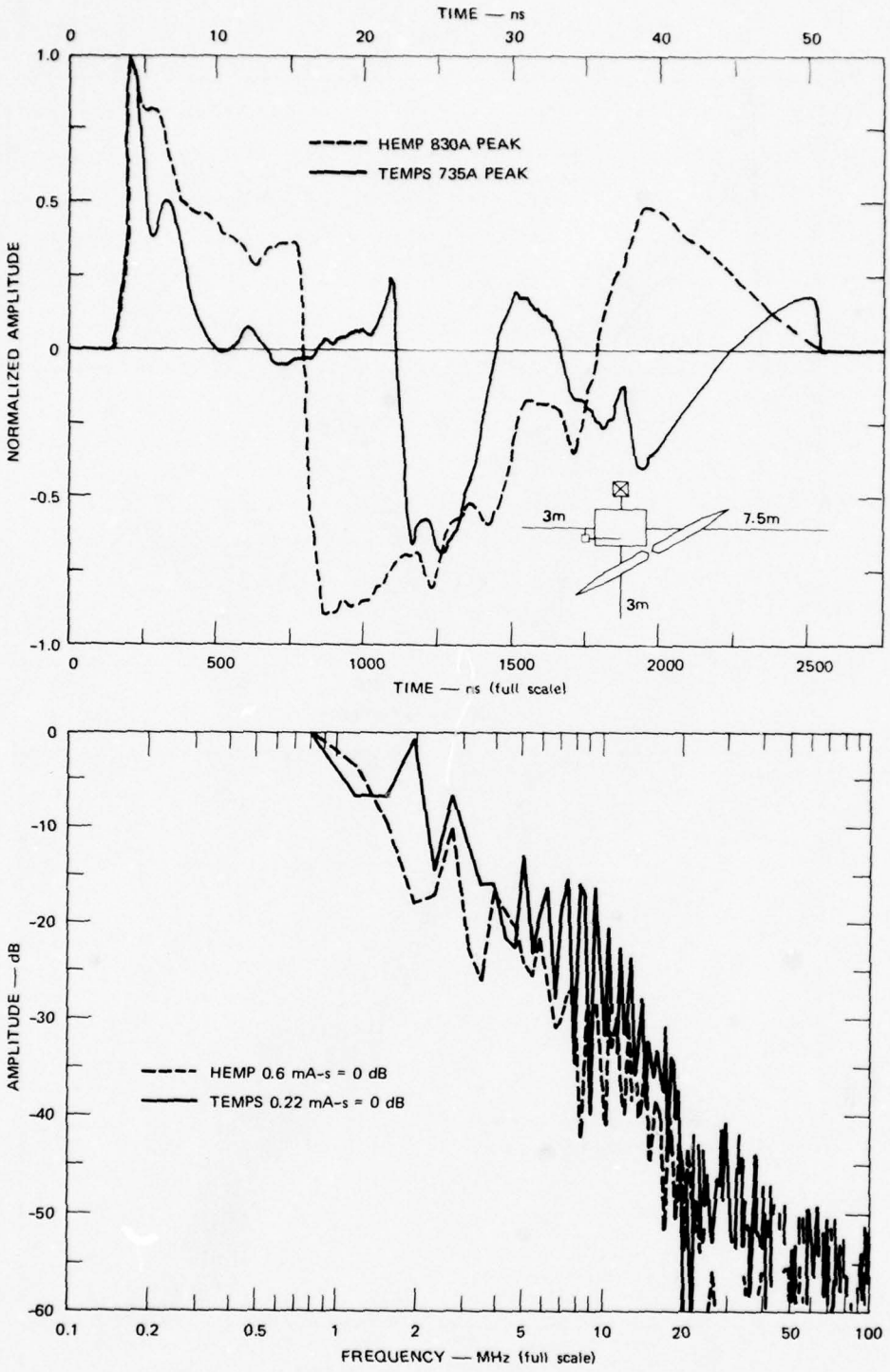

FIGURE 13 TEMPS AT 0.6 m (30-m full scale) AT 45° AND HEMP EXCITATIONS ON THE LEFT ABOVEGROUND WIRE

Comparing the response of the RIGHT aboveground wire (Figure 9) with the LEFT aboveground wire (Figure 13) for this configuration of TEMPS, reveals a difference in peak current of about 25 dB. The RIGHT aboveground wire is much more strongly excited. This is to be expected because the TEMPS straddles the RIGHT wire while the building shields the LEFT wire. Thus, bringing the TEMPS in close to achieve strong excitation of the site may be effective for only some penetrations because of the shielding of objects by parts of the facility being tested.

As a final example of the excitation of aboveground penetrations attached to large buildings the HEMPS and TEMPS response on the NEAR aboveground wire was compared (Figure 14). The NEAR aboveground wire crossed the polarization of the HEMP so that one would expect the

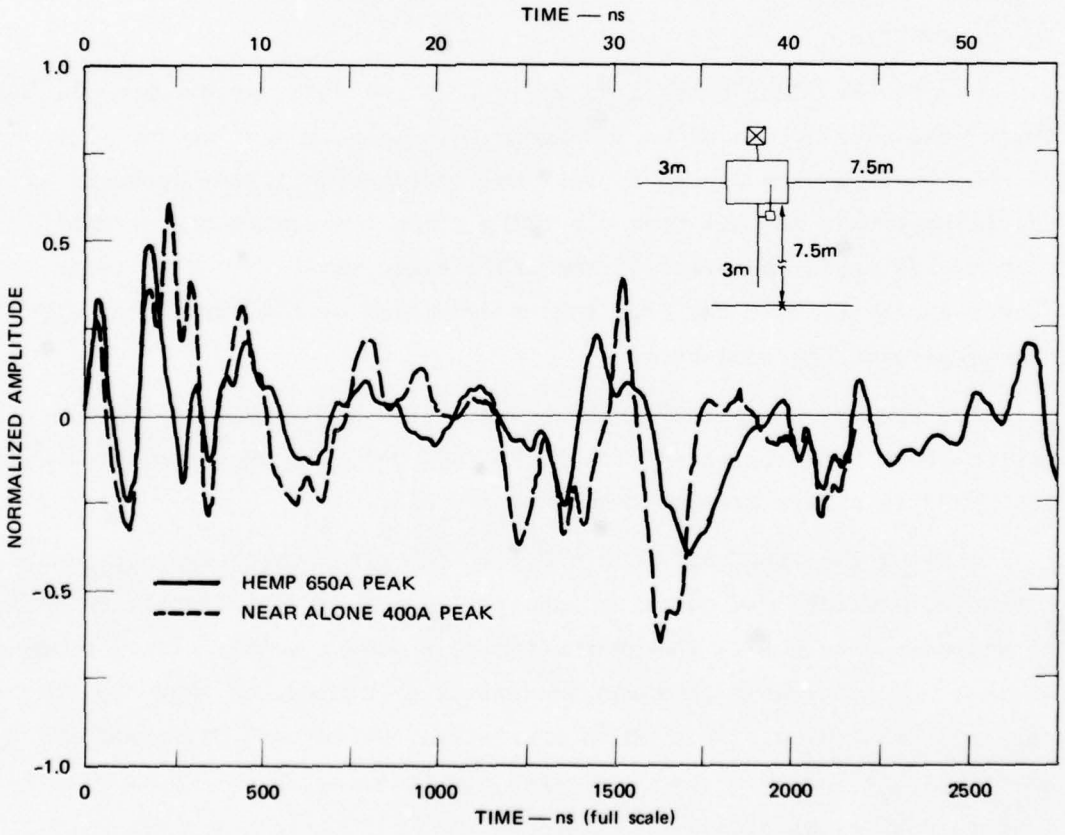

FIGURE 14 HEMP EXCITATIONS ON THE NEAR ABOVEGROUND WIRE

response to be weak. Indeed, the waveform was weak and considerably different from that of conductors parallel to the HEMP polarization (Figures 6 and 10). The peak time-domain response for the NEAR wire was reduced by 6 dB.

The TEMPS excitation for a distance of 1.5 m is shown in Figure 15. The TEMPS waveform (solid line) differs from the HEMP waveform (dashed line) and is much stronger (26 dB above the HEMP peak). The spectra shapes shown in Figure 15 are vastly different. HEMP produces more coupling by about 18 dB for frequencies above 2 MHz; this difference for frequencies above 2 MHz is less than the difference in spectra magnitude, which is a +30 dB.

Once again, the TEMPS straddles the NEAR aboveground wire and produces very high currents. Furthermore, the TEMPS vertically-polarized components produce fields that couple to the NEAR aboveground wire in this geometry.

Moving the TEMPS closer, to 0.6 m from the site, produces a slightly lower peak current, as shown in Figure 16. This is what would be expected if the coupling were caused by the interaction with fields produced by the current that travels down the TEMPS along its length rather than with fields produced normal to the TEMPS axis, which vary with range. Thus, we propose that the coupling is dominated by the portion of TEMPS that straddles the conductor.

The spectra shown in Figure 16 again show a decrease in TEMPS excitation above 5 MHz compared with HEMP. However, the spectrum magnitude for TEMPS is always greater than that for HEMP.

Angling the TEMPS 45° at 0.6 m from the site center again produces a changed waveform and different spectral shape from the parallel TEMPS as shown in Figure 17. The excitation is a wider, nearly cyclic waveform with an obviously enhanced low-frequency content as shown by the peak spectrum value. This TEMPS excitation, while very different in waveshape and spectrum shape, excites all frequencies at levels equivalent to HEMP excitation.

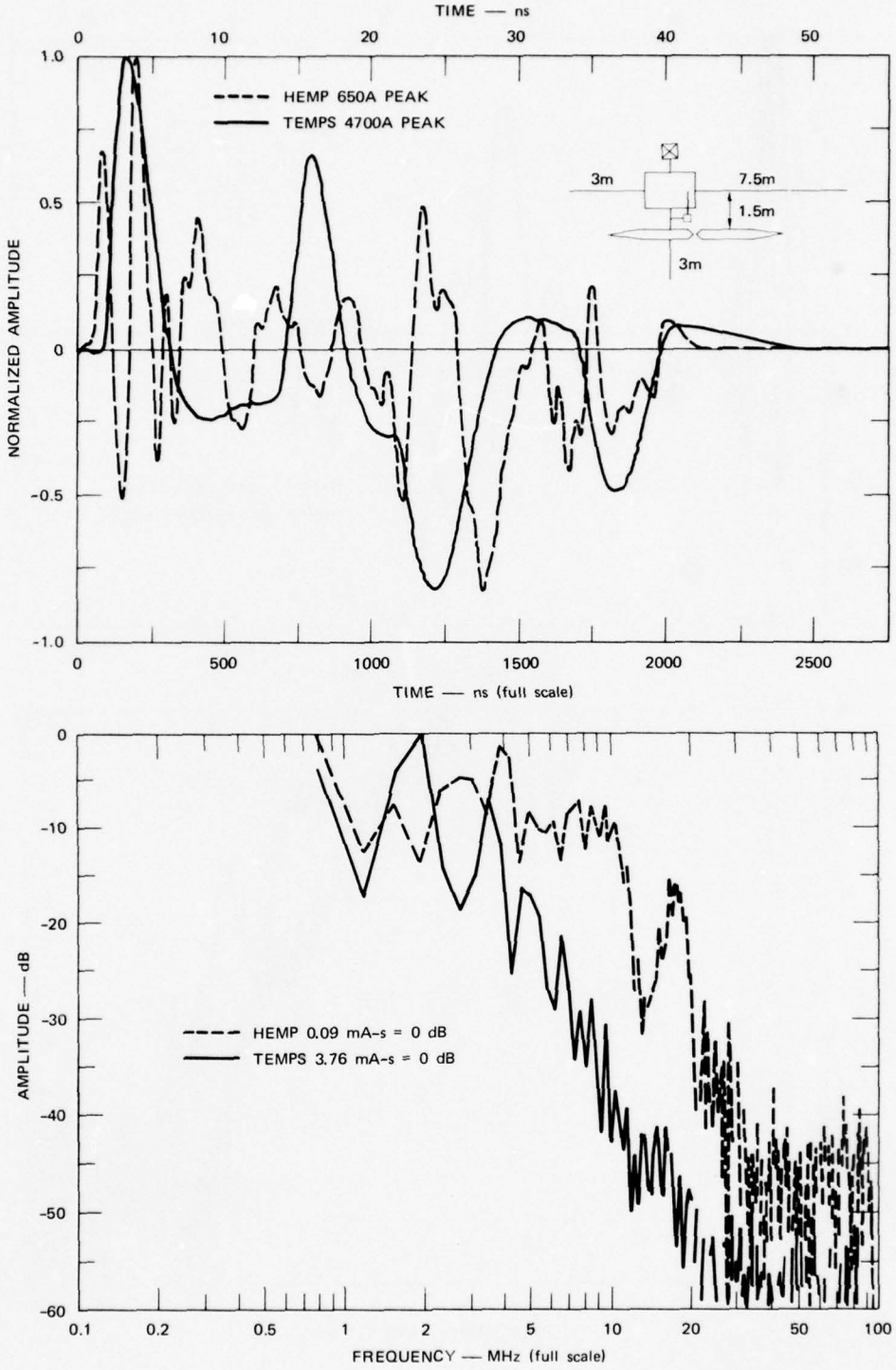

FIGURE 15 TEMPS AT 1.5 m (75-m full scale) AND HEMP EXCITATIONS ON THE NEAR ABOVEGROUND WIRE

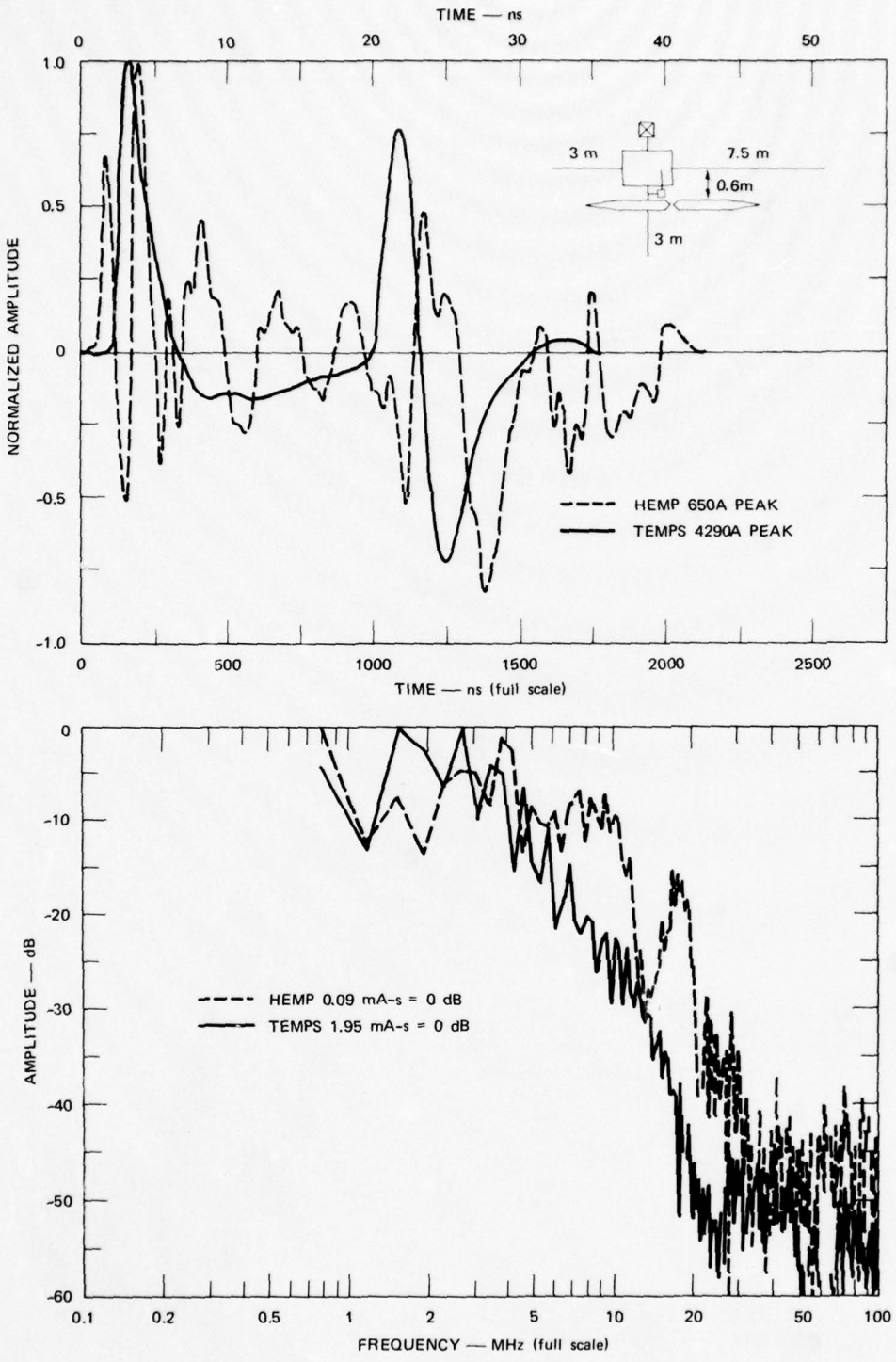

FIGURE 16 TEMPS AT 0.6 m (30-m full scale) AND HEMP EXCITATIONS ON THE NEAR ABOVEGROUND WIRE

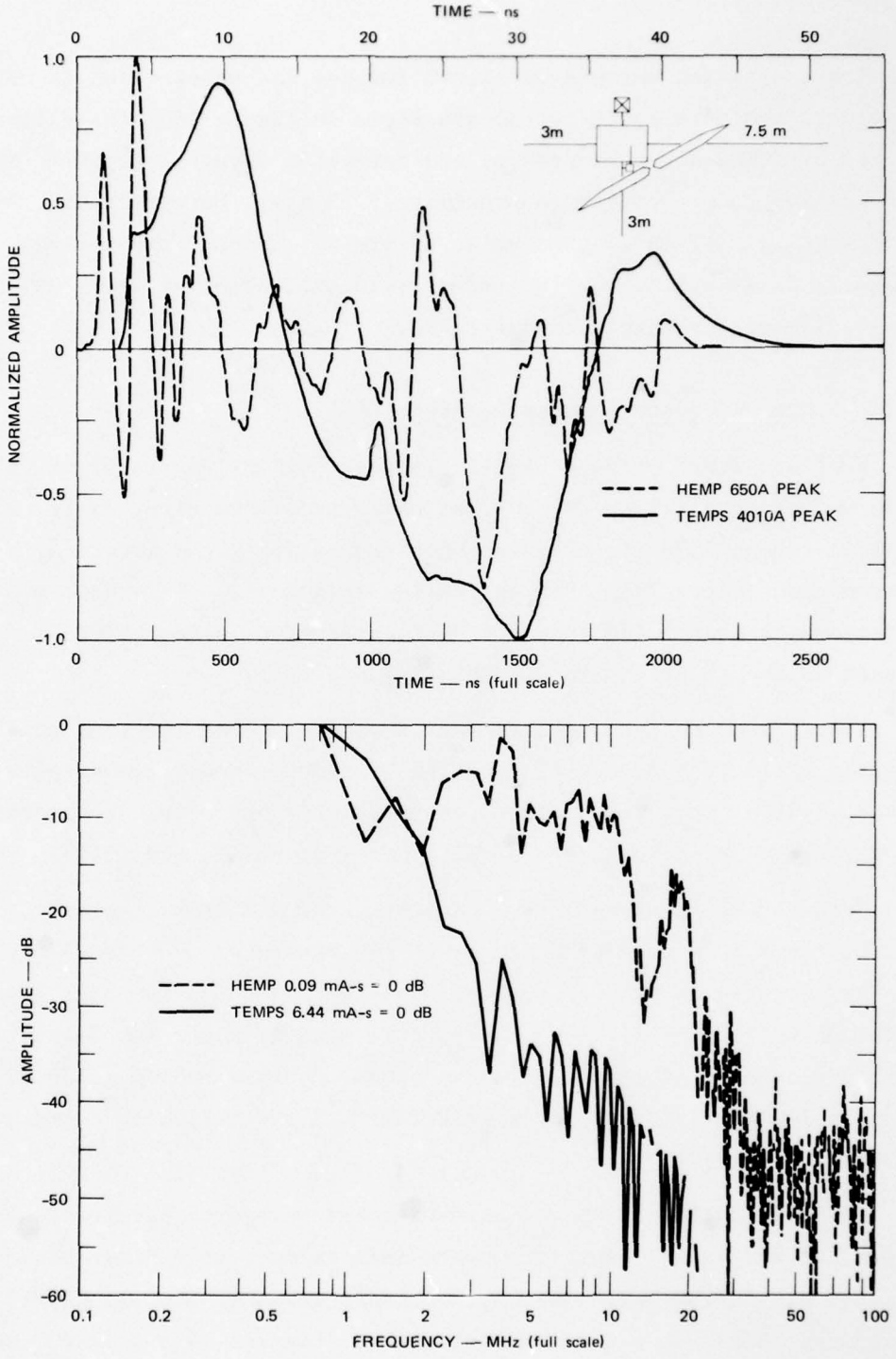

FIGURE 17 TEMPS AT 0.6 m (30-m full scale) AT 45° AND HEMP EXCITATIONS ON THE NEAR ABOVEGROUND WIRE

The excitation current waveforms for the FAR penetration (a waveguide attached to a radio tower) are shown in Figure 18. The excitations created by TEMPS are dominated by its late-time vertical electric field, which causes tower ringing (approximately 12 ns). For TEMPS at 1.5 and 0.6 m, the initial excitation pulse is similar to HEMP excitation. For angled TEMPS at 0.6 m, the late-time field excitation of the RIGHT aboveground wire distorts the initial pulse.

3.1.2 Summary for Aboveground Penetrations

HEMP and TEMPS produce similar coupled current waveforms for aboveground wires parallel to the excitation source (Figures 7, 8, 11, 12, and 13). When TEMPS straddles an aboveground wire, the waveform is altered and differs from HEMP excitation (Figure 9). This waveform difference is most evident on the NEAR aboveground wire, which is crossed to the polarization of HEMP (Figures 15-17).

The spectra shapes for HEMP and TEMPS excitation are also similar when the excitation source is parallel to aboveground wires (Figures 7, 8, and 11-13). When TEMPS straddles an aboveground wire, the spectra are different, being enhanced below 5 MHz (Figures 9, and 15-17).

When the TEMPS straddles a conductor, the difference between the peak currents from the TEMPS and HEMPS can become as much as 15 to 25 dB; the larger differences are produced when the conductor is cross-polarized to the HEMP (Figures 15-17). The spectra magnitude for TEMPS excitation of aboveground wires equals or exceeds HEMP excitation (up to 30 dB at lower frequencies) except for angled TEMPS on the LEFT wire between 2 and 6 MHz (Figure 13).

HEMP excitation of aboveground wire and waveguide penetrations has shown that individual excitations are independent, to a first order (Figures 6, 10, and 14). The way one penetration (e.g., the RIGHT) is excited by TEMPS can alter the excitations (Figures 13 and 17) of other penetrations. Figure 19 shows the major component of surface current on the building for different excitation conditions. The waveform is not affected by the presence of additional penetrations, nor by a different

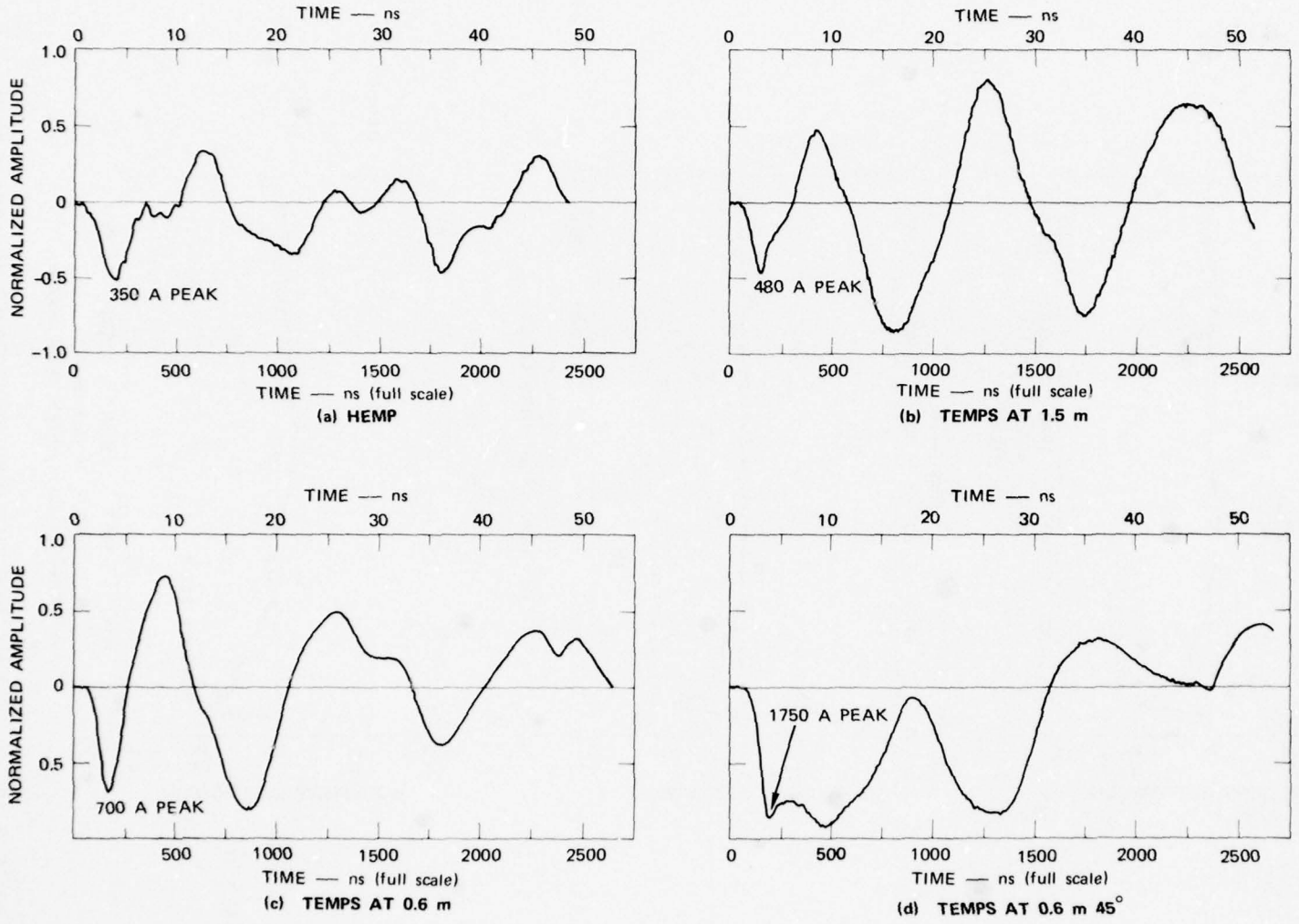

FIGURE 18 EXCITATION ON THE FAR TOWER WAVEGUIDE (for the aboveground wires)

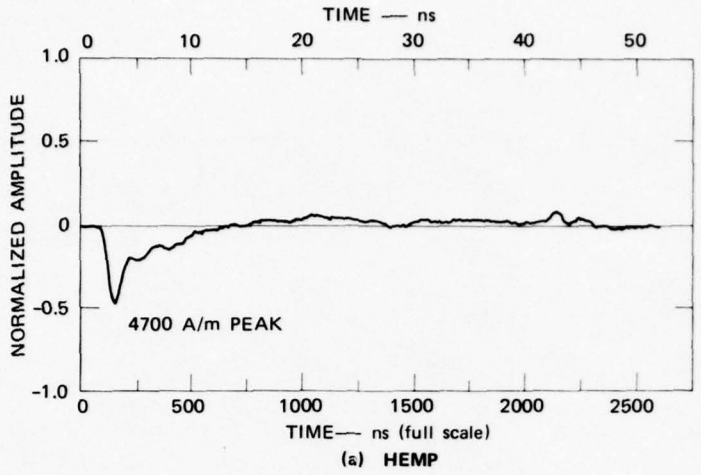

(a) HEMP

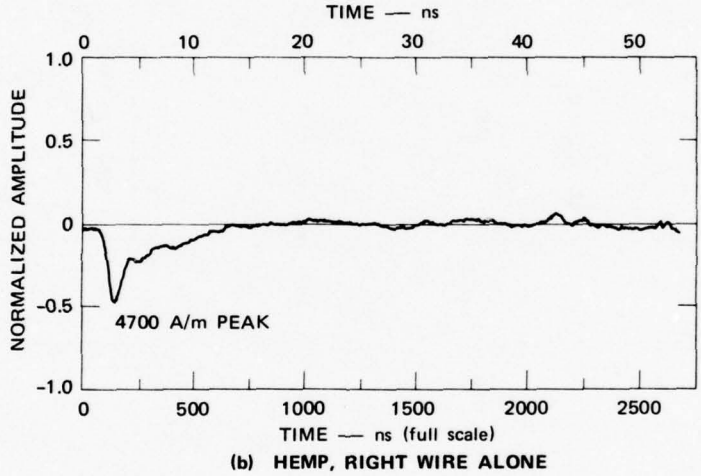

(b) HEMP, RIGHT WIRE ALONE

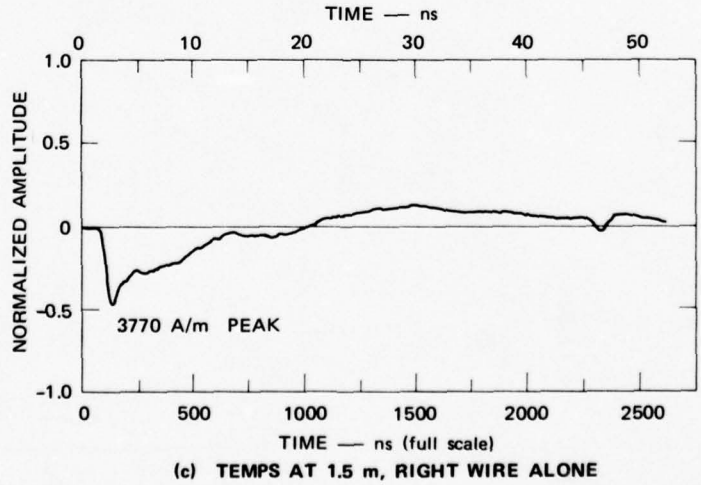

(c) TEMPS AT 1.5 m, RIGHT WIRE ALONE

FIGURE 19 HEMP AND TEMPS BUILDING EXCITATIONS *(aboveground wires)*

excitation source. However, the effects of the late-time TEMPS fields can be seen in Figure 19(c).

The effects of the position of TEMPS on building excitation is shown in Figure 20. The manner in which individual penetrations are excited does not appear to affect the building excitation. However, the distance of TEMPS from the building does show an effect in the initial pulse peak and width.

Excitation of aboveground wires can be easily predicted. Figure 21 shows the predicted and measured HEMP excitation of the RIGHT aboveground wire. The prediction given in Appendix D is highly accurate when one considers the simplifying assumptions used to make the prediction.

3.2 BURIED WIRES

3.2.1 Coupling to Buried Wires

In addition to excitation of aboveground wires, measurements were made of the coupling to buried conductors from a HEMP and a TEMPS placed in different positions relative to the conductor.

Once again, the HEMP was modeled by a long dipole about 7.5 m (375-m full scale) away from the buried wire. For this series of measurements, the RIGHT and NEAR conductors were buried 25 mm (Figure 5). The 7.5-m (375-m full scale) RIGHT aboveground penetration and the 3-m (150-m full scale) NEAR aboveground penetration were replaced by conductors buried 25 mm (1.25-m full scale) below the surface of the earth.

The waveform and spectrum of the RIGHT buried wire current are shown in Figure 22 for HEMP excitation. The risetime is slow compared with the HEMP incident risetime (Figures 2 and 4). The spectrum shows a decrease of amplitude of approximately f^{-2}. Because the field incident on buried waves decreases approximately as f^{-1}, the transfer coefficient must also be approximately f^{-1}.

The current waveform and spectrum for the RIGHT buried wire for TEMPS at 1.5 m (75-m full scale) from the building and parallel to the buried conductor are shown in Figure 23. The TEMPS waveform is similar

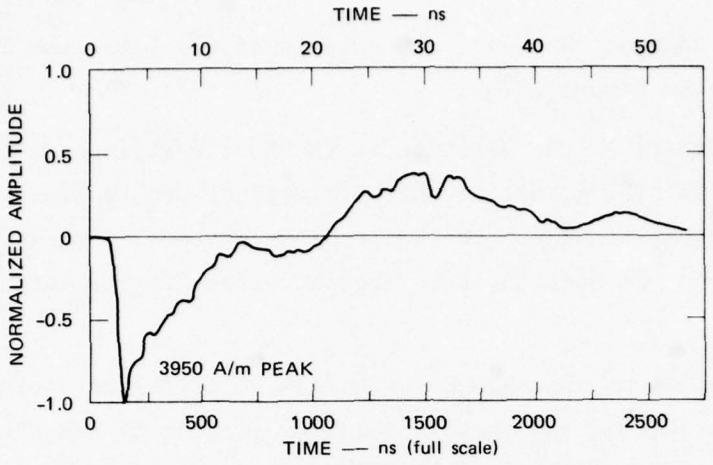

(a) **TEMPS AT 1.5 m**

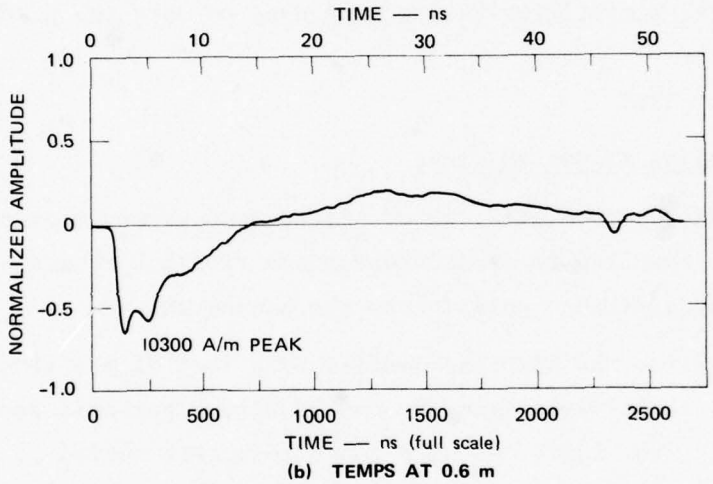

(b) **TEMPS AT 0.6 m**

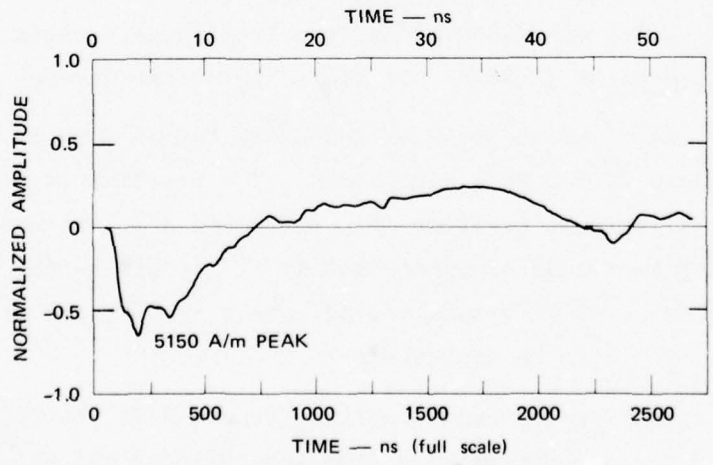

(c) **TEMPS AT 0.6 m, 45° ANGLE**

FIGURE 20 THE EFFECTS OF TEMPS POSITION ON BUILDING EXCITATION

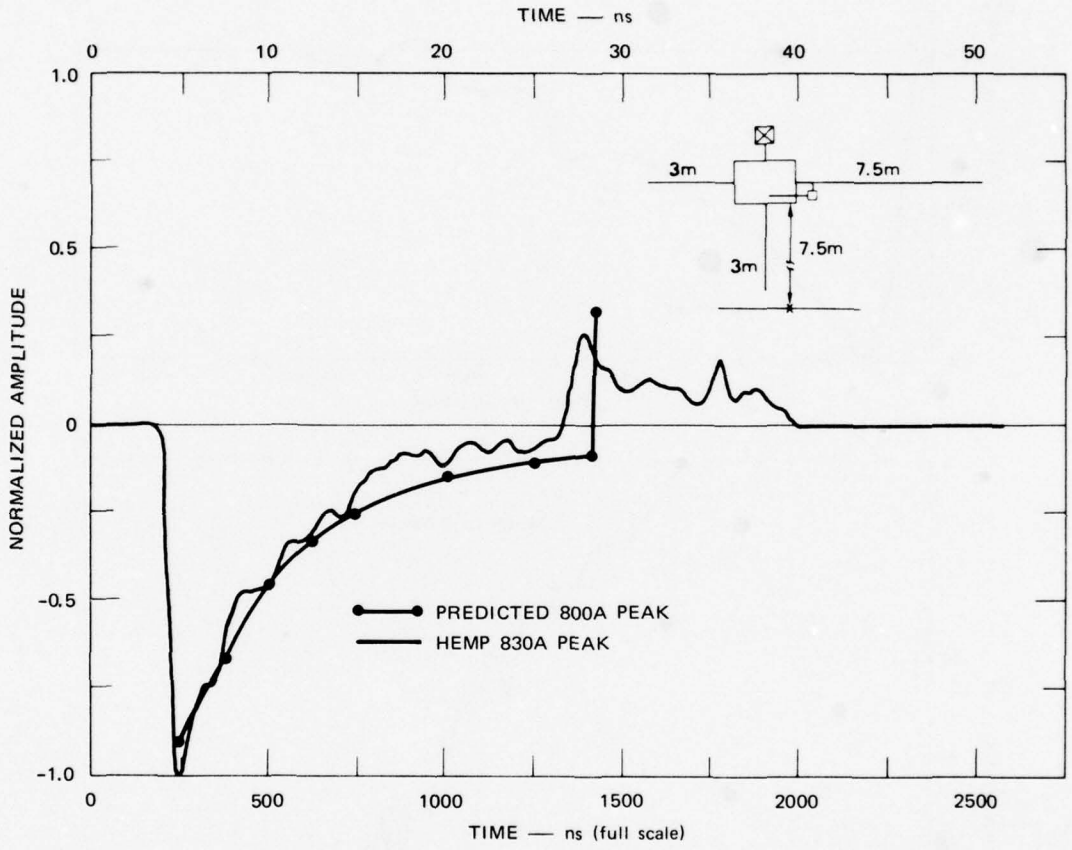

FIGURE 21 PREDICTED AND MEASURED RIGHT ABOVEGROUND WIRE FOR HEMP EXCITATION

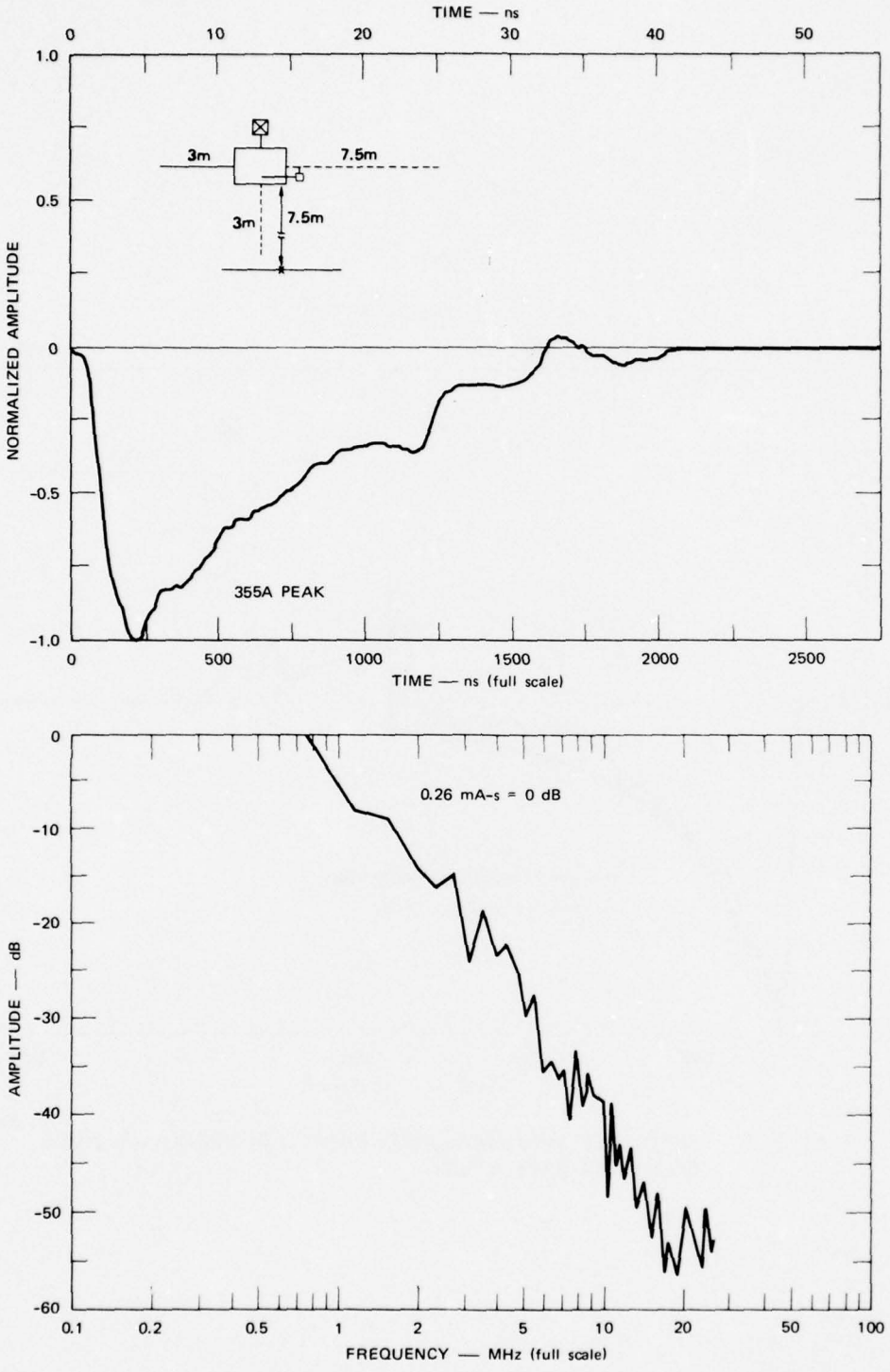

FIGURE 22 HEMP EXCITATION ON THE RIGHT BURIED WIRE

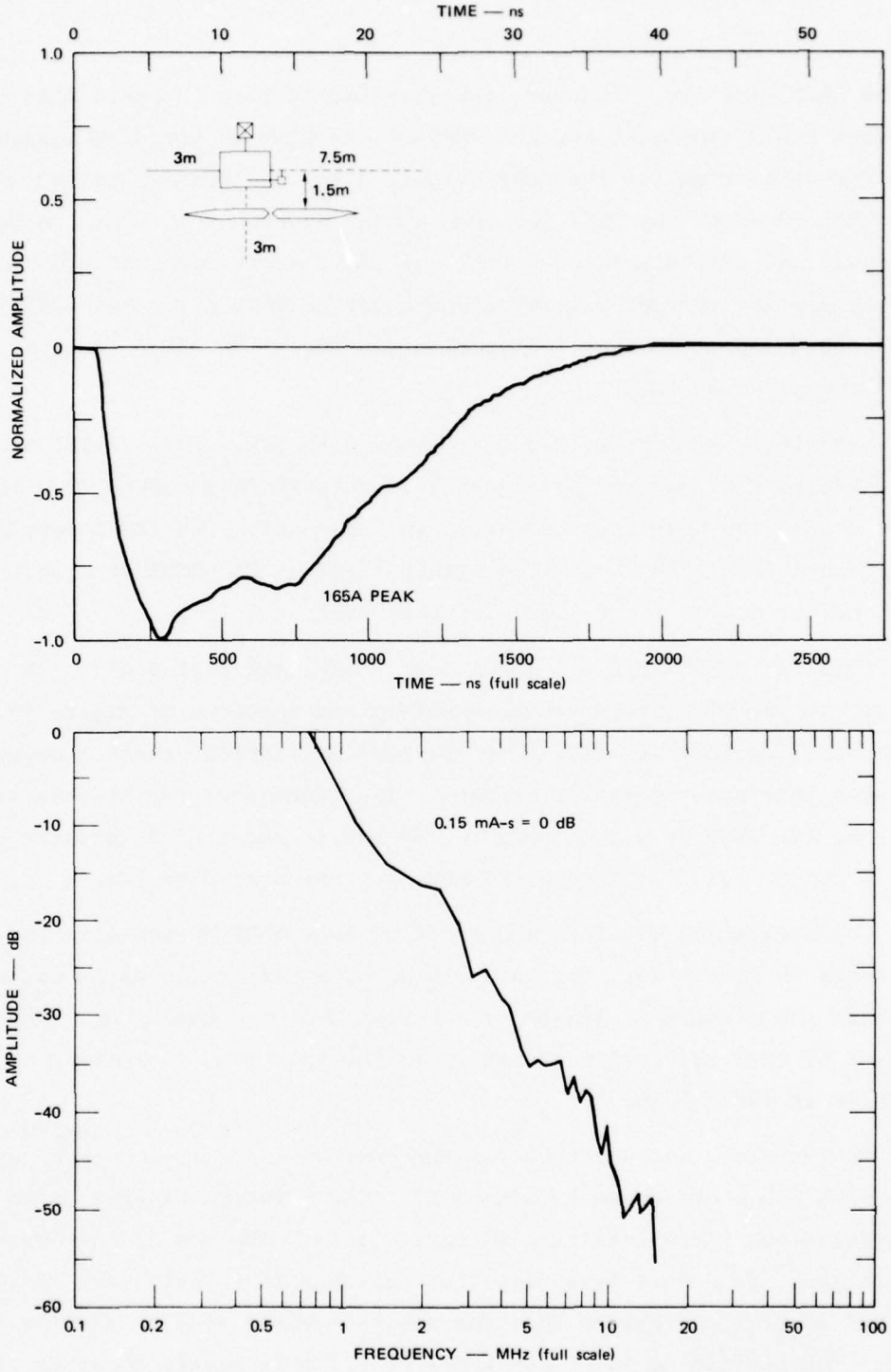

FIGURE 23 TEMPS AT 1.5 m (75-m full scale) EXCITATION ON THE RIGHT BURIED WIRE

to the HEMP waveform. However, the risetime is slow compared with the incident field risetime, and the TEMPS decay time is slightly longer than the decay time for the HEMP (Figure 22). The TEMPS spectrum shape is within ±2 dB of the HEMP spectrum almost everywhere. Thus, in both frequency and time domain, the HEMP and TEMPS excitations at 1.5 m produce similar current waveforms and spectrum shapes for the RIGHT buried conductor. However, the excitation level for TEMPS is about 6 dB lower than for HEMP.

Bringing the TEMPS to 0.6 m from the site (30-m full scale) produces the waveform and spectrum of Figure 24. This TEMPS waveform is almost identical to the HEMP waveform shown in Figure 22. The TEMPS spectrum shape shown in Figure 24 is also within ±2 dB of the HEMP at almost all frequencies, and is about 4 dB less than HEMP.

Finally, TEMPS at 0.6 m (30-m full scale) and angled 45° with respect to the wire produces the waveform and spectrum of Figure 25. Again, the waveform is similar to the HEMP excitation waveform except for some late-time crossover effects. The TEMPS spectrum has the same shape as the HEMP to within about ±2 dB and is about 12 dB greater than HEMP. TEMPS angled is the only TEMPS excitation at HEMP levels.

The excitation waveform and spectrum on a NEAR buried wire for HEMP are shown in Figure 26. The waveform shows a reflection at 12 ns, which is about the electrical length of a buried 3-m wire conductor. The effects of this reflection are shown in the spectrum, indicating a decrease at about 2 MHz.

The waveform and spectrum for the NEAR buried wire for TEMPS excitation at 1.5 m are shown in Figure 27. The waveform clearly shows the effects of the TEMPS late-time electric fields with the 37-ns-wide pulse excitation. The short time variations of this TEMPS pulse are similar to HEMP excitation (Figure 26); the spectrum shape is also similar to HEMP. The excitation level for TEMPS at 1.5 m is nearly an order of magnitude less than HEMP for waveform, and nearly equal for spectrum.

The TEMPS at 0.6 m (30-m full scale) produces the waveform and spectrum of Figure 28. The TEMPS waveform is similar to HEMP for the

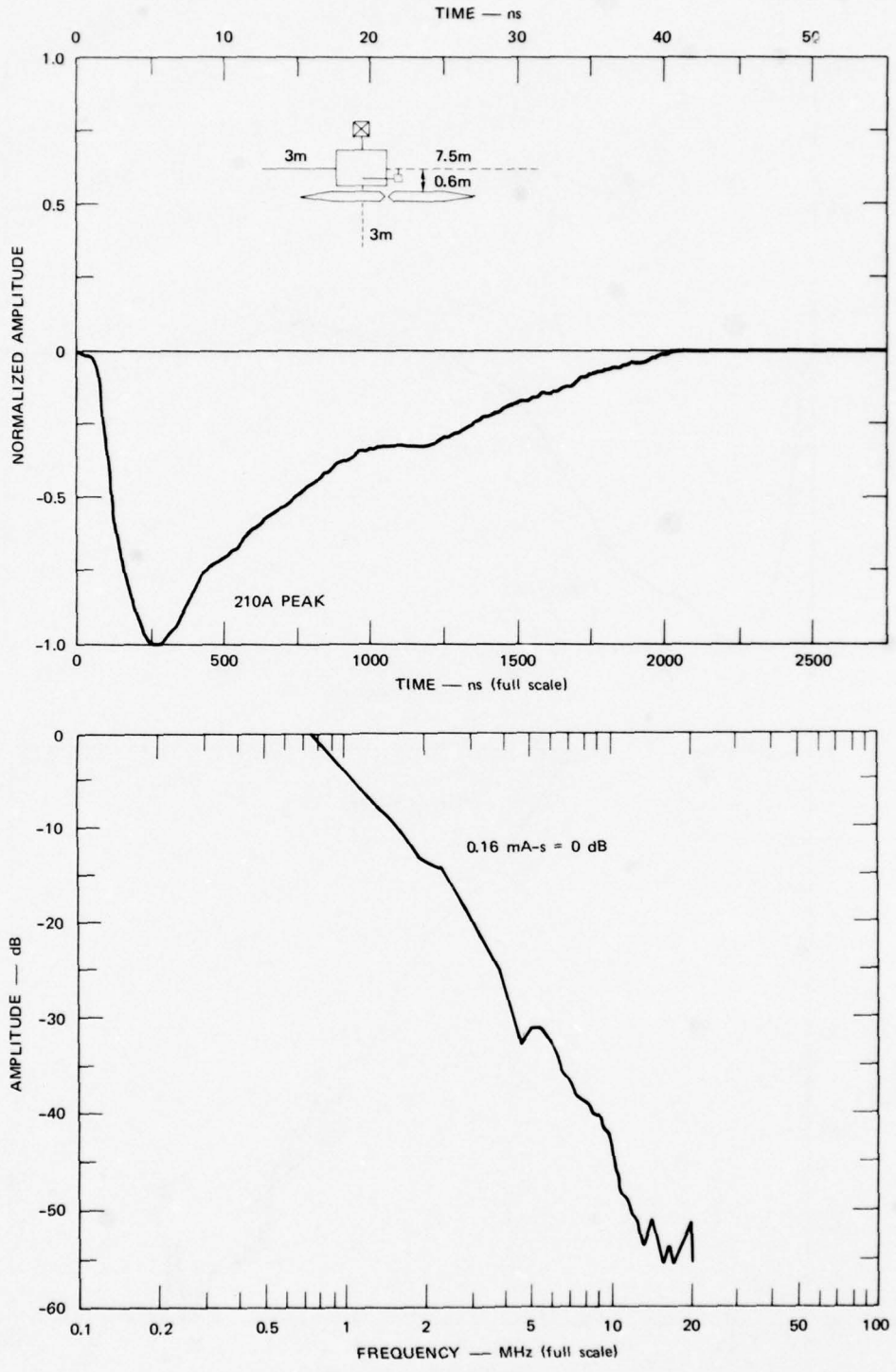

FIGURE 24 TEMPS AT 0.6 m (30-m full scale) EXCITATION ON THE RIGHT BURIED WIRE

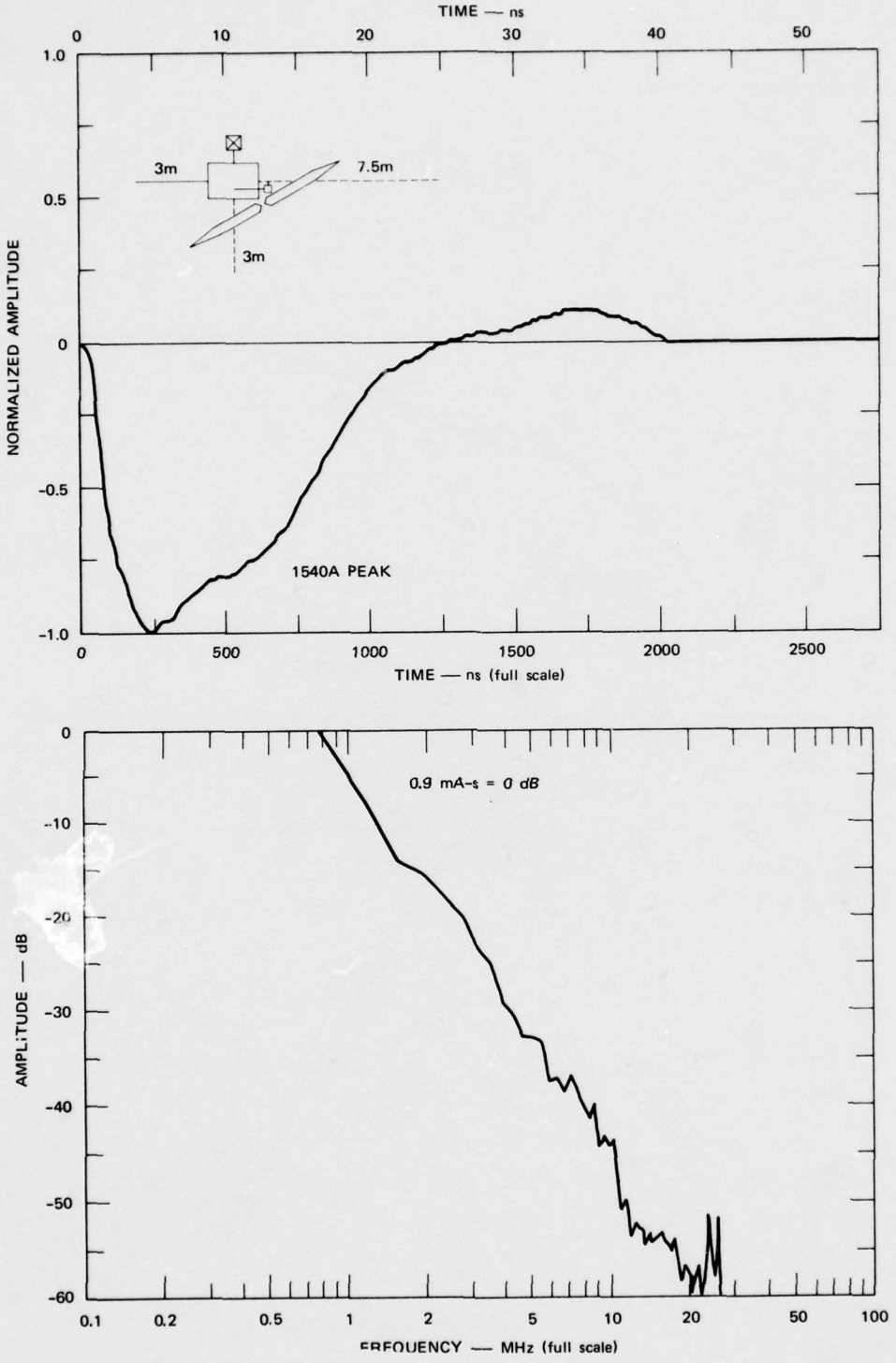

FIGURE 25 TEMPS AT 0.6 m (30-m full scale) AT 45° AND EXCITATION ON THE RIGHT BURIED WIRE

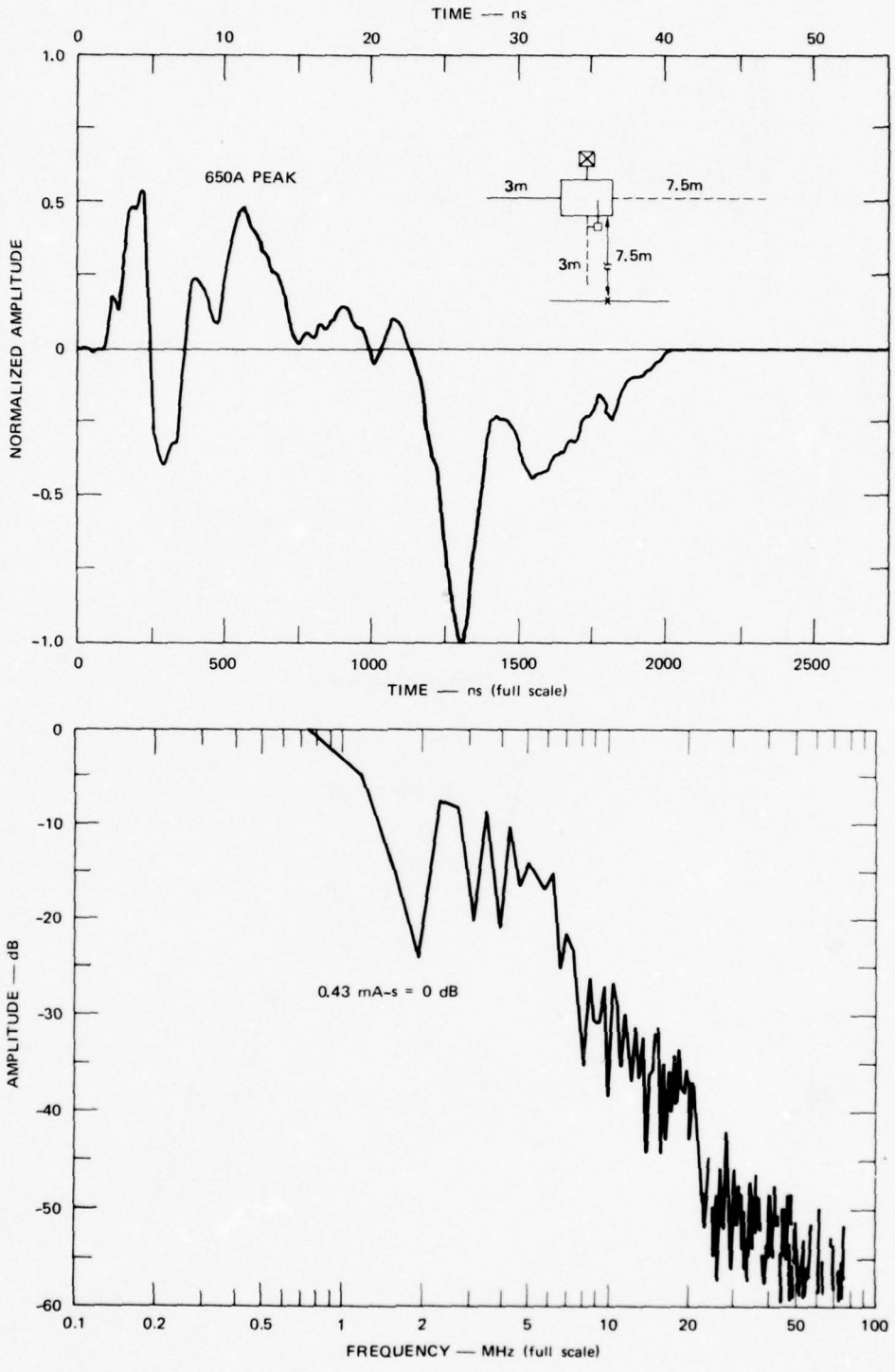

FIGURE 26 HEMP EXCITATION ON THE NEAR BURIED WIRE

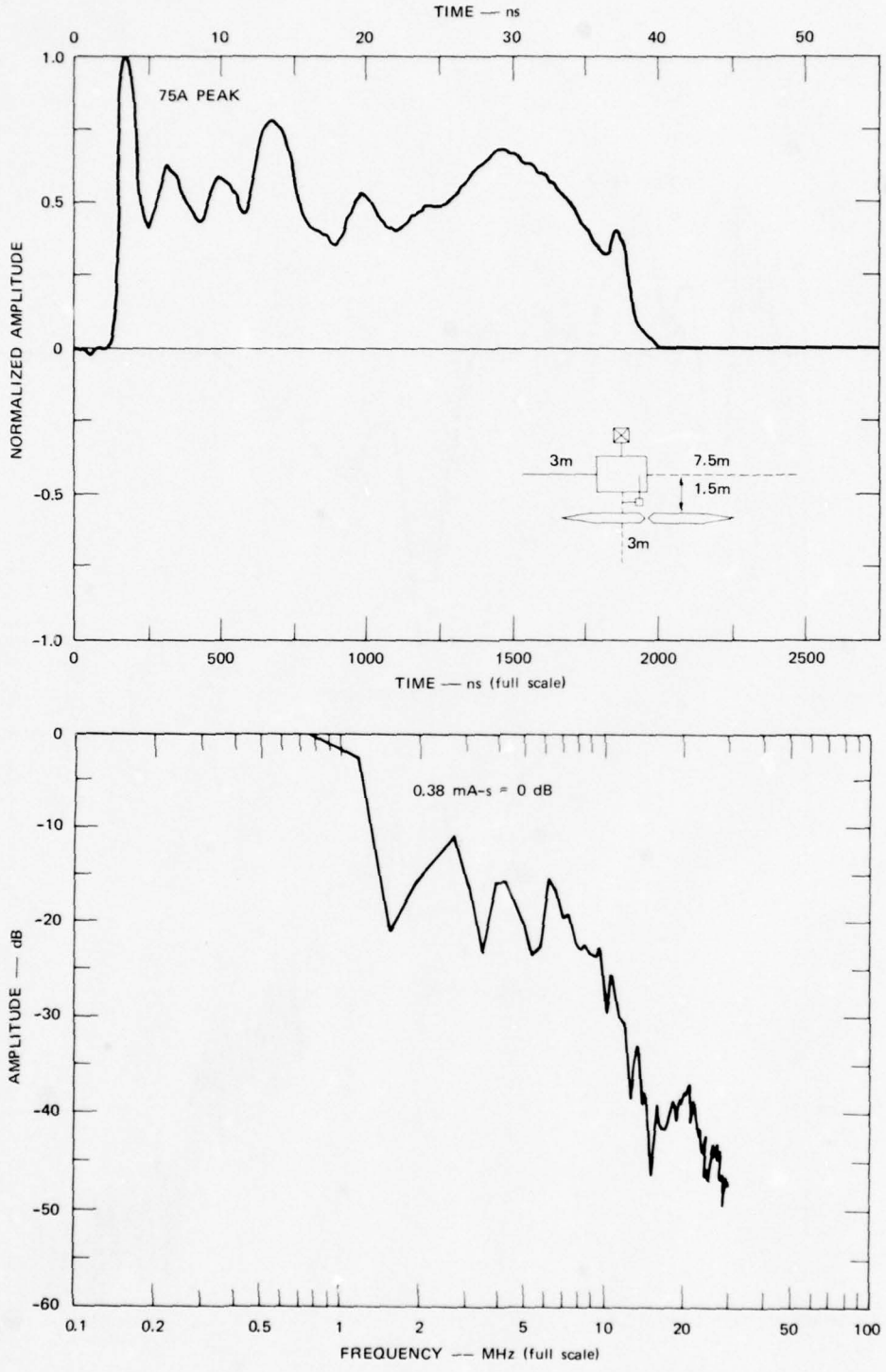

FIGURE 27 TEMPS AT 1.5 m (75-m full scale) EXCITATION ON THE NEAR BURIED WIRE

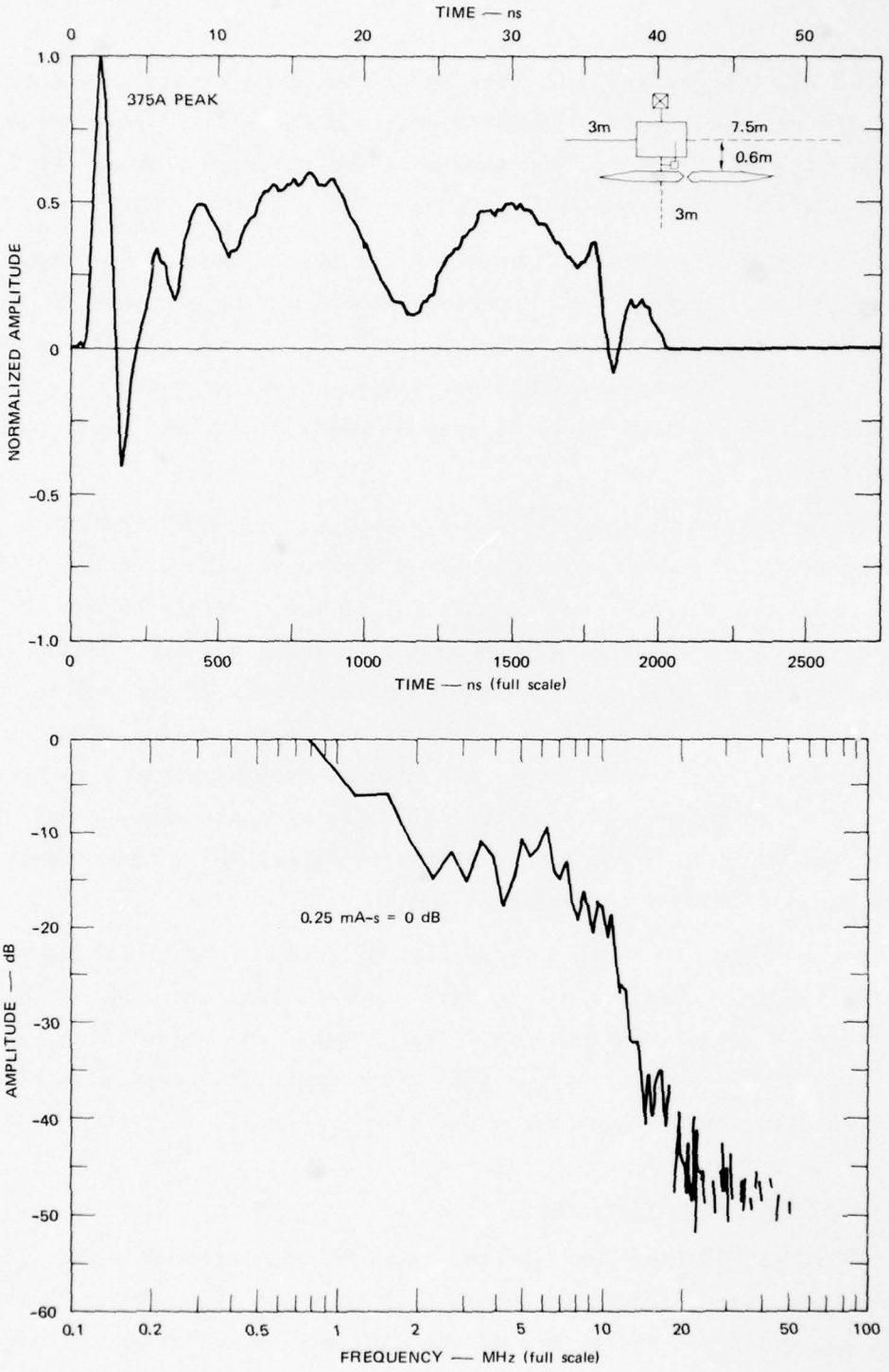

FIGURE 28 TEMPS AT 0.6 m (30-m full scale) EXCITATION ON THE NEAR BURIED WIRE

first 12 ns. Thereafter, the effects of the TEMPS late-time electric field are again evident. The TEMPS spectrum shape shows an enhancement from about 5 to 12 MHz and does not show the spectrum decrease at 2 MHz. The excitation level for TEMPS is about 3 dB less than HEMP.

Angling the TEMPS at 45° at 0.6 m results in the data of Figure 29. Except for the structure near the peak, the TEMPS waveform is considerably different from the HEMP waveform (Figure 26). The spectrum shape is also more like f^{-1}. The angled TEMPS excitation waveform is about 6 dB greater than HEMP; the spectrum is 12 dB greater below 3 MHz, and equal to HEMP above 3 MHz.

The waveforms of the LEFT aboveground wire for HEMP and TEMPS excitations with the NEAR and RIGHT wires buried are shown in Figure 30. These waveforms are all nearly identical to the waveforms shown in Figures 10-13 for the LEFT aboveground wire (with all aboveground wires). The reflection in the middle of the TEMPS waveforms is reduced for buried wires attached to the building, which is very apparent for TEMPS at 1.5 m (see Figure 11 for comparison). All the waveform magnitudes in Figure 30 are similar to the currents on the LEFT wire with all aboveground wires. Again, the excitations on each penetration appear to be independent of other wires connected to the facility.

The current waveforms for the FAR tower waveguide are shown in Figure 31. The waveforms on the waveguide are similar to those shown in Figure 18 for all aboveground wires attached to the building. However, there are distinct waveform differences, indicating that the building structure is coupled to the tower waveguide as a penetration.

3.2.2 Summary for Buried Wires

TEMPS and HEMP produce similar waveform and spectrum shapes for buried wires, and excitation levels for TEMPS are below HEMP. For TEMPS angled at 45° and at 0.6 m, the excitations are slightly more than HEMP, at the expense of waveform shape (Figures 22, 25, and 26, 29).

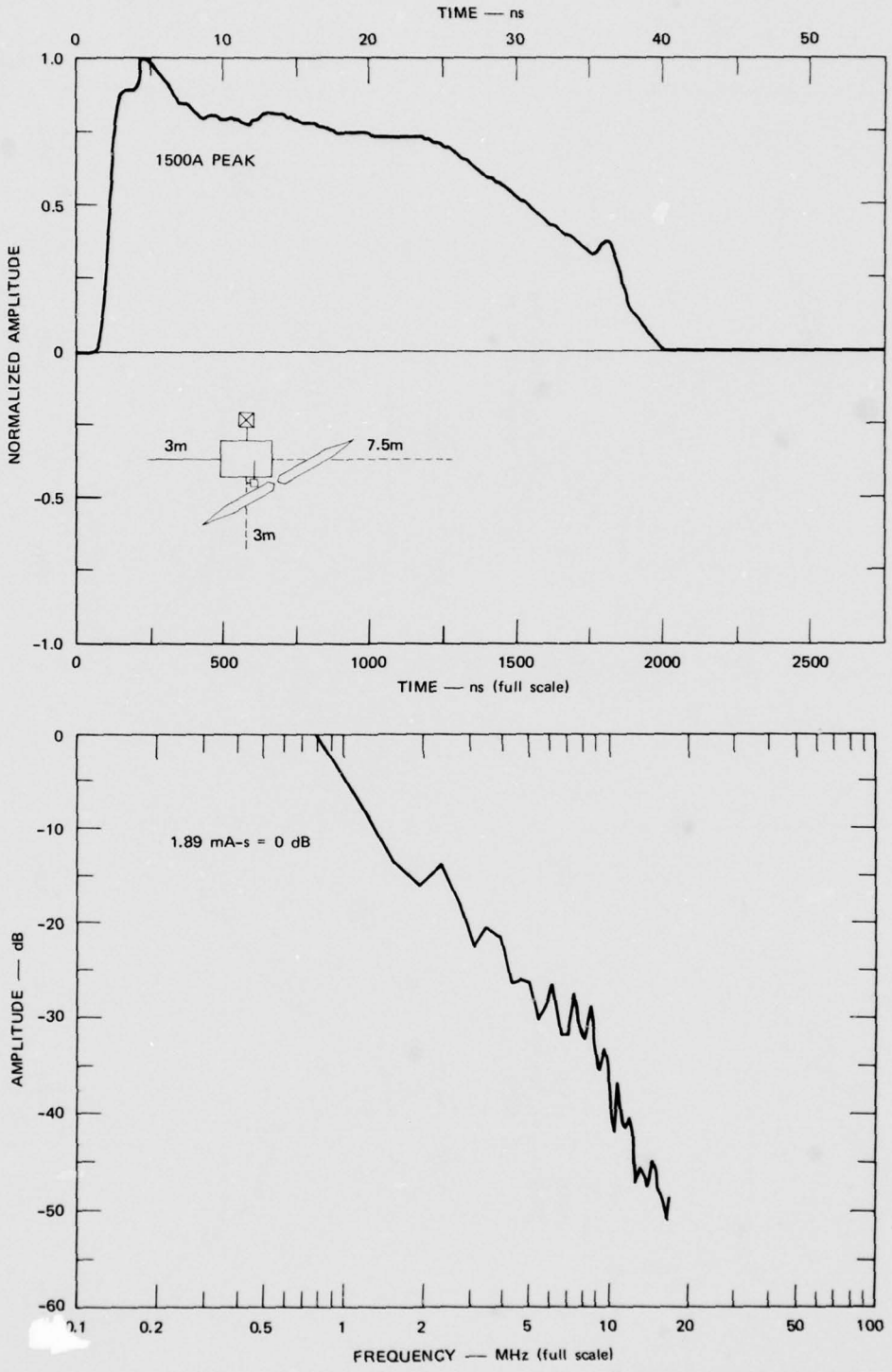

FIGURE 29 TEMPS AT 0.6 m (30-m full scale) AT 45° AND EXCITATION ON THE NEAR BURIED WIRE

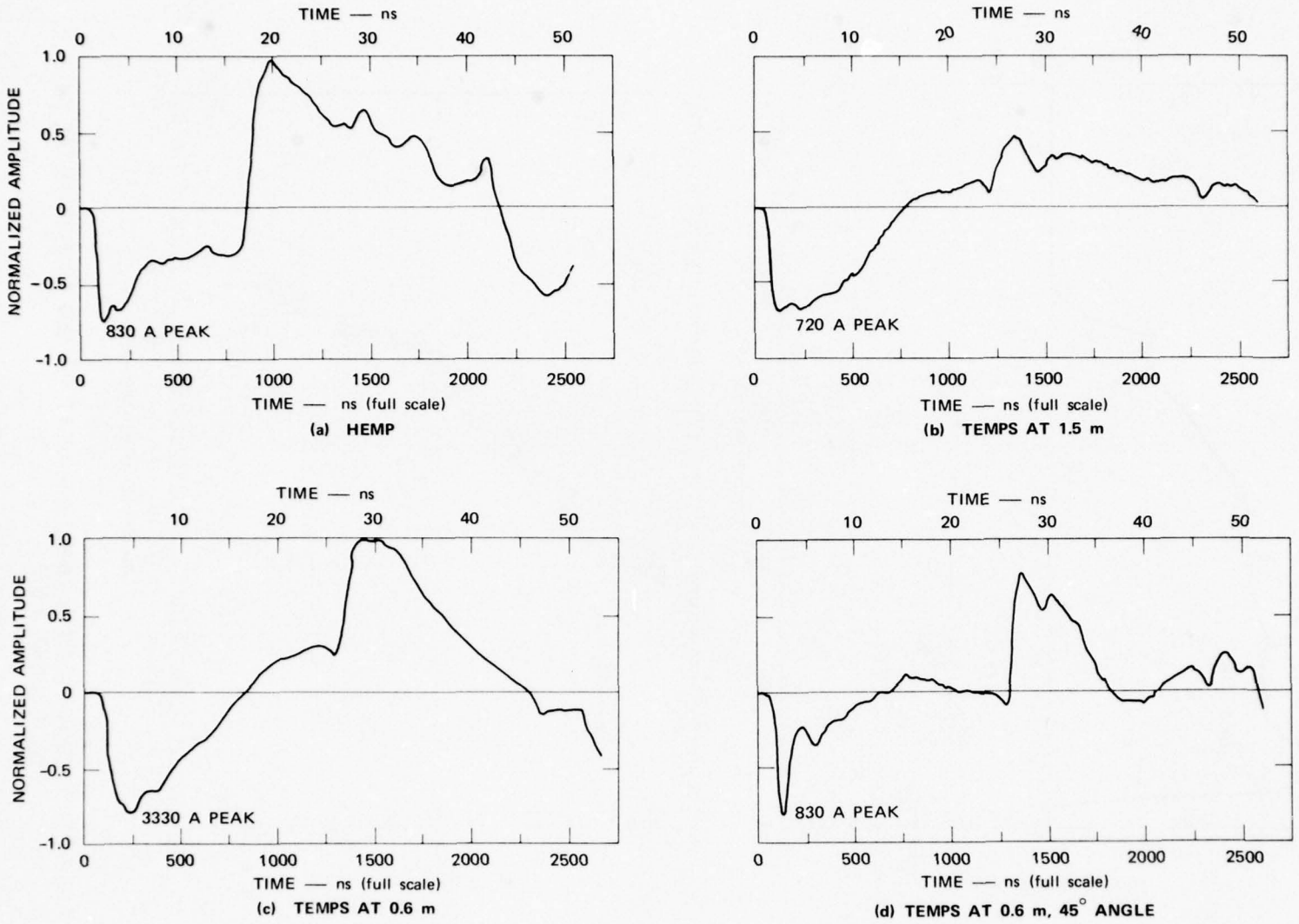

FIGURE 30 EXCITATION ON THE LEFT ABOVEGROUND WIRE (for buried wires)

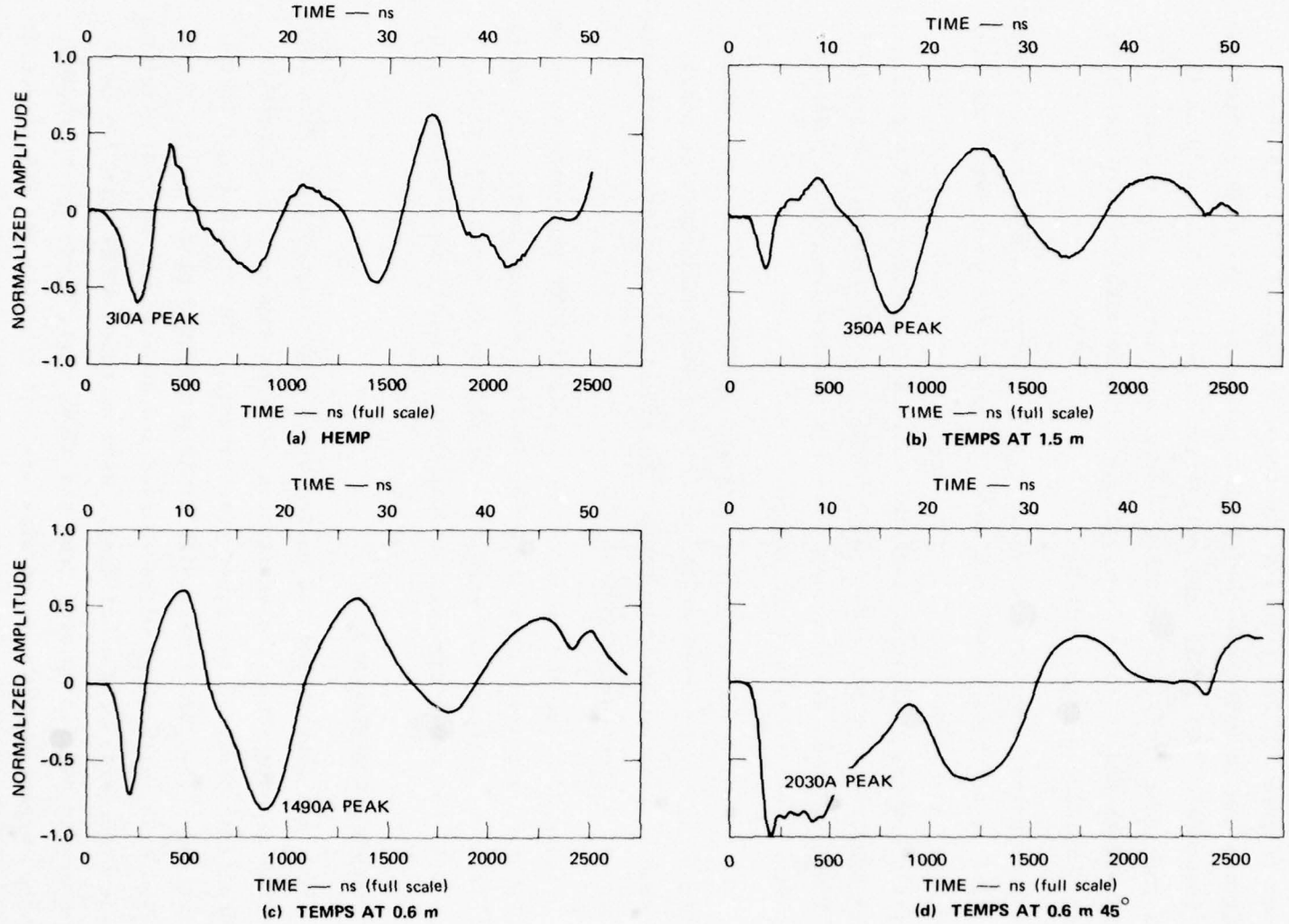

FIGURE 31 EXCITATION ON THE FAR TOWER WAVEGUIDE (for buried wires)

The waveforms for the LEFT aboveground wire with the other wires buried (Figure 30) are identical to those in Figures 10-13 in peak amplitude and in waveshape for the initial pulse. The HEMP excitations are identical. For TEMPS, the reflection signal at about 1200 ns is less than that for RIGHT and NEAR aboveground wires. The closeness of TEMPS excitation to those penetrations influences the current waveform on the LEFT above-ground wire.

The current waveforms shown in Figure 31 for the FAR tower waveguide are similar to those shown in Figure 18, except for peak magnitude and late-time ring frequency. The ring frequency for HEMP excitation is slightly higher, indicating that the building structure with buried wires appears to be smaller. This change in ring frequency is reduced for TEMPS as it is brought nearer the FAR penetration, which indicates that TEMPS is a localized excitation.

The building excitation for NEAR and RIGHT buried wires is shown in Figure 32. With TEMPS at 1.5 m, the building excitation is nearly the same as that produced by HEMP. The effects of the late-time vertical fields can be seen with TEMPS at 0.6 m.

Figure 33 shows the measured and predicted HEMP excitations for the RIGHT buried wire (see Appendix D for prediction equations). The agreement is good, although the predicted excitation is for a bare wire, which will not cross the axis at 30 to 40 ns as will an insulated wire.

3.3 COUPLED PENETRATIONS

For both aboveground and buried wires with single RIGHT, FAR, LEFT, and NEAR penetrations, the excitation currents appear to be independent to the first order of the other penetrations. The wire current in the aboveground 7.5-m RIGHT wire with RIGHT and NEAR buried wires is shown in Figure 34, with other wires (buried and aboveground angled) attached to the RIGHT side of the building. With an added RIGHT wire 7.5 cm above ground and 7.5 cm away from the RIGHT wire, there was no change in wire current when the added wire was orthogonal in the FAR direction (solid line curve). However, when the added wire was parallel at 7.5 cm

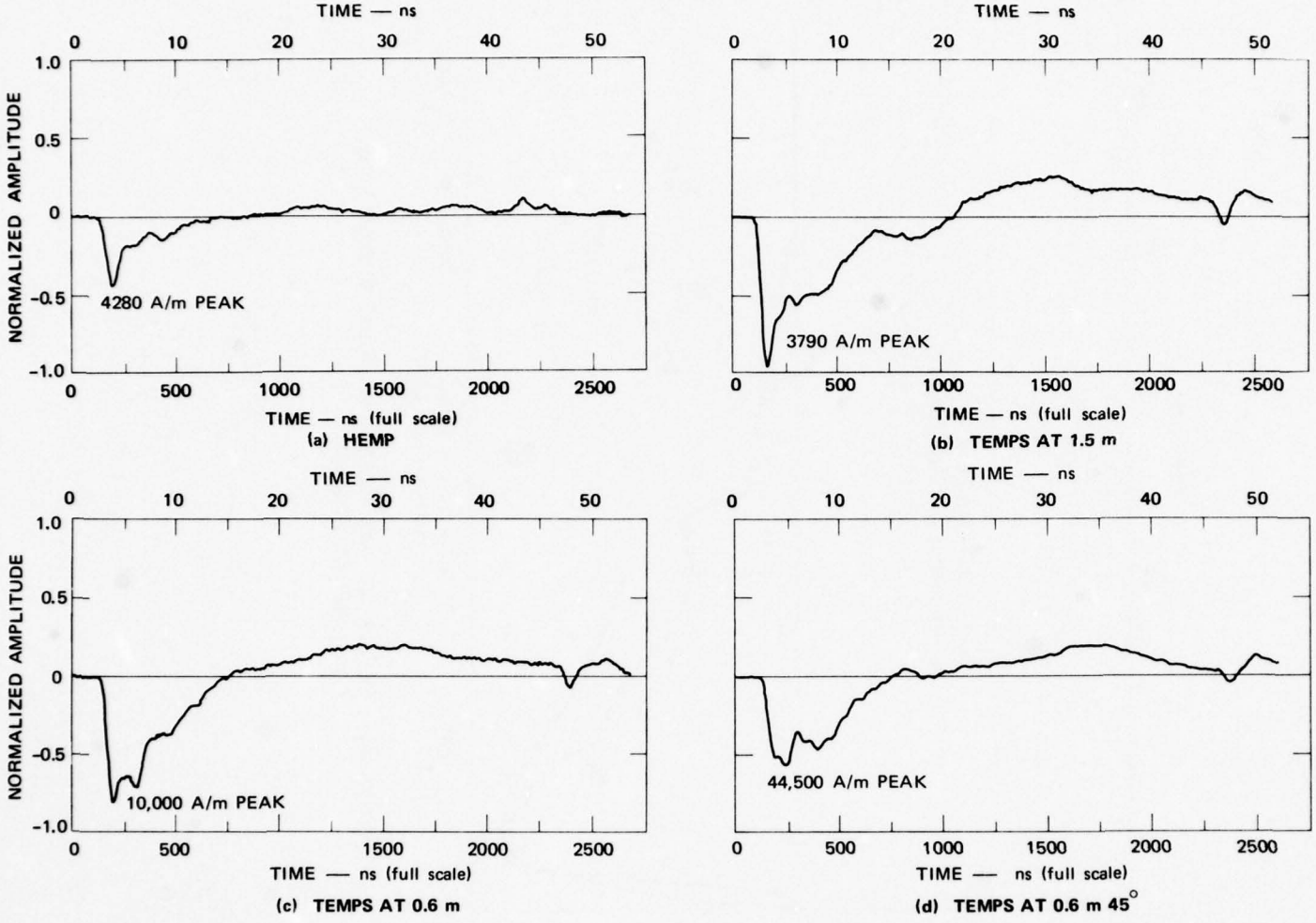

FIGURE 32 HEMP AND TEMPS BUILDING EXCITATIONS (for buried wires)

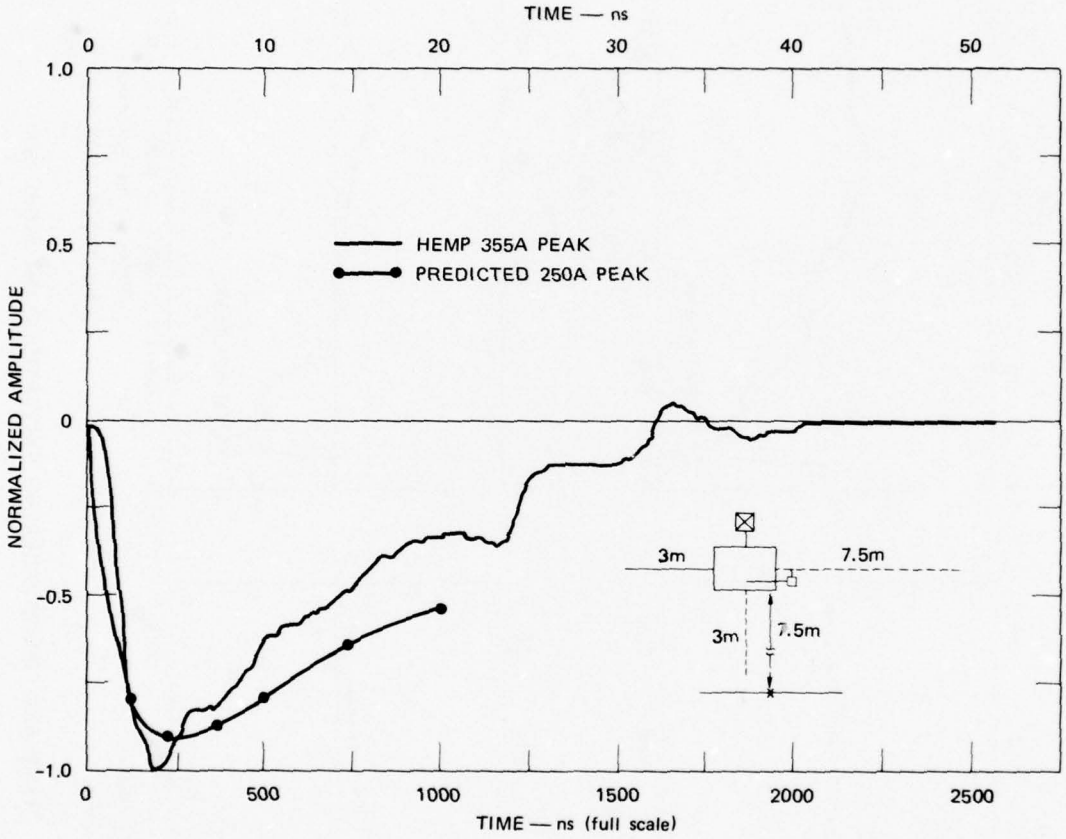

FIGURE 33 PREDICTED AND MEASURED RIGHT BURIED WIRE FOR HEMP EXCITATION

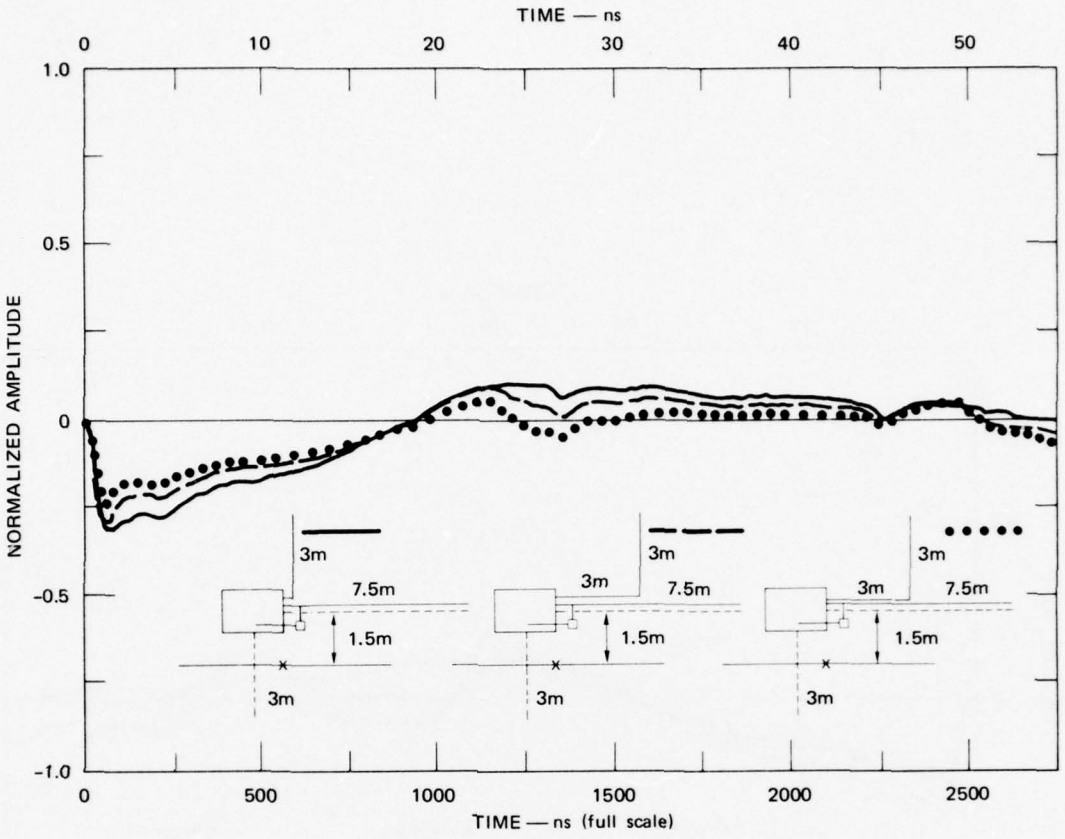

FIGURE 34 TEMPS AT 1.5 m (75-m full scale) EXCITATION OF ABOVEGROUND WIRE IN THE PRESENCE OF OTHER RIGHT PENETRATIONS

for 3 m before turning in the FAR direction, a reduction in current was observed (dashed curve). When the added wire was within 1.5 cm for 3 m along the RIGHT wire, a further reduction was observed (dotted curve).

With the 6-m aboveground RIGHT wire added on the NEAR side of the RIGHT wire, an amplitude reduction similar to the FAR amplitude reduction was observed, as shown in Figure 35. However, the effects of TEMPS late-time excitation on the added wire can be seen as the humps at about 20 and 30 ns. Since these humps change with the added-wire position, they appear to be directly coupled from the added-wire onto the RIGHT wire.

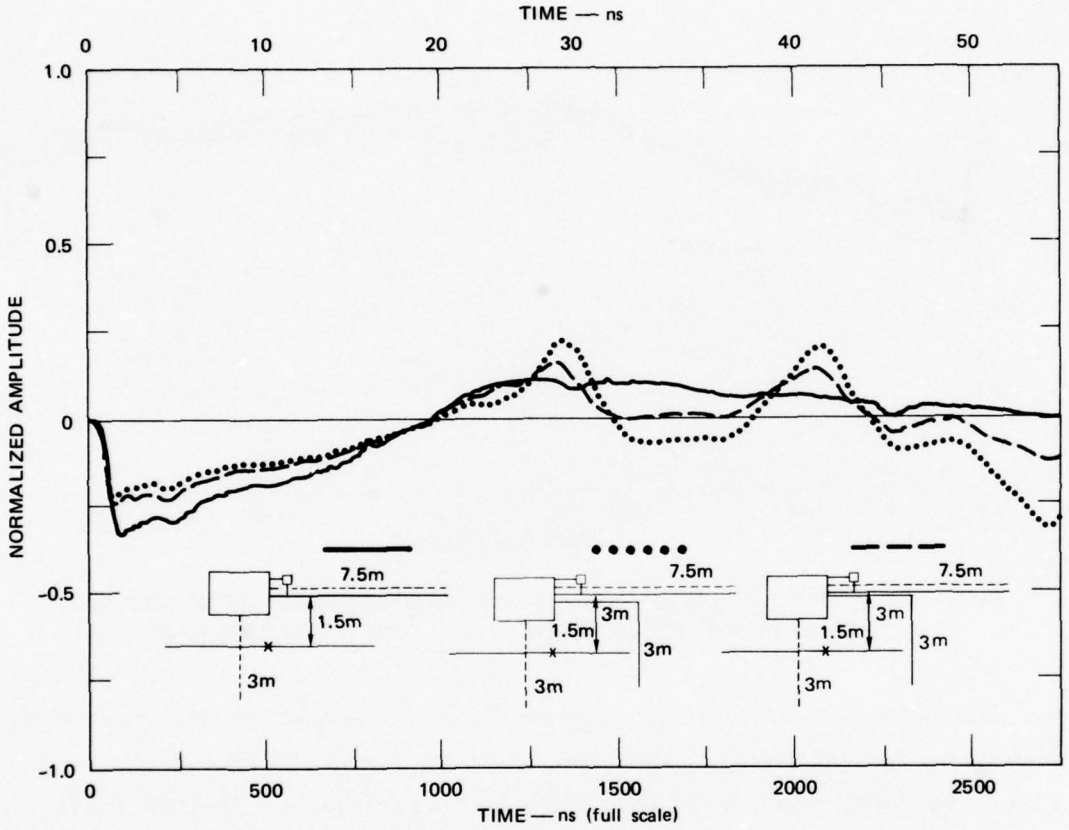

FIGURE 35 TEMPS AT 1.5 m (75-m full scale); FURTHER EXCITATION OF ABOVEGROUND WIRE IN THE PRESENCE OF OTHER PENETRATIONS

4. EMP SIMULATOR/FACILITY INTERACTION

The short-circuit wire currents have shown that the TEMPS excitation does not duplicate HEMP excitations. For individual currents, the non-HEMP fields for TEMPS distort the waveforms. Waveforms are also distorted by the interactions between TEMPS and the wire when they cross. In general, spectrum shapes are not distorted as much as waveforms.

4.1 SIMULATOR INTERACTION

For the RIGHT and LEFT wires, which are parallel to HEMP, TEMPS can best simulate HEMP if the aboveground wires do not intersect the simulator structure. For these wires, TEMPS excitations can equal or exceed HEMP excitation levels. HEMP excitation is cross polarized for the NEAR aboveground wire, resulting in a small, noise-like current. The TEMPS excitation for this wire is almost totally due to interaction between the wire, the simulator structure, and the simulator late-time vertical electric field.

Buried wires are shielded from interaction with the TEMPS structure by the earth, which also minimizes the differences in the HEMP and TEMPS excitation fields. For these wires, TEMPS waveshapes are similar to HEMP excitation. Spectrum shapes are very similar. Buried-wire current levels for TEMPS are less than HEMP excitation levels, except when the wires pass under the simulator structure.

The building structure excitation for TEMPS is similar to HEMP excitation except for a late-time, waveform crossover (typical of all TEMPS wire-current waveforms). The waveform-crossover magnitude is small if the building structure is within the simulator bicone working area (±57°).

The FAR tower waveguide excitation current is greatly influenced by the TEMPS vertical electric field, which is not present for HEMP excitation. This field results in excitation waveforms with exaggerated

tower ringing and larger excitation levels. The spectra, however, are less distorted, being somewhat similar to HEMP excitation.

4.2 SIMULATOR LOCATION

In general, a TEMPS position can be found for each of the measured facility excitations that will provide excitation levels, current waveforms, and spectrum shapes, within a few dB, that are equivalent to HEMP excitation. Application of TEMPS to simulate HEMP excitation for a facility can best be achieved by:

- Identifying and rank-ordering the energy-coupling paths (penetration-to-critical circuit) for each critical sensitive equipment.
- Selecting TEMPS locations that are "parallel" to aboveground wires and that cross buried wires to achieve HEMP level excitation of critical penetrations.
- Defining precise TEMPS positions that best fit the penetration rank-orderning for each sensitive equipment(s).

This TEMPS location procedure has been used to select TEMPS positions to achieve HEMP-relatable tests.[8] The final selection chosen for TEMPS (two positions) is shown in Figure 36 as positions F and G. Note the apparent minor position adjustments required to achieve best excitation.

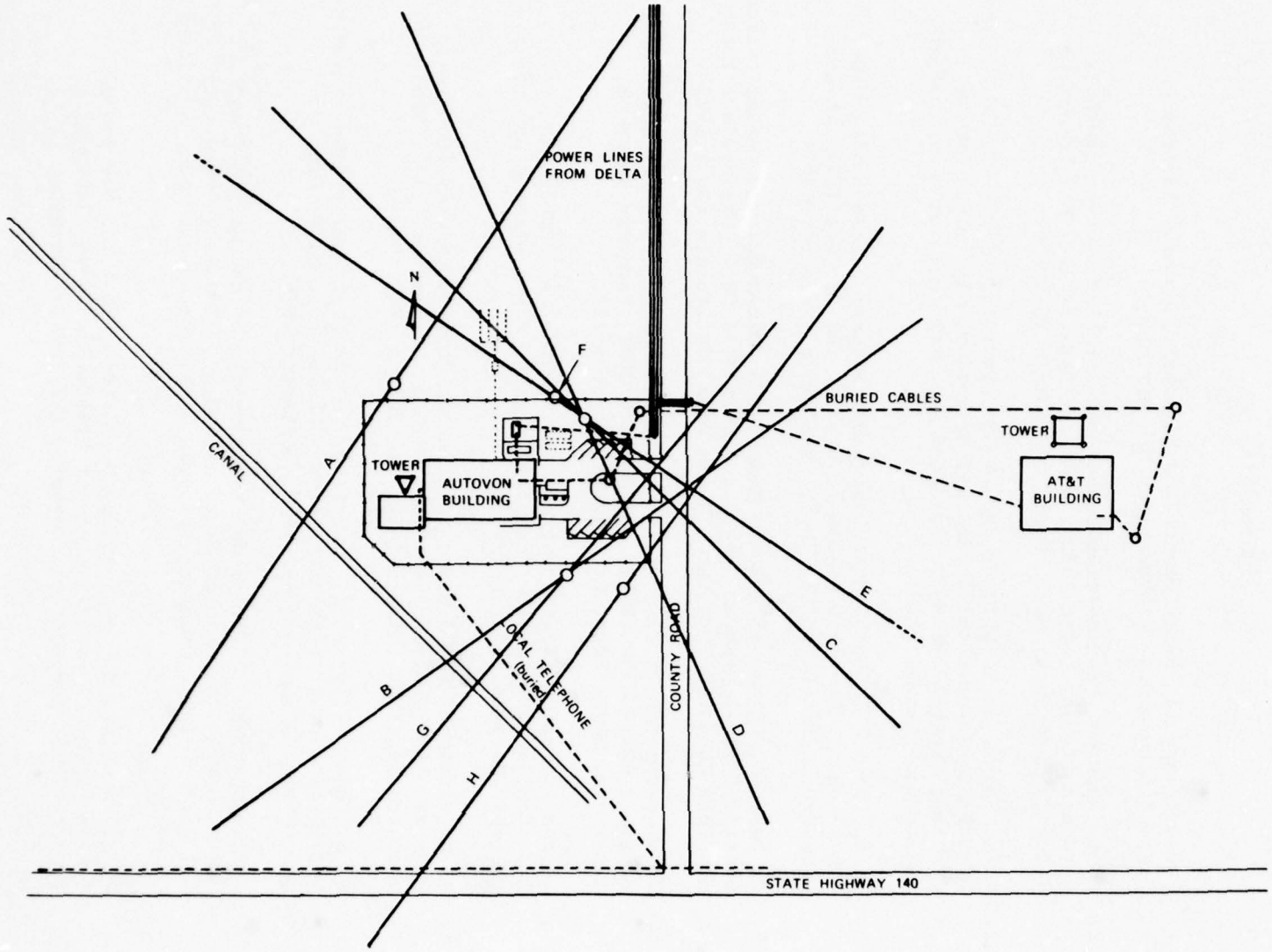

FIGURE 36 SIMULATOR POSITIONS FOR BEST FACILITY EXCITATION

REFERENCES

1. "Electromagnetic Pulse Sensor and Simulation Notes," Air Force Weapons Laboratory, Albuquerque, New Mexico.

2. A. L. Whitson, "Engineering Techniques for Electromagnetic Pulse Hardness Testing," DNA 3332F, Contract DASA01-71-C-0087, Stanford Research Institute, Menlo Park, California (September 1973).

3. G. S. Parks, A. L. Whitson, and G. B. Carpenter, "Some Considerations of EMP Simulator Construction and Operation," Technical Report 1, Contract F08606-76-C-0031, Stanford Research Institute, Menlo Park, California (Unpublished).

4. J. B. Chown, "EMP Simulator Design-Specification Sensitivity Study," Final Report, Contract DAAG39-72-C-0031, SRI Project 1391, Stanford Research Institute, Menlo Park, California (December 1971).

5. S. Dairiki, "Study of a Scale Model of a Common Carrier Communication Station," Final Report, Contract DAEA18-71-A-0204, SRI Project 2068, Stanford Research Institute, Menlo Park, California (July 1973).

6. J. B. Chown, "Polk City Scale Modeling," PREMPT Technical Note SRI-2, Contract DCA100-73-C-0042, SRI Project 2032, Stanford Research Institute, Menlo Park, California (March 1973).

7. Joseph R. Kreck, "Electromagnetic Scale Model of TEMPS/Polk City Test Configuration," HDL Technical Report, Harry Diamond Laboratories, Adelphi, Maryland (March 1976).

8. A. L. Whitson, "TEMPS Scale Modeling for Delta," PREMPT Technical Note SRI-14D, Contract DAC100-74-C-0025, SRI Project 3149, Stanford Research Institute, Menlo Park, California (May 1974).

9. A. A. Cuneo, Jr., and J. J. Loftus, "Scale Modeling for the Perimeter Acquisition Radar (PAR) EMP Test," HDL-TR-1761, Harry Diamond Laboratories, Adelphi, Maryland (September 1976).

10. W. E. Scharfman, "Scale Model Measurements of the Original and the Modified TORUS on Several Types of Ground," Contract F04701-72-C-0210, SRI Project 3035, Stanford Research Institute, Menlo Park, California (September 1974).

11. W. A. Baker, A. B. Sola, and J. V. Locasso, "B-1 1/5 Scale Model System," AFWL-TR-74-127, Contract F29601-73-C-0096, Rockwell International Corporation, Anaheim, California (November 1974).

12. E. F. Vance, "Determination of Incident Fields from Surface Field Measurements," Technical Memorandum 9, Contract F29601-69-C-0127, SRI Project 7995, Stanford Research Institute, Menlo Park, California (October 1970).

13. W. E. Scharfman, "A Laboratory Study of Horizontal Dipoles--TEMPS," Final Report, Subcontract 21-372-91, SRI Project 1484, Stanford Research Institute, Menlo Park, California (March 1972).

14. E. L. Patrick and S. L. Soo Hoo, "Transportable Electromagnetic Pulse Simulator (TEMPS) Field Mapping Report," HDL-TR-1743, Harry Diamond Laboratories, Adelphi, Maryland (September 1976).

15. E. F. Vance, "Coupling to Cables," DNA Handbook Revision, Chapter 11, Contract DAAG39-74-C-0086, Stanford Research Institute, Menlo Park, California (December 1974).

Appendix A

EMP SIMULATOR/FACILITY SCALE MODEL INTERACTION

A.1 SCALE MODEL OF SAFEGUARD SITE COMPLEX

In a study carried out by Stanford Research Institute in 1971, scale modeling was used to determine excitation field specifications for a proposed EMP simulator for SAFEGUARD. Some of the proposed simulator characteristics appeared overly stringent based on what was known about the coupling of EMP frequency electromagnetic waves to structures. Scale modeling was used to demonstrate that the simulator specifications could be relaxed without significantly affecting the induced coupling.[4]

A 100:1 scale model of the SAFEGUARD site was built (Figure A-1). Only the significant external electromagnetic features were modeled. The model was illuminated using a horizontal dipole antenna with an exponentially decaying pulse. The pulse simulated the decay characteristics of the canonical HEMP waveshape, but did not reproduce the rise time. Data were gathered and analyzed to times when reflections from the dipole ends and other obstacles perturbed the measurements.

The primary question addressed was that of the effects of deviations from planarity and uniformity upon the coupled currents. Perfect planarity occurs if the amplitude front is a plane wave over the target volume. Perfect uniformity occurs if the incident amplitude is constant throughout the target volume. A typical radiating simulator may emit, at certain times, a wave with a spherical wavefront, whose amplitude varies inversely as the range. The planarity and uniformity issues are linked together and cannot be separated easily in most cases.

The dipole illuminator was placed at various ranges, heights, and azimuths from a reference point on the model. Currents induced at ten different points on the model were measured for the various illuminations.

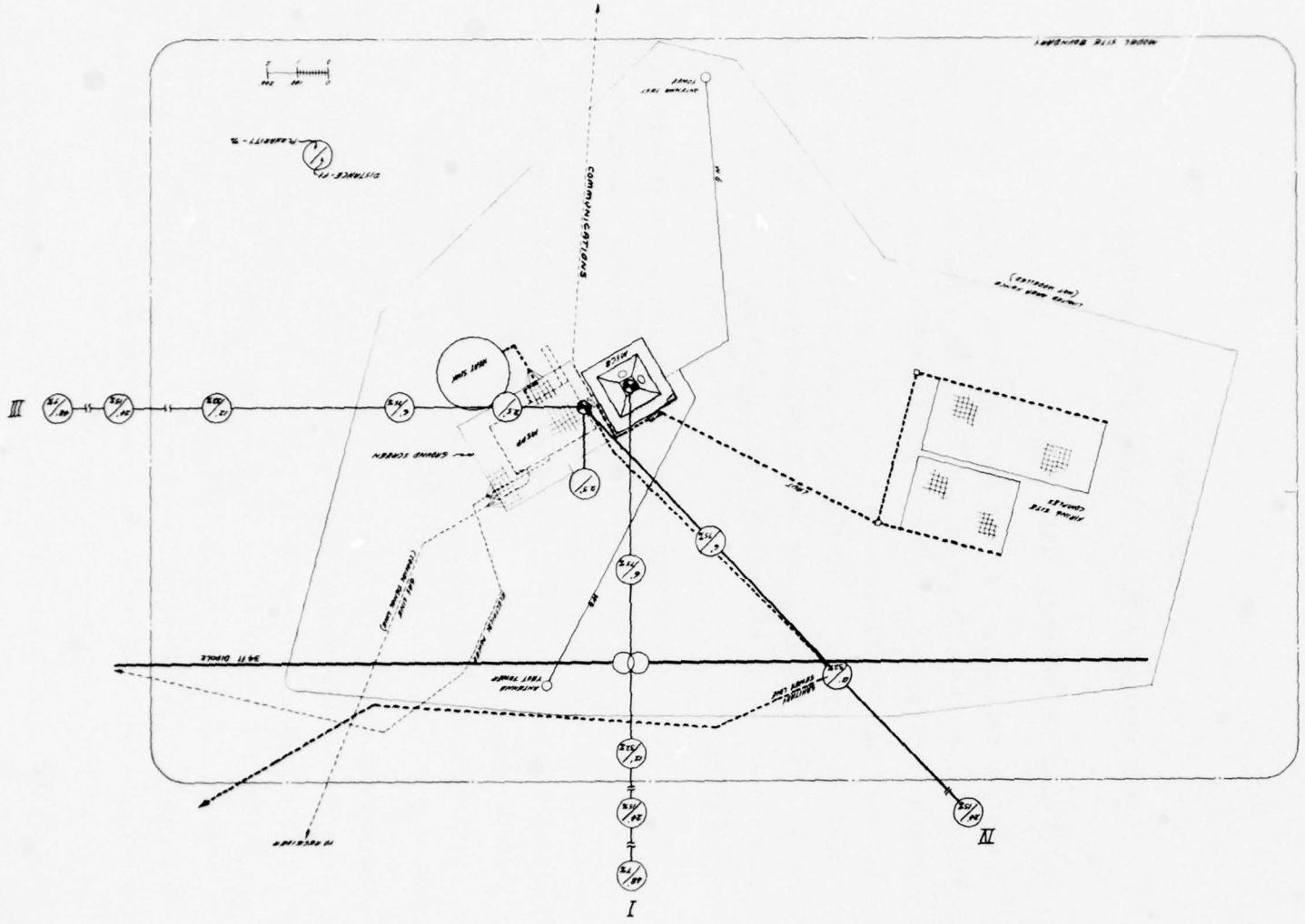

FIGURE A-1 DRAWING OF 1/100 SCALE MODEL OF SAFEGUARD SITE COMPLEX

For each current sensor location, the measurements were compared to a baseline condition. The farthest range illuminations, while not having perfect planarity or uniformity, served as the baseline conditions for HEMP illumination from the corresponding azimuth and elevation angles. Further comparisons were made among currents at different azimuths, for the same range and elevation angle.

The model illuminations as a function of azimuth and elevation angles were also used to address another important simulator question, that of the most effective simulator location, independent of planarity and uniformity considerations. There was no simple answer available, since coupling and equipment sensitivity must also be considered. Nonetheless, angular variations particularly address the adequacy of the simulation.

Planarity is defined as the ratio of the longitudinal field component to the transverse field component at a specific point. Planarity will vary with simulator range, simulator orientation relative to the site, and the dimensions of the target area (100x200-m full scale). Uniformity is defined as the fractional increase or decrease in transverse field amplitude within the target area in relation to a reference point. Normally, uniformity is measured in relation to the center of the target area, along a ray oriented in the illumination direction, passing through the reference point.

The dipole illuminator was placed at ranges of 17, 8.5, 4.25, 2.13, and 0.87 m (48, 24, 12, 6, and 2.5 ft) from a reference point (top of the modeled Missile System Control Building). This resulted in planarities of 7%, 15%, 32%, 75%, and greater than 100%, respectively, for the main MSCB/MSPP complex as shown in Figure A-2. All illuminations were at an elevation of 15° from horizontal. Illumination was from north, east, and northwest angles relative to the real site (Figure A-1). The dipole illuminator was 10.3-m (34-ft) long, resulting in a minimum clear-time of 17 ns (1.7-μs full scale).

Since the dipole fields vary inversely as range, each measured current was corrected for range to give a true indication of planarity and uniformity effects. The 14.6-m (48-ft) range (7% planarity) was

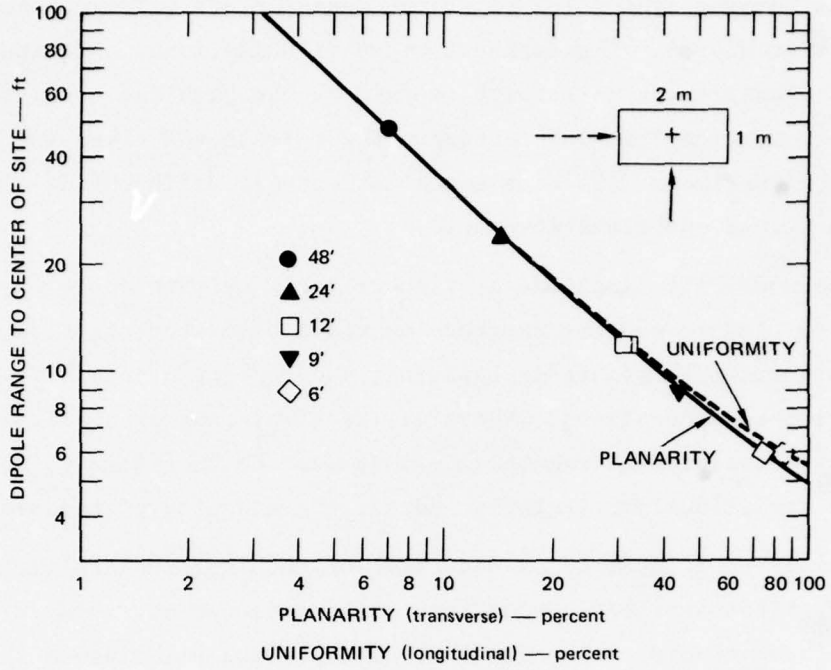

FIGURE A-2 PLANARITY AND UNIFORMITY AS A FUNCTION OF DIPOLE RANGE TO CENTER OF SITE

taken as the baseline value approximating perfect planarity. At that range, the uniformity, also shown in Figure A-2, was no worse than ±7.6%.

In general, the measured currents pass through zero in the time domain, or exhibit some nulls in their frequency spectra. Since some of the data have significant current peaks containing most of the signal energy, it was decided to make the comparisons on the basis of change in peak amplitude, rather than using other possible criteria. The results indicated that the individual waveshapes were quite similar in appearance as the range was varied, and in many cases were similar in appearance as the illumination direction was varied (Figure A-3). In 75% of the cases examined, a ±2 dB deviation in amplitude levels allowed the planarity specification to be relaxed to levels approaching 70% of the original value.

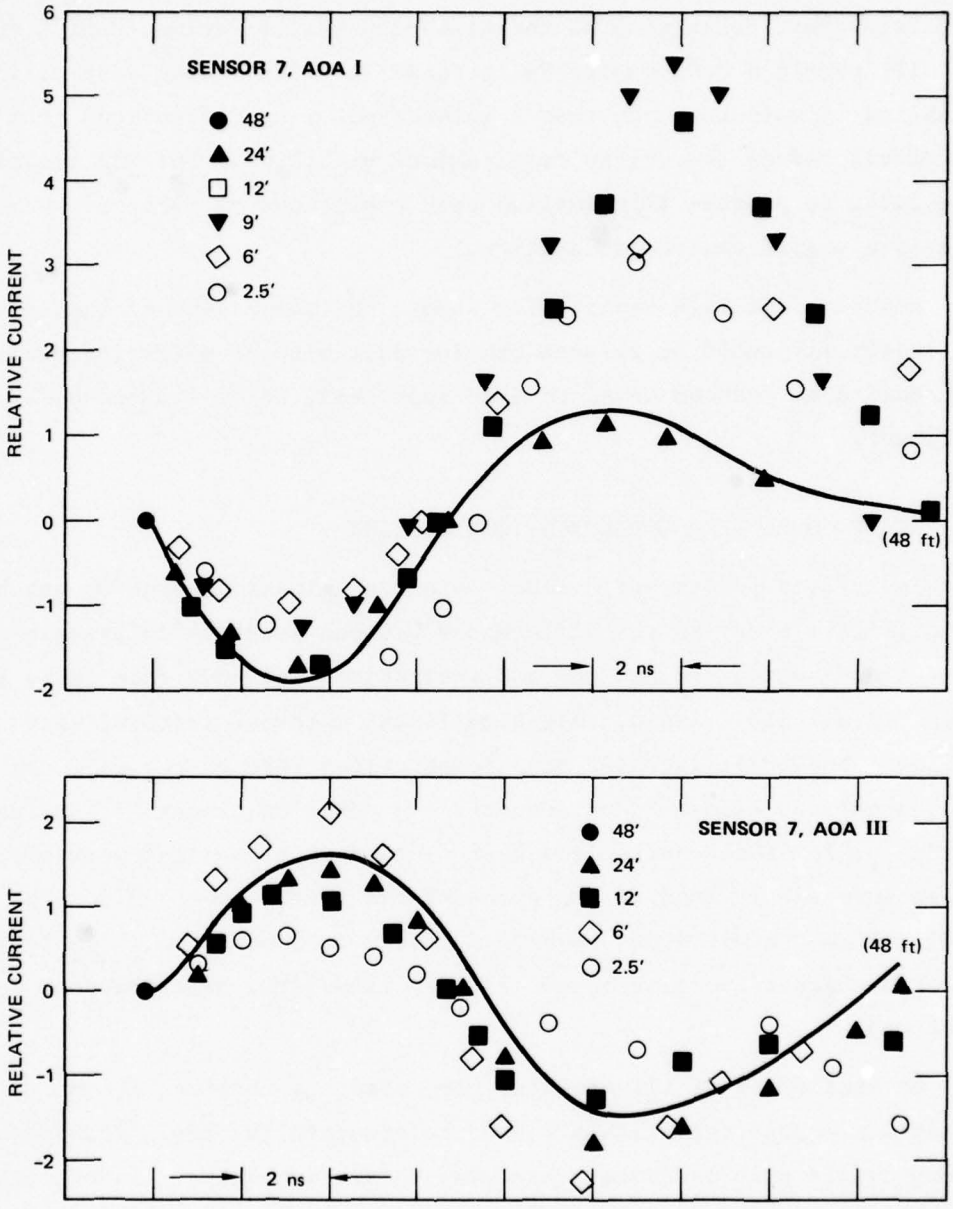

FIGURE A-3 COMPARISON OF SENSOR-CURRENT WAVEFORM AS A FUNCTION OF DIPOLE RANGE

The 75% level was nearly achieved at the 1.8-m (6-ft) range, which would correspond to a center line front-to-back illumination range of 2.83:1, or about ±68% deviation from uniformity. It can readily be calculated that relaxation of the planarity specification from 7% to 70% will permit a 7.63 amplitude increase (17.7 dB) using a specified radiating illuminator, and that a relaxation of specifications from 20% to 70% can reduce the driver requirements by 9.1 dB. For EMP simulators attempting to produce illumination peak amplitudes of about 50 kV/m, this is a significant consideration.

Results from this sensitivity study, therefore, showed that planarity and uniformity could be relaxed considerably without suffering serious degradation of induced waveform (and spectrum), or of induced peak amplitude.

A.2 SCALE MODEL OF A COMMUNICATIONS STATION

In 1973, a 1/40th scale model of a communications station was built to facilitate studying the differences between previous full-scale excitations[5] with TEFS and RES and excitations for HEMP (see Table 1 of the main text). Again, only significant external features were modeled. The model included some penetrations through the wall, as well as various skin-current sensors. In addition, internal terminating impedances for the penetrations were modeled to the extent possible, rather than simply bonding the penetrations to the model wall. The model included a microwave tower. Currents were measured at 10 locations, and skin currents were measured at 5 locations (two polarizations per location).

Several forms of illumination were used: a vertical monopole, a vertical monopole resistively loaded to simulate the RES waveshape, and a long dipole with canonical (decaying) HEMP wave shape. In addition, a short-pulse waveform (impulse) was used with the vertical monopole to deduce impulse responses of the structures. The dipole was oriented for both horizontal and vertical (E-field in the plane of incidence) polarization. Measurements were made at a variety of azimuth angles, at several elevation angles, and at a number of ranges from the site

center. However, not all these variations were made for any one illuminating situation.

An investigation of planarity and uniformity effects as a function of range was conducted using the RES waveshape (vertical polarization, grazing incidence). The structures selected for investigation were ac neutral, ac phase, antenna tower (leg), coaxial line, and water pipe. These structures were the most extensive in length, had impulse responses of the longest duration, and were expected to show the greatest effects of nonplanarity and nonuniformity.

The measurements were corrected for range variations to the site reference point (center of station roof). Comparisons were made not only on the peak amplitude, but on successive peaks within a waveform. For each waveform, the average of the absolute values of all the discernable peaks was computed and compared to a similar computation at a different range. As with the SAFEGUARD simulator specification study,[4] the waveshapes were basically similar as the planarity and uniformity were varied. Although the relative peak amplitudes varied somewhat, all the peaks of the responses on a structure for different antenna distances occurred practically at the same time.

When the waveshape was varied, rather than the uniformity or planarity, the resultant waveshapes at a specific model location were different both in form and amplitude. For equal peak-amplitude RES and HEMP illumination, the peak responses to RES illumination were less than the peak responses to HEMP illumination by as much as a factor of 5. This result was expected because the model response is the convolution of the model response to an impulse and the driving field time function. The HEMP illumination had a much slower decay time than did the RES illumination. For long structures, the impulse response of the model extended to low frequencies. Consequently, those long structures showed dramatic differences in peak amplitude for RES and HEMP illumination.

The same consideration will be true for all simulators--the current excited on a target will show variations for different simulator excitation and spectra, corresponding to the impulse response of the target. The effect is not directly uniformity or planarity dependent. The effect must be considered when comparing different simulators or different excitation techniques (e.g., different pulsers) of the same simulator. This effect must be considered when calculating results anticipated for true HEMP excitation.

Table A-1 shows some of the variations seen for changes in waveshape (RES and HEMP) and changes in incident polarization (vertical and horizontal). Note that vertical polarization almost always produced greater excitation than horizontal polarization, on the long structures listed. The HEMP waveshape which is usually assumed to be representative of threat is primarily horizontal, but it has about a 30% vertical component. It is clear from the table that the response to vertical excitation, even reduced to 30% of its listed value, is comparable to, and sometimes larger than the response to horizontal excitation.

In general, transmission line simulators produce vertical excitation. Hence, if 50-kV/m fields are available, most targets can be driven to adequate excitation levels. Radiating dipole simulators (TEMPS, for example) are generally horizontally polarized, but they have significant vertical components at large angles away from the centerline on the ground. Such simulators, however, may produce inadequate excitation of some targets.

Included in the RES illumination results is one column denoting the variation with azimuth of the illuminating antenna. The dominantly vertical structures (waveguide, tower leg) show relatively little effects of azimuthal orientation. As expected, the various structures responded most strongly when the electric field was polarized parallel to the orientation of the structure.

The planarity and uniformity aspects were carefully investigated. It was found that the radiating source could be located as c[illegible] the model as 3.8 m, or 153-m full scale, and the amplitudes of the responses

Table A-1

MAXIMUM PEAK PENETRATING CURRENTS FOR 100 kV/m*

	RES† Illumination				HEMP† Illumination					
	Vertical Polarization				Vertical Polarization			Horizontal Polarization†		
	Measured (mA)	Az (deg)	Variation with Az	Full-Scale (kA)	Measured (mA)	Az (deg)	Full-Scale (kA)	Measured (mA)	Inc (deg)	Full-Scale (kA)
ac phase: normal	18	90	4.1	1.3	83	90	5.6	9.2	0	0.77
Disconnect east power lines	--	--	--	--	102‡	270	8.5	50	0	4.1
ac neutral: normal	18	90	2.9	1.3	67	90	4.5	5.5	0	0.45
Disconnect east power lines	--	--	--	--	134‡	270	11.0	26	0	2.1
Periodic ground								33	0	2.7
Antenna tower leg	5.4	180	2.1	0.37	11	180	0.75	15	0	1.3
	--	--	--	--	13‡	270	1.1	--	--	--
Waveguide: normal	6.6	0	1.6	0.45	11	0	0.75	4.3	0	0.36
Raceway disconnected from building	--	--	--	--	49‡	270	4.1	31	0	2.6
Coaxial line: normal	4.1	90	5.3	0.28	14.3	90	0.97	10	0	0.83
Eastward coax only	--	--	--	--	--	--	--	17.7	0	1.5

*90° (grazing) incidence angle unless otherwise indicated.

†Polarization parallel to 90° azimuth angle.

‡65° incidence angle.

would be within 2 dB of the responses at 12.2 m when amplitudes were adjusted for R^{-1} range variation. At the close-in range of 3.8 m the uniformity was 1.27:1, and the planarity was 13%.

In this investigation, the largest peak amplitude was not used to make comparisons, as was done in the results cited earlier.[4] Instead, the individual peaks of the entire waveform were used. The data taken at 7.9 m (25.8 ft) served as a reference, with each positive or negative peak in that waveform serving as a reference for the corresponding peak in the waveforms taken at different ranges. The relative values of the successive peaks were averaged, and the average value was compared for different ranges, using the same azimuth and polarization, however. Table A-2 shows results of that process for the five extended structures that were investigated.

Table A-2

AVERAGED RELATIVE PEAK AMPLITUDE COMPARISON
FOR DIFFERENT RADIATING SOURCE DISTANCES

Source	Averaged Relative Peak Amplitude						
Antenna range (m)	3.3	4.8	6.3	7.9	9.4	10.9	12.4
ac phase	0.94	9.98	1.00	1.00	1.02	1.01	0.95
ac neutral	0.89	0.97	0.96	1.00	1.09	0.98	0.97
Antenna tower leg	0.95	1.03	1.06	1.00	0.89	1.16	1.50
Coaxial line	0.75	0.88	0.87	1.00	0.99	1.08	1.04
Water pipe	0.75	0.84	0.96	1.00	1.09	1.08	1.04

With the single exception of the tower leg at 14.5-m range, all the results are within 3.3 dB. Except for the odd result, the results for 7.9 m are within 0.3 dB of the results for 14.5 m. Of the results shown in Table A-2, 23 have relative amplitudes within ±1 dB, 27 within ±2 dB, and 29 within ±3 dB. The other structures investigated, being smaller, had lesser variations.

With the exception of one odd point, the range could be varied from 10.9 m to 3.3 m with a maximum change of 3.2 dB in averaged amplitudes of the peaks of a specific waveform. At the shortest range, the uniformity was 1.32:1 and the planarity was 15%.

A.3 SCALE MODEL TEMPS SIMULATOR STUDY OF AN AUTOVON STATION

A scale model investigation of TEMPS illumination on the Polk City, Florida, AUTOVON station (General Telephone of Florida) was made in 1973. The model TEMPS illumination was compared to a HEMP model illumination. The latter was produced by a horizontal dipole antenna driven with a canonical HEMP waveshape, correct except for the rise-time. The station and TEMPS models were built to a 1/50th scale. The resulting data are useful for comparing radiating dipole simulators. TEMPS, Martin-Orlando long-wire facility, and other ground-based facilities are listed in Table 1 of the text.

The investigation focused on two items: (1) an inquiry into the effect of positioning TEMPS in two alternate locations; (2) a comparison of the currents produced by TEMPS with the currents produced by simulated HEMP excitation, including maximum excitation. Thus, excitations were measured for the horizontal dipole at a variety of elevation and azimuth angles including those corresponding to the TEMPS angles. However, the dipole was kept at a long range, and no attempt was made to study issues of planarity and uniformity.

Four major penetrants to the AUTOVON facility were modeled: telephone cable entry, ac power lines, condenser pipes and conduits, and external lighting standards. The adjacent microwave building, with its ring ground, tower ac leads, and connecting cables, also was modeled.

The horizontal dipole was 24.4-m (80-ft) long, and located 10.7 m (35 ft) from the model. An earlier study,[4] had demonstrated that this configuration gave excellent planarity and uniformity. The 24.4-m length resulted in minimum full-scale clear-times of 2 μs, and maximum full-scale clear-times of almost 4 μs, which was quite adequate to handle the simulated HEMP waveshape (750 ns, e-folding time).

The TEMPS model was located 1 m from a reference point between the model AUTOVON and microwave buildings in one position, and 1.67 m from the reference point in the alternate position (Figure A-4).

The TEMPS-model spectrum (and also the actual TEMPS spectrum) is not a fixed function of frequency at different ranges and angular positions because of clear-time limits associated with the biconic section. There is an initial high-amplitude, short-duration spike that gradually vanishes as the angle away from the centerline increases. The TEMPS waveform has this spike superimposed on a double-exponential waveshape, which simulates the canonical HEMP waveshape fairly well. If the spike is ignored, the peak amplitude of this remaining waveshape is about 61% of the total amplitude, including the spike (as measured on the centerline of TEMPS).

The TEMPS model (and the actual TEMPS) produces vertical electric fields at off-axis locations. Those vertical fields are a larger fraction of the horizontal field than occurs for the horizontal dipole antenna. Consequently, the TEMPS model is expected to produce different waveshapes and amplitudes than those produced by the horizontal dipole antenna. The TEMPS model is 6.1-m long (304.8-m full scale), whereas the dipole antenna is 24.4-m long. Clear-time limits on TEMPS data are 10-ns model time (500-ns full scale), but the resistive termination of TEMPS minimizes reflection and reradiation from the ends, and allows longer time periods of useful data to be achieved.

In general, the excitations produced by the TEMPS model matched very closely those produced by the dipole antenna. This was true for both amplitude and waveshape. In this excitation comparison, the spike produced by TEMPS was ignored, and the amplitude of the remaining TEMPS waveform was kept equal to the amplitude of the dipole antenna waveform, both adjusted for range effects. Figure A-5 shows the waveforms and amplitudes of the induced currents for the TEMPS model and the HEMP dipole antenna model. Except for the waveguide (an extended vertical structure) and the ac phase leads of the microwave facility (labeled R_2), the waveforms and amplitudes match very closely.

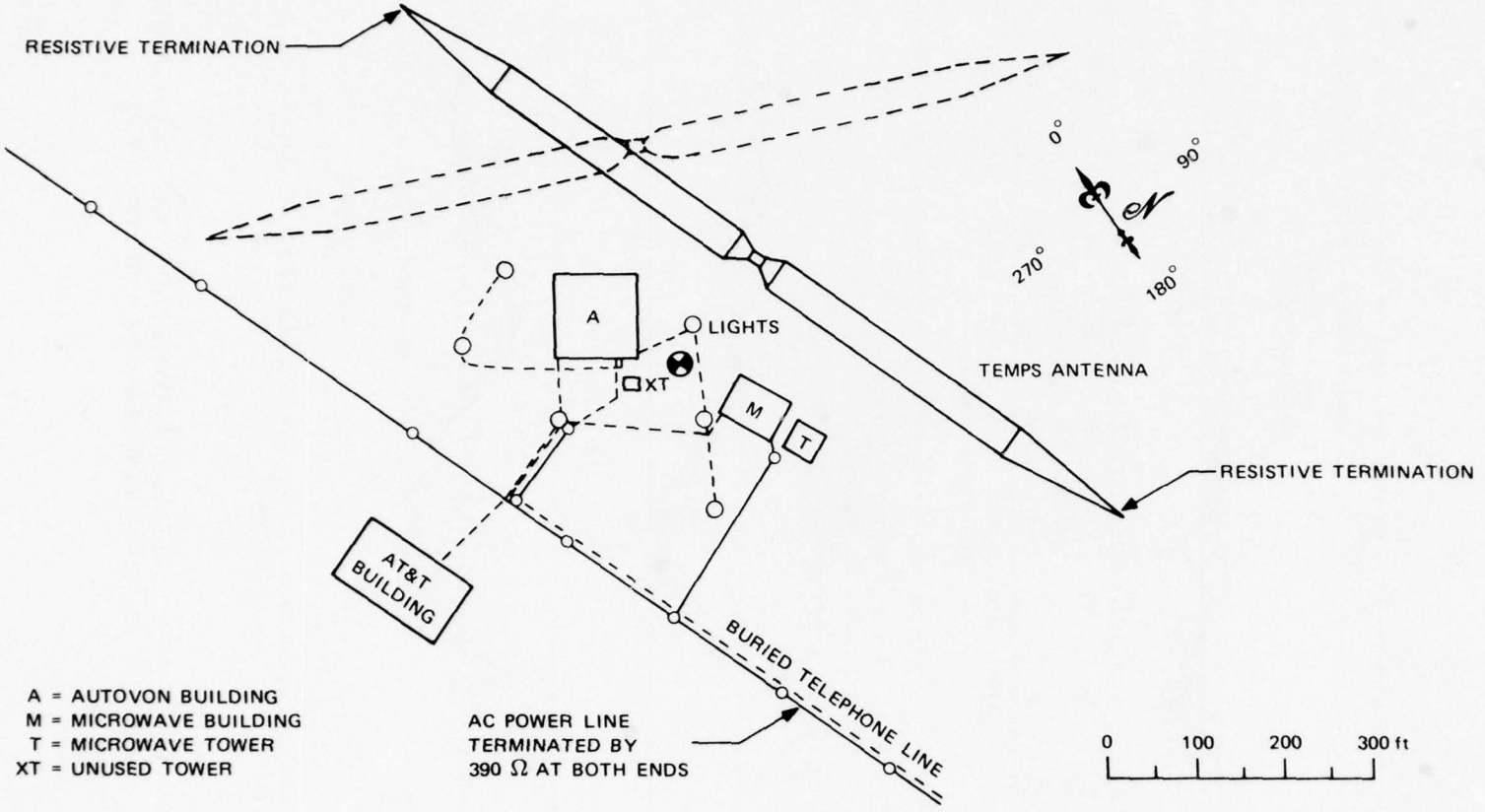

FIGURE A-4 DRAWING OF POLK CITY SWITCHING CENTER

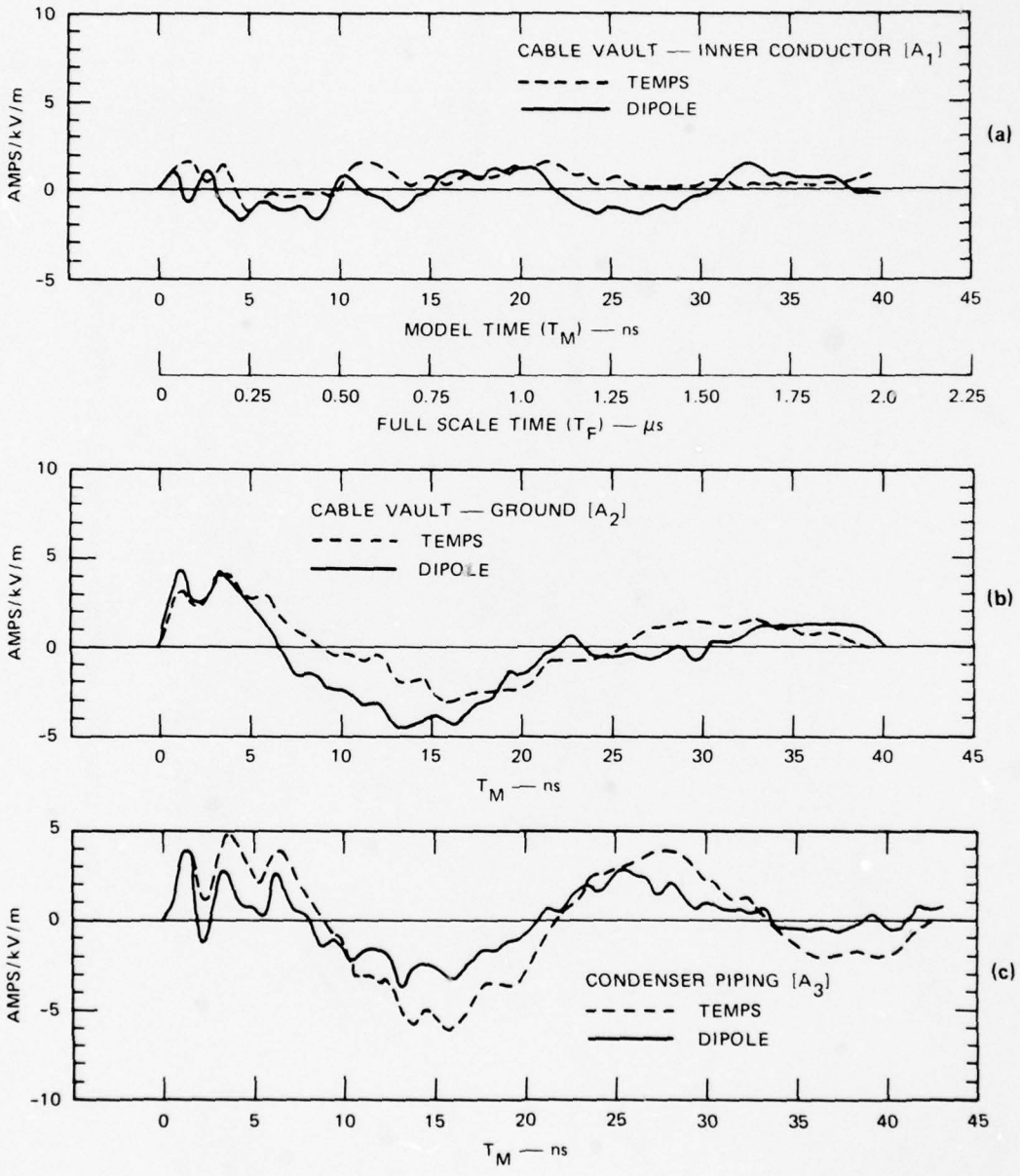

FIGURE A-5 PENETRATION CURRENTS FOR TEMPS AND DIPOLE ILLUMINATION OF POLK CITY SWITCHING COMPLEX (AOA = 70°, AOI = 23°)

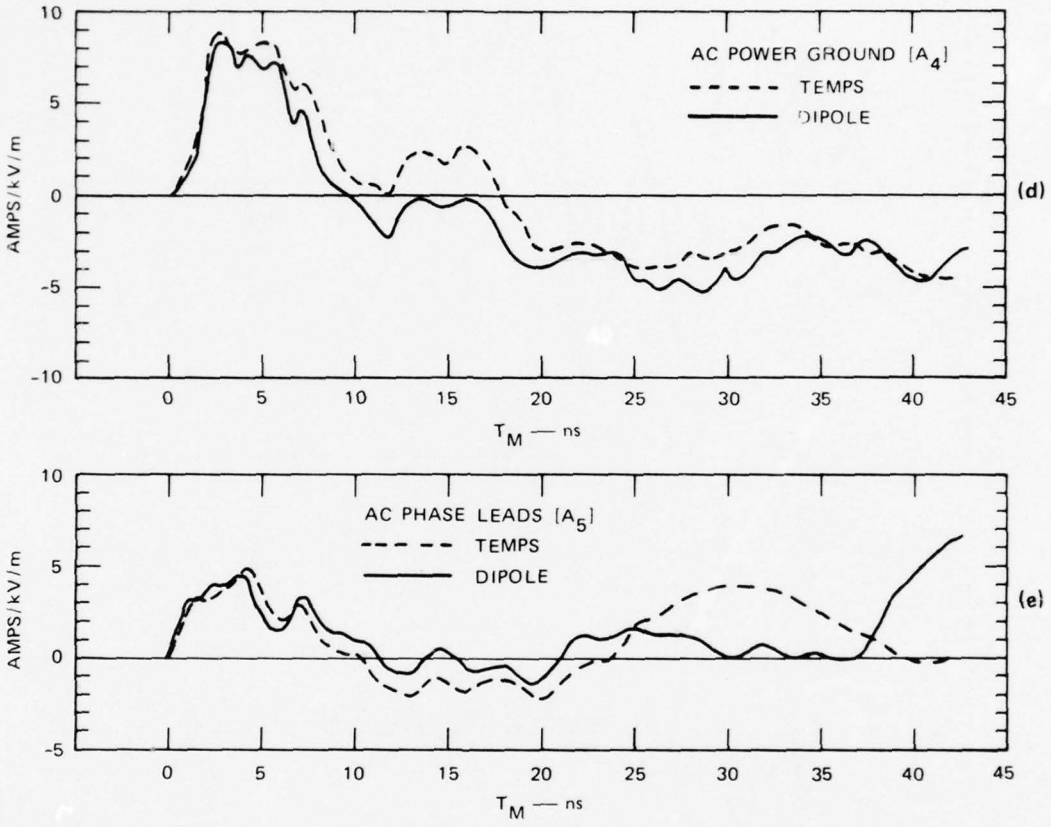

FIGURE A-5 (Continued)

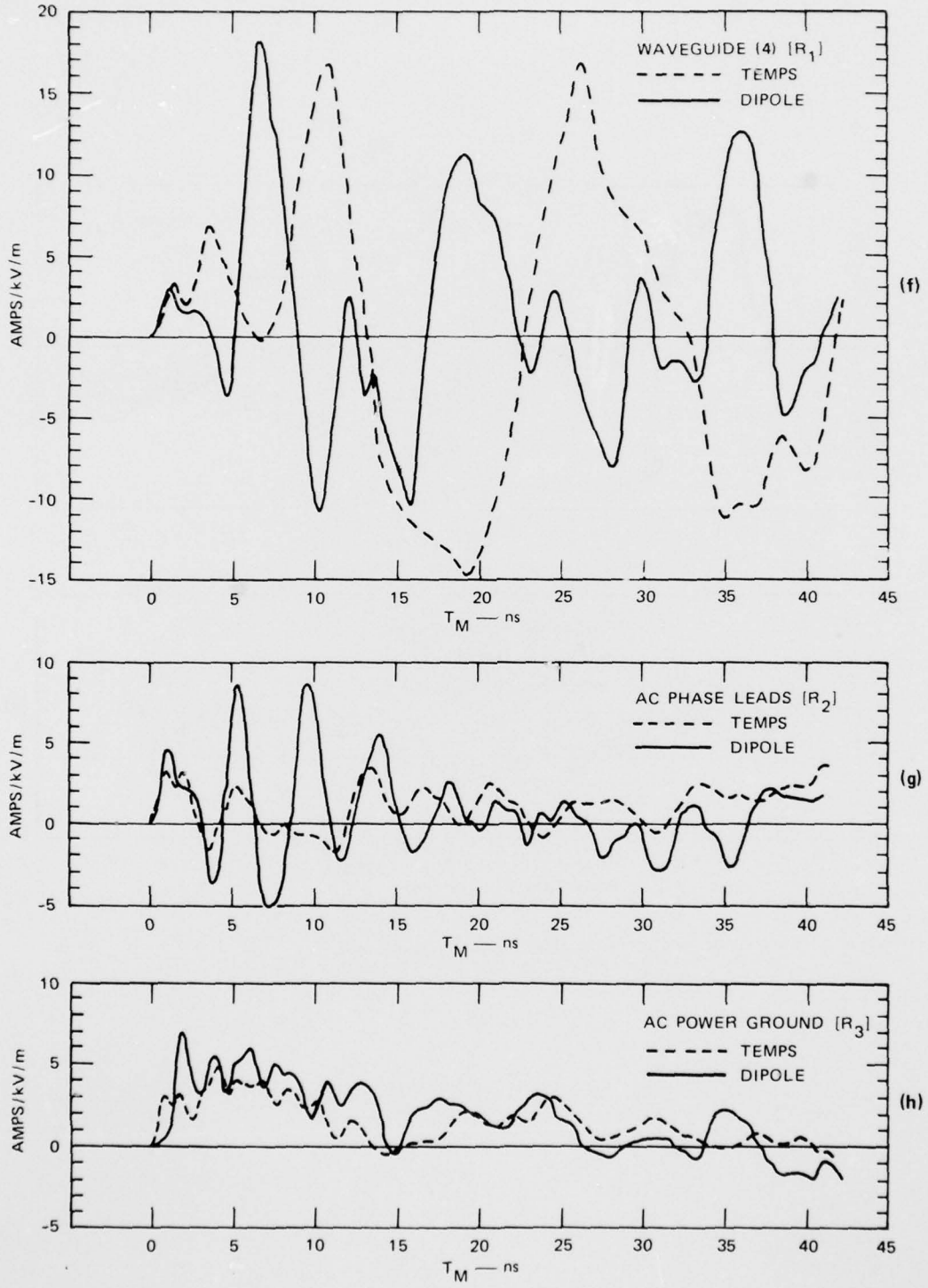

FIGURE A-5 (Concluded)

Figure A-5 shows that through the first 10 ns of model time, the peak magnitude of the envelopes amplitudes are well within 3 dB (exception: the microwave building phase leads). In fact, the waveshapes during that time period have almost identical variations in time of peaks and troughs. An exception is the waveguide, where TEMPS simulated the amplitude well, but produced a phase shift relative to the dipole antenna. This was attributed to fringe field illumination of the tower and waveguide with significant vertical field components. The peak magnitudes excited by the TEMPS model on the microwave building model phase leads were low (by about 3 dB) compared with the dipole antenna excitation. This was attributed to nonuniformity effects and fringe field illumination produced by the TEMPS model. Those effects were much more severe for the TEMPS model than for the dipole antenna model.

It was concluded that radiating dipole antenna simulators, such as TEMPS, that are resistively terminated and close to the ground adequately simulate HEMP excitation. When the structure being excited is sensitive to vertical polarization, there are some discrepancies in waveshape, but the amplitude of the excitation is nearly correct.

Appendix B

MODEL FACILITY SOIL CONDUCTIVITY

B.1 INTRODUCTION

The soil in which the facility and simulator model was located was salted with sodium chloride to a depth of 0.9 m (3 ft), so that when the soil was watered, a suitable value of soil conductivity was obtained. The soil from locations around the facility and simulator was sampled about once a week, using a four-electrode Wenner bridge configuration. The plastic bubble sheltering the modeling range prevented rapid evaporation and rain from controlling the soil conductivity.

To substantiate the model range measurements when the Wenner configuration was used, samples of soil were placed in a parallel plate geometry in the laboratory. The measurements of the resistance of the soil indicated that the conductivity was essentially the same for the laboratory control as it was for the model range.

B.2 MEASUREMENT OF SOIL CONDUCTIVITY

Extensive investigation has shown that electrical resistance of a soil can be measured by noting the voltage required to force a measured current through it. To avoid the interference of contact potentials, low-frequency alternating current is generally used, as it was in the model.

The soil in the immediate vicinity of the electrodes, where the current is concentrated, provides a greater part of the resistance measured than does the surrounding soil. Thus, local inhomogeneities have a significant effect on the measured value of resistivity. Because of this, it is common practice to use four electrodes as shown in Figure B-1. The outer two electrodes introduce the current into the ground. Voltage is measured between the inner two electrodes. If the

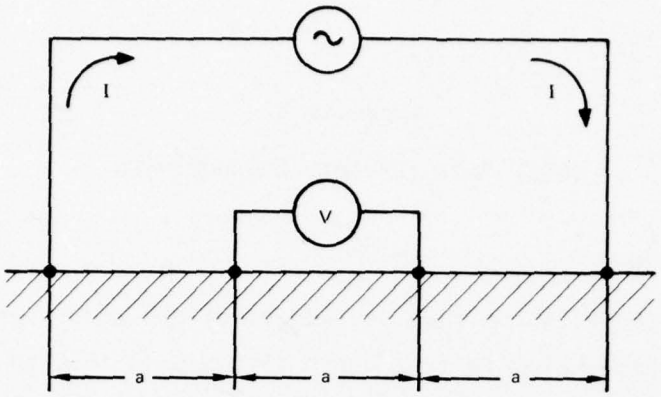

FIGURE B-1 FOUR-ELECTRODE ARRANGEMENT FOR MEASURING SOIL CONDUCTIVITY

electrodes are equally spaced, the configuration is called a Wenner configuration and the mathematics is simplified. The potential (voltage) drop measured is that between the two equipotential surfaces on which the inner electrodes lie. This is equivalent, in effect, to increasing the area of the current electrodes to that of the equipotential surfaces. With this configuration the effect of contact resistance is largely eliminated.

Soil conductivity, σ (the inverse of soil resistance), is given for the Wenner configuration as $\sigma = I/2\pi aV$, where I is the measured current, V is the measured voltage, and a spacing a of 0.1 m was used. Measurements are made at an audio frequency of 10 kHz so that the soil is a good conductor ($\sigma/\omega\varepsilon \gg 1$).

B.3 LABORATORY MEASUREMENT OF SOIL CONDUCTIVITY

For this investigation, the soil conductivity was also measured in a plastic cylinder 11.4-cm long and 5 cm in diameter. The plastic cylinder was filled with soil, which could be compressed with a brass screw cap to as little as 7.6 cm. The measurement of the resistance of the soil was accomplished by connecting a signal generator across the soil container with a known resistor, in series. The resistance,

R_s, of the soil was determined by measuring the voltages, V_s, across the soil container and across the known series resistor, R_K. Thus, the resistance of the soil was $R_s = V_s R_K / V_K$. Measurements showed that the same value of resistance was obtained over a wide range of frequencies above 1 kHz. Only at very low frequencies of about 100 Hz, where polarization effects occur, did the resistance value start to change. The high-frequency limit was restricted by the relationship $\sigma/\omega\varepsilon > 1$, where σ is the soil conductivity, ω is the angular frequency of the signal generator, and ε is the dielectric constant of the soil. The high-frequency restriction ensures that the soil behaves as a conductor and not as a dielectric. The conductivity in s/m determined by $\sigma = 4\ell/(\pi d^2 R_s)$, where ℓ is the length of the compressed soil in meters, and d is the diameter of the cylinder in meters.

B.4 SOIL CONDUCTIVITY FOR MODELING

In the model range, the conductivity was measured between 0.35 and 0.62 s/m. This corresponds to a full-scale conductivity between 0.007 and 0.012 s/m, which is typical of dry average soil.

Conductivity at specific locations in the model range was essentially constant to within 10% of its nominal value. However, because the model range is not perfectly homogeneous and isotropic, a variability of up to 2 to 1 existed between all locations. Table B-1 lists some nominal conductivities at mapping locations shown in Figure 2 of the main text.

B.5 VARIABILITY OF RESPONSE CAUSED BY SOIL CONDUCTIVITY

Model measurements indicated that the peak-current response to an EMP illumination varies according to whether the structure is above or below ground. For structures considered to be above-ground, such as antenna, waveguide, antenna tower leg, ac phase lines, and building roofs and walls, the measured peak-current variation with soil conductivity was small; the largest variation was 30%. For the above structures, peak current increased as the soil conductivity changed from dry (0.2 s/m) to wet (1 s/m). For structures below ground, such

Table B-1

MODEL RANGE SOIL CONDUCTIVITIES

Location	Conductivity (s/m)
Model facility center (X = 0, Y = 0)	0.57
TEMPS center (X = 0, Y = 1.5 m)	0.44
TEMPS termination (X ≈ 3 m, Y ≈ -1.5 m)	0.41
3-m wire appendage (X = +33 m, Y = 0)	0.47
Location (X = 0, Y = -4.5 m)	0.62
Location (X = 1.5 m, Y = 1.5 m)	0.58
Location (X = 1.5 m, Y = -3 m)	0.60

as cables and pipes, the measured peak current decreased by a slightly larger amount; the largest decrease was about 40%. Peak current decreased as the soil conductivity changes from 0.2 s/m to 1 s/m. For the average soil conductivity of 0.35 to 0.65 s/m used throughout the test, the variation in peak-current response amplitude varied less than 1 dB.

Appendix C

MODEL FACILITY INSTRUMENTATION SYSTEM

C.1 DESCRIPTION

The instrumentation system in Figure C-1 consists of the following components, taken in order from the signal end to the final data output: sensing device (current transformer or field sensor), sensor cable, signal cable, HP 1817A sampler, HP 183A oscilloscope mainframe with HP 1815B time base, and HP 136A X-Y recorder.

A special sensor unit is required for measuring tangential magnetic field. This sensor unit is a slot that is short-circuited at its center by a wire. The sensing device (current transformer) measures the short-circuit current flowing through the wire, except that some load impedance is transformed back into the short-circuited wire. The slot is calibrated, using a known magnetic field.

The sensor units are SRI-designed and built, and consist of: a 6.4-cm (2.5-in.) diameter brass outer plate with a slot, a 6.4-cm (2.5-in.) diameter inner retaining ring, hardware for fastening the outer plate to the ring, and hardware for fastening the wire to the slot. To use the unit, a 5-cm (2-in.) diameter hole is cut in the metal surface. The metal surface is then clamped between the outer plate and inner ring, using the fastening hardware. The slot can be rotated by loosening the hardware, rotating the entire unit, and then fastening the hardware, without requiring removal of the unit. Since the slot is a directional device, rotation of it permits measurement of magnetic field direction, or measurement of orthogonal components.

The slot width is 1 cm (3/8 in.), to accommodate a CT-1 transformer, and is 4-cm (1-9/16-in.) long. The present slots are actually butterfly-shaped rather than rectangular--i.e., tapered at the ends to make them

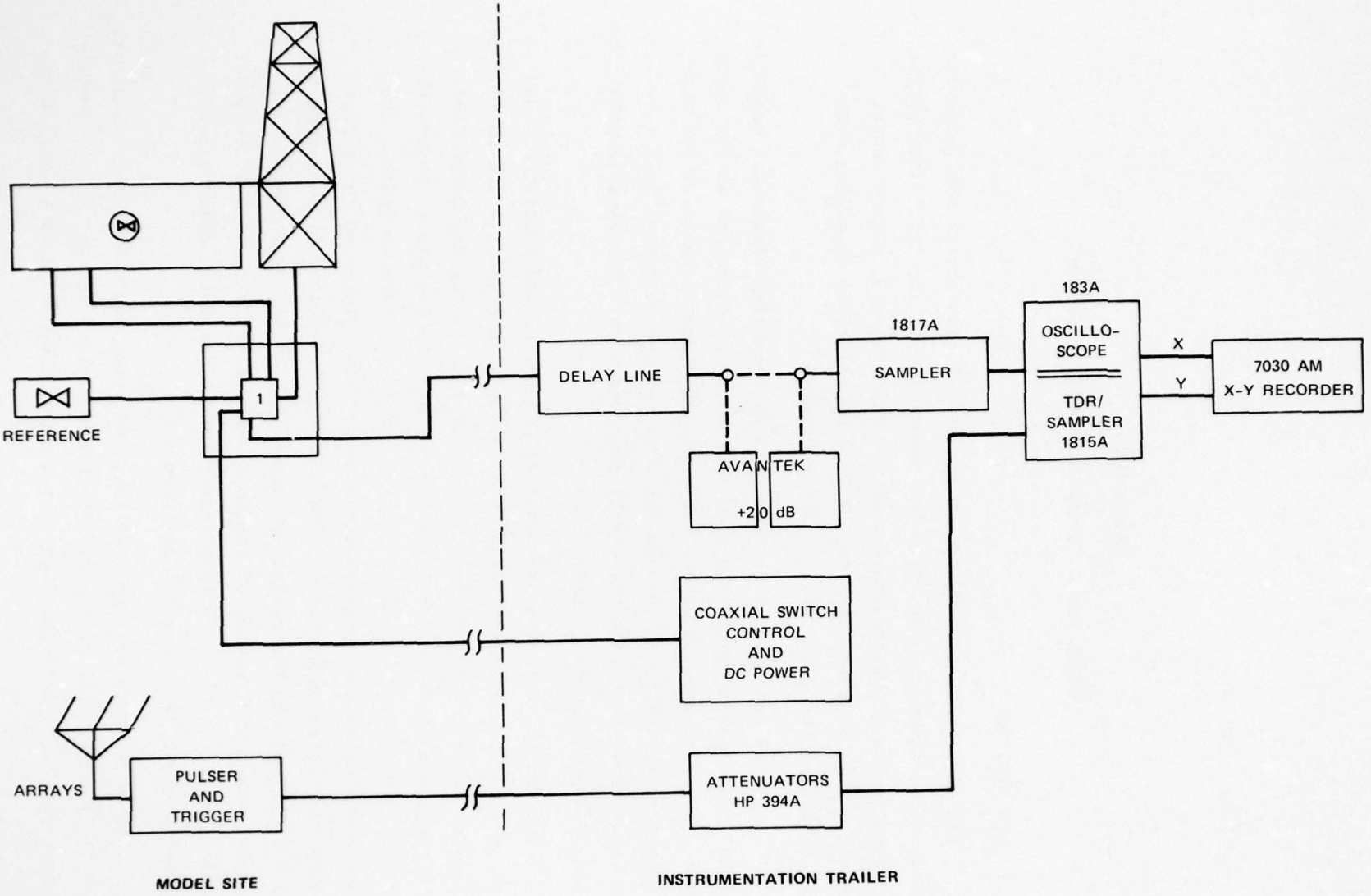

FIGURE C-1 MODELING FACILITY INSTRUMENTATION SYSTEM

more broadband. The slots retain the 1-cm (3/8-in.) width only over the central 1.3 cm (1/2 in.), and then taper out to 1.9 cm (3/4 in.) at the ends.

The principal sensing devices used are Tektronix CT-1 current transformers. These have a sensitivity of 5 mV/mA into a 50-Ω load, rise-time less than 350 ps, and aberrations of less than 5% during the first 5 ns. The lower frequency limit is 35 kHz (3 dB point). The decay of the CT-1 is less than 1% over the first 50 ns. The insertion impedance with a 50-Ω termination is 1 Ω shunted by 5 μH. These were used for all wire current measurements, and also with the sensor units.

When the CT-1 is used with the sensor units, the insertion impedance of the CT-1 loads the slot inductance so the decay-time of the sensor unit is about 13 to 14 ns. This is slower than the slowest decay-time of the pulses to be radiated (about 8 ns), but is fast enough to cause the sag of a rectangular pulse over the anticipated 20-ns test time. The sag caused by this L/R decay-time can be compensated for by analytical treatment of the data. However, the L/R decay-time distorts the waveforms as viewed in real time during testing.

The sensor-unit decay-time can be increased by decreasing R or by increasing L. Both methods reduce the sensitivity below 5 mV/mA. After considering several methods of modifying slot inductance to preserve rise time while extending decay time, it was decided after observing the shortness of the waveforms in the measurements that the 20-ns decay-time can be tolerated.

The sensor cable is a Tektronix P6040 cable, 0.4-m (1.5-ft) long, which connects to the CT-1. It is a miniature cable that provides a delay of 2.4 ns, has a rise-time of less than 200 ps, and has 0.7-dB loss at 1 GHz. It has a GR-874 output connector.

A GR-874-to-type-N between-series adapter is used to connect the sensor cable to a coaxial switch, Transco model 136C00100. The coaxial switch is SP6T, solenoid-actuated. At 1 GHz, the nominal VSWR of the coaxial switch is less than 1.20, and the insertion loss is less than 0.15 dB. The isolation is greater than 60 dB between channels.

The signal cable is a special low-loss cable, which combines the functions of signal transmission path plus delay cable needed for properly triggering the sampling oscilloscope. The signal cable consists of 37.5 m (110 ft) of Aluminispline cable (Times Wire and Cable Co., model AS-5078PJ). This is 50-Ω, solid-outer-sheath, splined dielectric cable with a velocity of propagation 90% of the speed of light, and having 1.65-dB loss at 1 GHz.

The model is essentially a rectangular metal box about 89-cm (35-in.) long, 61-cm (24-in.) wide, and 22.8-cm (9-in.) high, buried to a depth of 10.1 cm (4 in.). The signal cable runs from the model to the instrumentation van. To avoid pickup on the signal cable from flowing only to the building, or the converse, the signal cable is taken out through the bottom of the model. A 5-cm (2-in.) diameter brass pipe, 10.1-cm (4-in.) long projects downward from the bottom of the building for about 9 cm (3.5 in.). The pipe prevents model currents from directly flowing into the building aperture--instead, they must flow downward along the pipe and then back up along the inside of the pipe. Because the building currents have a flow path of less impedance elsewhere, little current will take this path and the pipe acts as a choke section. The signal cable is floating with respect to the model--i.e., the signal cable has no conducting connection to the model. Therefore, a high impedance exists between the outer conductor of the signal cable, or the shields of the control cables, and the model. Only capacitive coupling exists. Finally, the signal drops about 17.8 cm (14 in.) below the building before becoming horizontal (bent in a quarter circle). The signal cable, therefore, run 45.6 cm (18 in.) below the soil surface (18.3-cm or 60-ft full scale), which further minimizes any electrical pickup on the cable. This method of taking the signal cable out of the model minimizes any disturbance of the signals to be measured.

The signal cable is connected to an HP 1817A sampler at the instrumentation van. The sampler is used with an HP 183A oscilloscope mainframe equipped with an HP 1815B timebase. An HP-supplied cable connects the sampler to the timebase, which plugs in to the bottom of the mainframe.

The specifications for the above sampling system are: rise-time less than 28 ps, 50-Ω input impedance, low-frequency distortion less than 3%, normal noise less than 8-mV or 10-mV/division scales and above, plus a signal-averaging function that reduces noise and jitter by 2:1.

The 1815B has recorder outputs connected to an HP 136A X-Y recorder. Although the measured data can be photographed, it is generally taken as X-Y pen recordings on standard 8-1/2x11-in. graph paper.

C.2 SPECIFICATIONS

C.2.1 Rise-Time

The system rise-time is made up of three major components: the sensor rise-time, the transmission-system rise-time and the detection-system rise-time. The sensor and detection rise-times correspond nearly to a ramp response as a function of time. However, the transmission-system rise-time is a complementary error-function response, except for minor deviations caused by dielectric losses.

For a coaxial-cable transmission system, in which skin-effect losses are solely responsible for attenuation, the response to a unit amplitude step function is

$$E_{out} = 1 - \text{erf } bL/(2T)^{1/2} \qquad \text{(C-1)}$$

where $T = t - \tau$, τ is the transit time of the system; L is the cable length (m); b is a constant for the cable, 1.45×10^{-8} A m^{-1} $s^{1/2}$; A is cable attenuation at 1 GHz, dB/30.5 m (100 ft); and erf is the error function. Quantity bL is proportional to the total attenuation of the cable in dB.

The response is not a linear ramp in time. Instead, the response is very rapid initially, and then goes to unity very slowly. A characteristic time for the system is T_o, the time to rise to 50% of the peak amplitude.

The times to reach various percentages of the unit step amplitude are given below:

X (%)	0 to X Rise-Time (T_o)
10	0.17
20	0.28
50	1.00
70	3.1
80	7.3
90	29
95	110

The 10-to-90% rise-time is 28.83 T_o, but the 10-to-80% rise-time is 7.13 T_o, about 1/4 the 10-to-90% rise-time.

When pulses of other shapes are transmitted through a cable, the resultant pulse shape must be obtained either graphically, or with a convolution integral. For rectangular pulses having a ramp front whose 10-to-90% time is larger than T_o, the resultant pulse shape is approximately the initial pulse shape until it crosses the complementary error-function curve; then the resultant pulse shape follows the complementary error-function shape.

The time, T_o, is given by

$$T_o = 4.56 \times 10^{-16} (AL)^2 = (bL/0.6745)^2 \quad . \qquad (C\text{-}2)$$

Note that T_o varies directly as the square of the total attenuation of the length of cables. Therefore, when cables are in series, the overall T_o is

$$T_o = \left[\sum_{j=1}^{n} \left(T_{o_j} \right)^{1/2} \right]^2 \quad . \qquad (C\text{-}3)$$

The system rise-time specifications are:

- Detection system, 28 ps (10-to-90%).
- Sensor, CT-1: 350 ps (10-to-90%), including P6040 cable, P6040 sensor cable alone, T_o = 2.08 ps, 10-to-90%, time = 60 ps.
- Signal cable: T_o = 12.4 ps, 10-to-90%, time = 358 ps.
- RG 9/U cable: T_o = 0.037 ps, 10-to-90%, time = 1.06 ps.
- Various connectors and coaxial switch: 10-to-90% time of less than 1 ps (estimated).

The CT-1 sensor response limits the system rise-time until the complementary error-function response is reached. Since the CT-1 rise-time is much longer than the various T_o's, or an appropriate summation of them, the response to a step function with a ramp front will be to reach the 90% amplitude at about 350 ps, then slowly climb to 100% climb amplitude. The estimated overall instrumentation system rise-time is 400 ps.

C.2.2 Decay Time

Only the magnetic-field-sensor-unit/sensing-device combination has a significant decay time. The exponential decay time for this combination unit is 13 ns.

C.2.3 Transmission-System Loss at 1 GHz

The transmission-system loss at 1 GHz is determined as follows:

P6040 cable	0.7 dB
Signal cable	1.65 dB
RG 9/U cable	0.09 dB
Coaxial switch	0.15 dB
Adapters (est.)	0.10 dB
Total loss	2.7 dB

AD-A067 280 SRI INTERNATIONAL MENLO PARK CA F/G 20/14
EMP SIMULATOR - SITE INTERACTION.(U)
MAR 78 A L WHITSON, W E SCHARFMAN DNA001-76-C-0026
UNCLASSIFIED DNA-4553F NL

2 OF 2
AD
A067280

END
DATE
FILMED
6-79
DDC

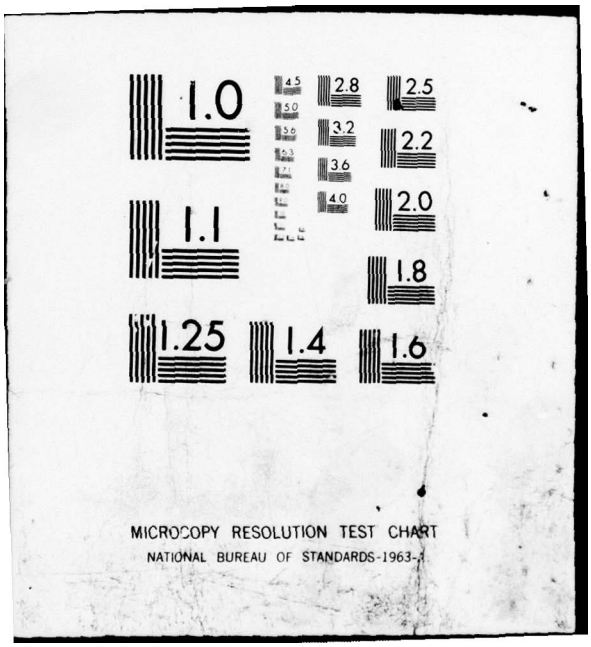
1.0
1.1
1.25
1.4
1.6
1.8
2.0
2.2
2.5
2.8
3.2
3.6
4.0
4.5
5.0
5.6
MICROCOPY RESOLUTION TEST CHART
NATIONAL BUREAU OF STANDARDS-1963-A

C.2.4 Delay Time

The HP 1817A sampler and HP 1815B time base require a minimum 55-ns delay between the trigger and signal inputs. Reliable triggering, with some baseline preceding the signal arrival, requires about 70-ns delay.

The following system delays are provided:

CT-1	0.4 ns	
P6040 cable	2.4 ns	
RG 9/U cable	1.5 ns	
Signal cable	124. ns	
Coaxial switch and adapters	1. ns	(est.)
Total system delay	129.3 ns	

Appendix D

EXCITATION PREDICTIONS FOR HEMP

The excitation current at the end of the 7.5-m RIGHT wires for broadside, horizontal polarization HEMP (normalized to peak incident electric field E_o) have been calculated and plotted. The calculations were performed to 25-to-30 ns (model time). The overhead wire short-circuit current waveform repeats with a period of 50.8 ns if attenuation is neglected, as it is in the calculated results. The RIGHT buried-wire current eventually sags to zero; it does not repeat.

The calculated current was for a bare buried wire. At an approximate time of 30-to-40 ns, the current should swing negative for insulated wire. The differences between the insulated wire and the bare wire are fairly trivial until the end effects show up at 30-to-40 ns.

D.1 ABOVEGROUND WIRE, BROADSIDE HORIZONTAL POLARIZATION

The current enclosed in the RIGHT aboveground wire is obtained from Vance,[15] Eq. (11.4-35), for the following conditions:

Soil conductivity, σ = 0.55 mho/m

Wire height, h = 6 in. (15 cm)

Wire diameter, 2a = 0.812 mm

Wire length, l = 25 ft (7.62 m)

Angle of incidence: elevation, $\psi = 20.8°$
azimuth, $\varphi = 90°$

Decoy time constant of incident pulse, τ = 4.1 ns.

For a period $t_o = (2h \sin \psi)/C$, where C is the speed of light, the incident wave alone is acting on the wire, and the induced current in the wire is

$$\frac{i(t)}{E_o} = \frac{e\tau D}{Z_o} (1 - e^{-t/\tau}) \quad (t < t_o) \qquad \text{(D-1)}$$

where D is the directivity function given by

$$D = \frac{\sin \varphi}{1 - \cos \varphi \cos \psi} = 1.0 \qquad \text{(D-2)}$$

and Z_o is the characteristic impedance of the wire above ground, given by

$$Z_o = \frac{M}{2\pi} \ln \frac{2h}{a} = 356\ \Omega \quad . \qquad \text{(D-3)}$$

For the wire height and angle of incidence shown, the clear-time $t_o = 0.36$ ns.

The normalized current in Eq. (D-1) above is the response to an exponential incident pulse of the form

$$E(t) = E_o e^{-t/\tau}$$

which is approximately the form of the pulse delivered by TEMPS (see Figure 11.5-10 of Patrick and Soo Hoo[14]). As is evident in Eq. (D-1), the wire current is normalized to amplitude E_o. That part of the response defined by Eq. (D-1) is the fast-rising portion lasting 0.36 ns in Figure D-1.

At $t = t_o$, the wave reflected from the ground arrives at the wire, and the induced current then has the form

$$\frac{i(t)}{E_o} = \frac{c\tau D}{Z_o} \left[\left(e^{t_o/\tau} - 1 \right) e^{-t/\tau} + 2\sqrt{\tau_e/\tau} \sin \psi \ f(t') \right] \quad (t < t_o < \ell/c) \qquad \text{(D-4)}$$

where $\tau_e = \varepsilon_o/\sigma$ is the soil time constant, and

$$f(t') = \frac{2}{\pi} e^{-t'/\tau} \int_o^{\sqrt{t'/\tau}} e^{u^2} \, du \qquad \text{(D-5)}$$

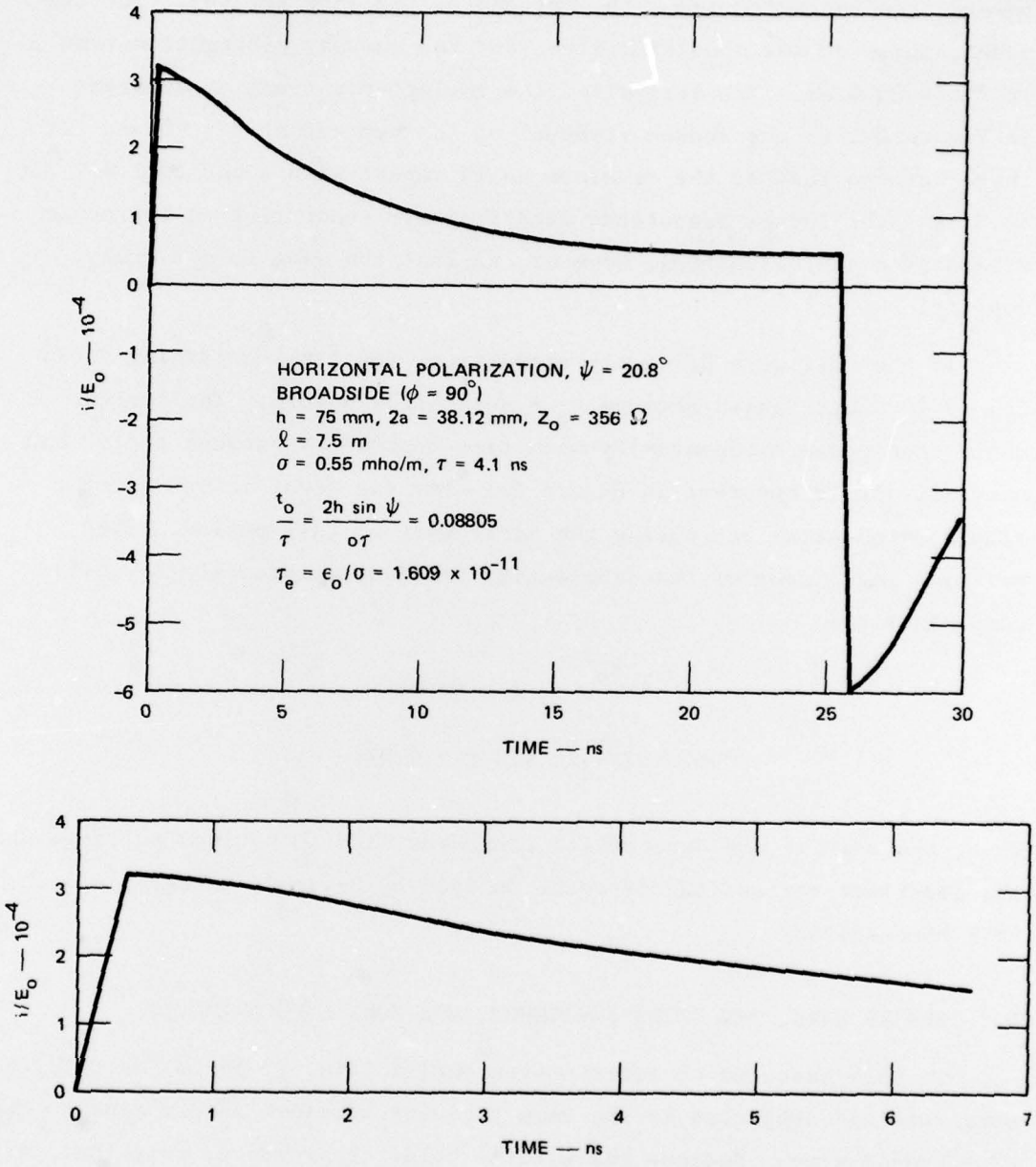

FIGURE D-1 PREDICTED CURRENT IN ABOVEGROUND RIGHT WIRE

in which $t' = t - t_o$. In the time ℓ/c it takes for a wave to propagate from one end of the line to the other, the induced current propagating toward, and reflected from, the far end of the line arrives. For the model, this end was open-circuited, and the one-way propagation time is $\ell/c = 25.4$ ns. The arrival of the reflected current is apparent in Figure D-1 by the sudden reversal of the current at t = 25 ns. If there were no losses, the waveform would repeat with a period $T = 2\ \ell/c = 50.8$ ns. The losses associated with finitely conducting soil produce attenuation and distortion, however, so that the wave is not truly repetitious.

If the soil were perfectly conducting, the term containing τ_e in Eq. (D-4) would vanish because $\tau_e = \varepsilon_o/\sigma$ becomes zero. The current would then decay exponentially with time-constant τ between $t = t_o$ and $t = \ell/c$. It is apparent in Figure D-1 that the decay is not quite a simple exponential one during the first part of this period. The relative magnitudes of the exponential and Dawson integral (Eq. D-5) components are

$$e^{-t_o/\tau} - 1 = 0.084$$

$$0.61 \times 2\sqrt{\tau_e/\tau}\ \sin\psi = 0.027 \quad .$$

Thus, the peak of the exponential component is 3 to 4 times as large as the imperfect reflection component defined by Dawson's integral and the soil conductivity.

D.2 BURIED WIRE, BROADSIDE INCIDENCE, HORIZONTAL POLARIZATION

In this case, we consider a wire buried 1-in. (2.54-cm) deep in the same soil and subjected to the same incident waveform as pertains to the aboveground wire. Because the wire is below the surface, only that part of the wave that propagates into the soil interacts with it. The short-circuit current at the end of the cable is given by Vance,[15] Eq. (11.5.-20) for $[\ln(\sqrt{2\delta/\gamma_o}a] \approx 10$. In our case, $\ln(\sqrt{2\delta/\gamma_o}a) \approx 5.8$, so we will correct the results by a factor 10/5.8. The short-circuit current is then

$$\frac{i(t)}{E_o} \approx 10^6 \left(\frac{10}{5.8}\right) \sqrt{\tau_e \tau}\, D_6(\psi,\psi)\, f(t,p) \quad (t < \ell/v) \tag{D-6}$$

where

$$D_6(\psi,\psi) = \sin\psi \sin\psi = 0.355$$

and

$$f(t_q p) = \frac{2}{\pi} e^{-t/\tau} \int_o^{\sqrt{t/\tau}} e^{-p/u^2} e^{u^2}\, du \tag{D-7}$$

in which

$$p = \frac{1}{4\tau\tau_e} \left(\frac{d}{c}\right)^2$$

where d is the depth of burial of the wire.

In the experimental model, the wire dimensions were:

Diameter, 2a = 31.96 mils = 0.812 mm

Depth of burial, d = 1 in. = 2.54 cm

Length, l = 25 ft = 7.62 m.

The depth-of-burial factor is then p = 0.027, and the peak value of the modified Dawson integral of Eq. (D-7) is about 0.5. The normalized peak current is then

$$\frac{i(t)}{E_o} \text{ peak} \approx 10^6 \frac{10}{5.8} \cdot \sqrt{\tau_e \tau} \cdot 0.355.0.5$$

$$\approx 7.5 \times 10^{-5} \text{ A/V/M} \quad .$$

The current waveform is shown in Figure D-2, which is taken from Figure 11.5-13 of Vance.[15]

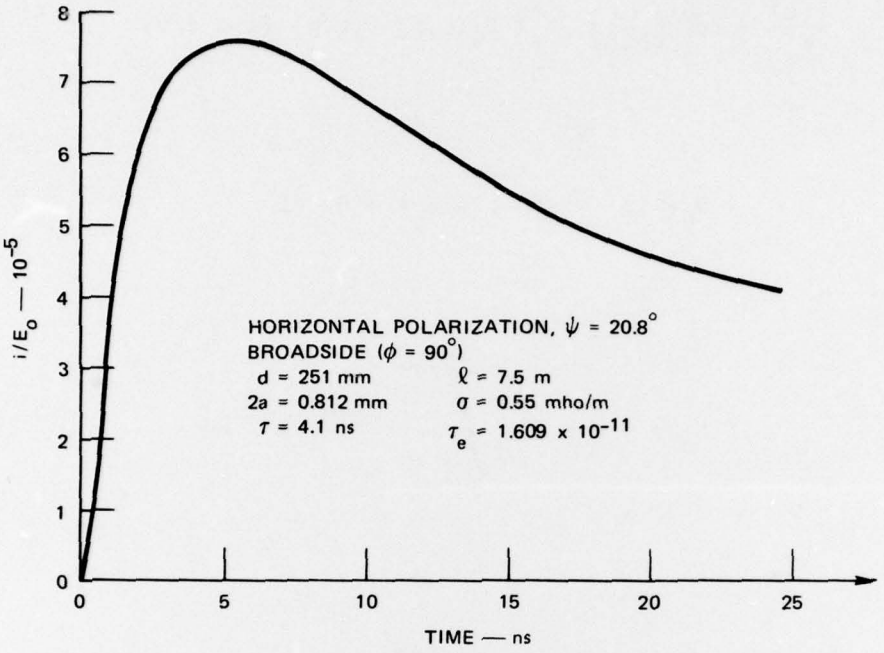

FIGURE D-2 PREDICTED CURRENT INDUCED IN BURIED RIGHT WIRE

At $t = \ell/v$, a reflection from the far end of the cable arrives at the terminals. For an insulated cable, v is often of the order c/10, and $\ell/v \approx 10\ \ell/c$ = 250 ns. In addition, for the buried cable, the attenuation is large; thus the reflected wave does not cause a sudden change as was observed for the aboveground wire in Figure D-1. Instead, the reflection from the open circuit manifests itself as a faster-than-normal decay and a zero crossing in the vicinity of 250 ns. In the vicinity of the current peak shown in Figure D-2, there is little difference between the current in the bare wire and that in the insulated wire (for the length of wire used in the experiment). For the bare wire, the reflection is even less distinct and the attenuation is even greater than for the insulated wire. These factors would make the reflection from the far end of a bare wire even less noticeable than the reflection from the end of an insulated wire.

DISTRIBUTION LIST

DEPARTMENT OF DEFENSE

Assistant to the Secretary of Defense
Atomic Energy
ATTN: Executive Assistant

Defense Civil Preparedness Agency
ATTN: Admin. Officer
ATTN: RE (EO)
ATTN: PO (SE)

Defense Communication Engineer Center
ATTN: Code R123
ATTN: Code R400
ATTN: R720, C. Stansberry

Defense Documentation Center
12 cy ATTN: DD

Defense Intelligence Agency
ATTN: RDS-3A

Defense Nuclear Agency
ATTN: RAEV
ATTN: RATN
ATTN: DDST
ATTN: STVL
4 cy ATTN: TITL

Field Command,
Defense Nuclear Agency
ATTN: FCSPM, J. Smith
ATTN: FCLMC
ATTN: FCPR

Field Command,
Defense Nuclear Agency
Livermore Division
ATTN: FCPRL

Interservice Nuclear Weapons School
ATTN: TTV

Joint Chiefs of Staff
ATTN: J-3

Joint Strat. Tgt. Planning Staff
ATTN: NRI-STINFO, Library
ATTN: JSAS

National Communications System
Department of Defense
ATTN: NCS-TS, D. Bodson

National Security Agency
ATTN: TDL
ATTN: S232, D. Vincent
ATTN: R-52, O. Van Gunten

Under Secretary of Defense for Rsch. & Engrg.
ATTN: Strategic and Space Systems (OS)

DEPARTMENT OF THE ARMY

BMD Systems Command
Department of the Army
ATTN: BMDSC-AOLIB

Deputy Chief of Staff for Rsch. Dev. & Acq.
Department of the Army
ATTN: DAMA-CSS-N, N. Barron

ERADCOM Technical Support Activity
Department of the Army
ATTN: DELET-IR, E. Hunter
ATTN: DELSD-L, W. Werk
ATTN: DRDCO-COM-ME, G. Gaule
ATTN: DELCS-K, A. Cohen

Fort Huachuca
Department of the Army
ATTN: CCH-PCA-TR

Harry Diamond Laboratories
Department of the Army
ATTN: DELHD-N-EM-C
ATTN: DELHD-N-EME Lab.
ATTN: DELHD-N-EMD
ATTN: DELHD-N-RB
ATTN: DELHD-N-EME
ATTN: DELHD-N-EMB
ATTN: DELHD-N-TI
ATTN: DELHD-N-RCC
ATTN: DELHD-N-EMA
ATTN: DELHD-N-TF
ATTN: DELHD-N-NP
ATTN: DELHD-N-TD
2 cy ATTN: DELHD-N-RBC

U.S. Army Armor Center
ATTN: Technical Library

U.S. Army Ballistic Research Labs.
ATTN: DRSTE-EL
ATTN: DRDAR-BLB, W. Vanantwerp
ATTN: DRDAR-BLE

U.S. Army Communications Command
Combat Development Division
ATTN: ATSI-CD-MD

U.S. Army Communications Command
ATTN: CC-LOG-LEO
ATTN: CC-OPS-OS
ATTN: CC-OPS-PD

U.S. Army Communications Sys. Agency
ATTN: CCM-RD-T CCM-AD-SV

U.S. Army Electronics Rsch. & Dev. Command
ATTN: DRDCO-SEI

U.S. Army Engineer Division, Huntsville
ATTN: HNDED-SR

DEPARTMENT OF THE ARMY (Continued)

U.S. Army Intelligence & Sec. Command
ATTN: Technical Library

U.S. Army Materiel Sys. Analysis Activity
ATTN: DRXSY-PO

U.S. Army Missile R&D Command
ATTN: DRDMI-EAA
ATTN: DRDMI-TBD
ATTN: DRCPM-LCEV, H. Henriksen
ATTN: DRCPM-PE-EA, W. Wagner
ATTN: DRCPM-PE-EG, W. Johnson

U.S. Army Test and Evaluation Command
ATTN: DRSTE-FA

U.S. Army Training and Doctrine Command
ATTN: ATORI-OP-SW

White Sands Missile Range
Department of the Army
ATTN: STEWS-TE-AN, J. Okuma

DEPARTMENT OF THE NAVY

Naval Construction Battalion Center
Civil Engineering Laboratory
ATTN: Code L08A

Naval Air Systems Command
ATTN: AIR 350F

Naval Electronic Systems Command
ATTN: PME 117-215

Naval Ocean Systems Center
ATTN: Code 8123, S. Lichtman
ATTN: Code 54, C. Fletcher

Naval Ordnance Station
ATTN: Standardization Division

Naval Postgraduate School
ATTN: Code 1424

Naval Research Laboratory
ATTN: Code 6701, J. Brown
ATTN: Code 2627, D. Folen
ATTN: Code 6750
ATTN: Code 6624

Naval Ship Engineering Center
ATTN: Code 6174D2, E. Duffy

Naval Surface Weapons Center
White Oak Laboratory
ATTN: Code F30
ATTN: Code F32, E. Rathbun
ATTN: Code R43, L. Libelo

Naval Weapons Center
ATTN: Code 233

Naval Weapons Evaluation Facility
ATTN: Code AT-6

Naval Weapons Support Center
ATTN: Code 11E

DEPARTMENT OF THE NAVY (Continued)

Office of the Chief of Naval Operations
ATTN: Op-981N1

Strategic Systems Project Office
Department of the Navy
ATTN: NSP-27334
ATTN: NSP-230, D. Gold
ATTN: NSP-2701, J. Pitsenberger
ATTN: NSP-43

DEPARTMENT OF THE AIR FORCE

Aeronautical Systems Division, AFSC
ATTN: ENFTV
ATTN: ASD-YH-EX

Aerospace Defense Command
Department of the Air Force
ATTN: DEEDS, J. Brannan

Air Force Weapons Laboratory, AFSC
ATTN: SUL
ATTN: ELP
ATTN: ELA, J. Castillo
ATTN: NXS
ATTN: NT
ATTN: CA
ATTN: ELXT
ATTN: EL, C. Baum
ATTN: ELT, W. Page

Air University Library
Department of the Air Force
ATTN: AUL-LSE-70-250

Deputy Chief of Staff
Research, Development, and Acq.
Department of the Air Force
ATTN: AFRDQSM

Electronic Systems Division, AFSC
ATTN: YSEA

Foreign Technology Division, AFSC
ATTN: TQTD, B. Ballard

Air Logistics Command
Department of the Air Force
ATTN: MMEDO, L. Kidman
ATTN: R. Blackburn
ATTN: MMETH, P. Berthel

Rome Air Development Center, AFSC
ATTN: TSLD

Space and Missile Systems Organization
Air Force Systems Command
ATTN: IND

Space and Missile Systems Organization
Air Force Systems Command
ATTN: MNNH, R. Lawrence
ATTN: MNNH, M. Baran

Space and Missile Systems Organization
Air Force Systems Command
ATTN: YAPC

DEPARTMENT OF THE AIR FORCE (Continued)

Strategic Air Command
Department of the Air Force
ATTN: XPFS, B. Stephan
ATTN: NRI-STINFO Library
ATTN: G. Matzke
ATTN: DEL

DEPARTMENT OF ENERGY

Department of Energy
Albuquerque Operations Office
ATTN: Operational Safety Division
ATTN: Technical Library

Department of Energy
Economic Regulatory Administration
Office of Utilities Systems
ATTN: EEPA for L. O'Neill

OTHER GOVERNMENT AGENCIES

Central Intelligence Agency
ATTN: RD/SI for OSI/NED/NWB

Department of Transportation
Federal Aviation Administration
ATTN: Sec. Div., ASE-300

DEPARTMENT OF DEFENSE CONTRACTORS

Aerospace Corporation
ATTN: R. Crolius
ATTN: J. Reinheimer
ATTN: R. Mortensen
ATTN: Library
ATTN: C. Pearlston
ATTN: I. Garfunkel

Agbabian Associates
ATTN: Library

Avco Research and Systems Group
ATTN: W. Lepsevich

Battelle Memorial Institute
ATTN: E. Leach
ATTN: R. Blazek

BDM Corporation
ATTN: Corporate Library

BDM Corporation
ATTN: Library

Bendix Corporation
Communication Division
ATTN: Document Control

Bendix Corporation
Research Laboratories Division
ATTN: M. Frank

Boeing Company
ATTN: KENT Technical Library
ATTN: D. Isbell
ATTN: D. Kemle
ATTN: B. Hanrahan

DEPARTMENT OF DEFENSE CONTRACTORS (Continued)

Booz-Allen and Hamilton, Inc.
ATTN: R. Chrisner
ATTN: Technical Library

Brown Engineering Company, Inc.
ATTN: F. Leonard

Burroughs Corporation
Federal and Special Systems Group
ATTN: A. Mauriello

Calspan Corporation
ATTN: Library

Charles Stark Draper Lab., Inc.
ATTN: TIC MS 74
ATTN: K. Fertig

Cincinnati Electronics Corp.
ATTN: L. Hammond

Computer Sciences Corporation
ATTN: R. Briggs

Comnputer Sciences Corporation
ATTN: R. Dickhauut
ATTN: A. Schiff

Control Data Corporation
ATTN: J. Meehan

Cutler-Hammer, Inc.
AIL Division
ATTN: E. Karpen

Dikewood Industries, Inc.
ATTN: Technical Library
ATTN: L. Davis

Dikewood Industries, Inc.
ATTN: K. Lee

E-Systems, Inc.
ECI Division
ATTN: R. Frank

E-Systems, Inc.
Greenville Division
ATTN: J. Moore

Effects Technology, Inc.
ATTN: S. Clow

EG&G Washington Analytical Services Center, Inc.
ATTN: C. Giles

Ford Aerospace & Communications Corp.
ATTN: K. Attinger
ATTN: E. Poncelet, Jr.

Ford Aerospace & Communications Corp.
ATTN: J. Mattingley
ATTN: Technical Library

Franklin Institute
ATTN: R. Thompson

DEPARTMENT OF DEFENSE CONTRACTORS (Continued)

General Dynamics Corporation
Electronics Division
ATTN: Research Library

General Dynamics Corporation
ATTN: Research Library

General Electric Company
Space Division
ATTN: J. Andrews

General Electric Company
Aerospace Electronics Systems
ATTN: C. Hewison

General Electric Company
ATTN: Technical Library

General Electric Company-TEMPO
Center for Advanced Studies
ATTN: R. Rutherford
ATTN: W. McNamara
ATTN: DASIAC

General Electric Company-TEMPO
Alexandria Office
ATTN: DASIAC

Georgia Institute of Technology
Georgia Tech. Research Institute
ATTN: R. Curry

Georgia Institute of Technology
Office of Contract Administration
ATTN: H. Denny

Grumman Aerospace Corporation
ATTN: L-01 35

GTE Sylvania, Inc.
Electronics Systems Grp-Eastern Div.
ATTN: C. Thornhill
ATTN: L. Blaisdell

GTE Sylvania, Inc.
ATTN: C. Ramsbottom
ATTN: D. Flood
ATTN: J. Waldron
ATTN: M. Nurefora
ATTN: E. Motchok

Harris Corporation
Harris Semiconductor Division
ATTN: A. Strain
ATTN: V. Pres. & Mgr. Prgms. Div.

Hazeltine Corporation
ATTN: M. Waite

Honeywell, Inc.
Avionics Division
ATTN: S&RC, Library
ATTN: R. Johnson

Honeywell, Inc.
Avionics Division
ATTN: S. Graff
ATTN: W. Stewart

DEPARTMENT OF DEFENSE CONTRACTORS (Continued)

Hughes Aircraft Company
ATTN: J. Singletary
ATTN: CTDC 6/E110
ATTN: K. Walker

IIT Research Institute
ATTN: J. Bridges
ATTN: T. Mindel

Institute for Defense Analyses
ATTN: Tech. Info. Services

International Tel. & Telegraph Corp.
ATTN: Technical Library

Ion Physics Corporation
ATTN: R. Evans
ATTN: H. Milde

IRT Corporation
ATTN: D. Swift

JAYCOR
Santa Barbara Facility
ATTN: W. Radasky

JAYCOR
ATTN: R. Stahl
ATTN: E. Wenaas

JAYCOR
ATTN: Library

Kaman Sciences Corporation
ATTN: A. Bridges
ATTN: W. Ware
ATTN: J. Lubell
ATTN: F. Shelton
ATTN: W. Rich

Lawrence Livermore Laboratory
University of California
ATTN: L-96, T. Donich
ATTN: L-10, H. Kruger
ATTN: L-153, D. Meeker
ATTN: L-156, E. Miller
ATTN: Technical Information Dept. Lib.

Litton Systems, Inc.
Data Systems Division
ATTN: M848-61
ATTN: EMC Gp.

Litton Systems, Inc.
AMECOM Division
ATTN: J. Skaggs

Lockheed Missiles and Space Company, Inc.
ATTN: M. Bernstein
ATTN: E. Smith
ATTN: L. Rossi
ATTN: G. Heath
ATTN: H. Thayn
2 cy ATTN: S. Taimuthy

Lockheed Missiles and Space Company, Inc.
ATTN: Tech. Info. Center

DEPARTMENT OF DEFENSE CONTRACTORS (Continued)

Los Alamos Scientific Laboratory
ATTN: J. Malik
ATTN: C. Benton

MIT Lincoln Laboratory
ATTN: L. Loughlin

Martin Marietta Corporation
Orlando Division
ATTN: M. Griffith

Maxwell Labs., Inc.
ATTN: A. Travelpiece

McDonnell Douglas Corporation
ATTN: T. Ender

McDonnell Douglas Corporation
ATTN: S. Schneider
ATTN: Technical Library Services

Mission Research Corporation
ATTN: EMP Group
ATTN: W. Hart

Mission Research Corporation
EM System Applications Division
ATTN: L. McCormick
ATTN: D. Merewether

Mission Research Corporation-San Diego
ATTN: V. Van Lint

Mitre Corporation
ATTN: M. Fitzgerald

Norden Systems, Inc.
ATTN: Technical Library

Northrop Corporation
Electronic Division
ATTN: L. Smith
ATTN: B. Ahlport
ATTN: V. Demartino

Palisades Inst. for Rsch. Services, Inc.
ATTN: Records Supervisor

Physics International Company
ATTN: Document Control

R & D Associates
ATTN: C. Mo
ATTN: R. Schaefer
ATTN: S. Rogers
ATTN: Document Control
ATTN: C. MacDonald

R & D Associates
ATTN: J. Bombardt

Rand Corporation
ATTN: W. Sollfrey
ATTN: C. Crain
ATTN: Library-D

Raytheon Company
ATTN: G. Joshi

DEPARTMENT OF DEFENSE CONTRACTORS (Continued)

Raytheon Company
ATTN: H. Flescher

RCA Corporation
Government Systems Division
ATTN: G. Brucker

RCA Corporation
ATTN: L. Minich

RCA Corporation
Camden Complex
ATTN: O. Whitehead

Rockwell International Corp.
ATTN: V. Michel
ATTN: J. Monroe

Rockwell International Corp.
Space Division
ATTN: B. White

Rockwell International Corp.
ATTN: B-1 Div.

Rockwell Interntional Corp.
ATTN: F. Shaw

Sandia Laboratories
ATTN: G. Yonas
ATTN: T. Martin
ATTN: R. Parker

Science Applications, Inc
ATTN: R. Parkinson

Science Applications, Inc.
ATTN: W. Chadsey

Sidney Frankel & Associates
ATTN: S. Frankel

Singer Company
ATTN: Security Manger for
Tech. Info. Center

Sperry Rand Corp.
Sperry Division
ATTN: Technical Library

Sperry Rand Corp.
Sperry Flight Systems
ATTN: D. Schow

Spire Corporation
ATTN: J. Uglum
ATTN: R. Little

SRI International
ATTN: G. Carpenter
ATTN: A. Whitson
ATTN: W. Scharfman

SRI International
ATTN: Mr. Hullings

Systems, Science & Software, Inc.
ATTN: A. Wilson

DEPARTMENT OF DEFENSE CONTRACTORS (Continued)

Texas Instruments, Inc.
ATTN: D. Manus
ATTN: Technical Library

Texas Tech. University
ATTN: T. Simpson

TRW Defense & Space System Group
ATTN: L. Magnolia
ATTN: H. Holloway
ATTN: O. Adams

DEPARTMENT OF DEFENSE CONTRACTORS (Continued)

Varian Associates, Inc.
ATTN: H. Jory

Westinghouse Electric Corp.
Advanced Energy Systems Div.
ATTN: Technical Library